Doctoral Dissertation

Dynamic Properties of Helical Assemblies of Chiral Organic Molecules Containing Steroidal Moieties

ステロイド骨格を含むキラル有機分子のらせん集合体の動的性質

Wen-Tzu Liu

July 2013

Department of Material and Life Science

Graduate School of Engineering

Osaka University

Contents

General Introduction

A vast amount of researches were devoted to supramolecular assemblies involving secondary interactions, such as hydrogen bonding, π-π stacking, charge transfer, hydrophobic interactions, and chelation of metal cations.[1-3] For the past two decades, our group has studied on the crystalline assemblies of steroidal bile acids and their derivatives because of their fascinating molecular structures. Their representative, cholic acid (CA) (Figure G-1(a)), has an arched polycyclic skeleton with eleven chiral carbons, a short side-chain, and four discrete hydrogen-bonding groups. Such a structure enables CA to form the crystalline assemblies which hold many kinds of guest molecules in channels through multiple hydrogen bonds. This indicates that CA serves as the host for including a wide variety of the guest components.[4-7]

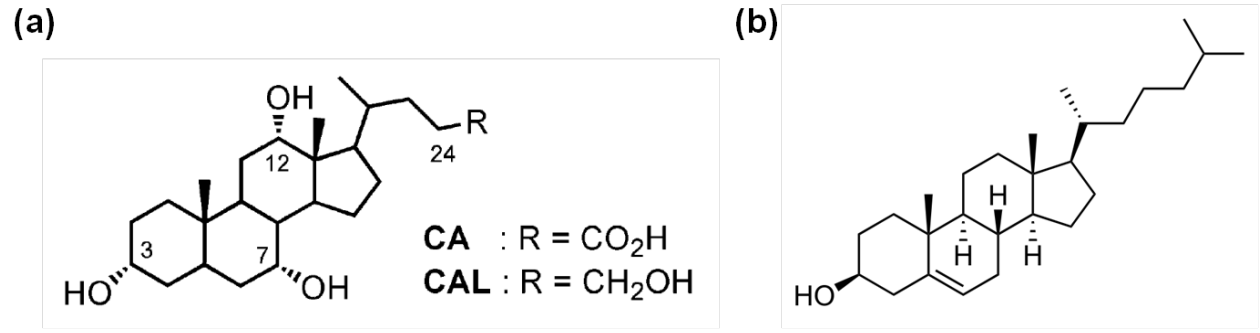

Figure G-1. (a) Cholic acid (CA) and its derivative (CAL) and (b) cholesterol.

CA has intermediate properties between small molecules, such as benzene, and large molecules, such as biopolymers. The former presents the inclusion properties in rare cases, while the latter does in most cases. The intermediate compounds, CA and other steroidal bile acids as well as over 50 of their derivatives, may be expected to construct host–guest assemblies, termed as inclusion compounds, and function as chiral diverse synthons for supramolecular architectures. The inclusion properties are related to various supramolecular features, involving cooperative interactions, self-organization, host–guest relationship, recognition, dynamics, sequential information, chirality, and so on. Therefore, a systematic study on the steroidal assemblies would clarify any relations between organic molecules and their assemblies through cooperative interactions, bridging the gap between small molecules and biopolymers.[8-10]

Helicity of polymers and assemblies in common

It is well-known that many substances involve helical structures, as exemplified in biopolymers such as proteins and DNA as well as stairs in daily life, and that such helices originate functional properties in various states (Figure G-2). The long study by our group exhibits the following remarkable feature; the CA inclusion crystals are composed of bundles of one-dimensional helical assemblies, which play a key role for understanding the above mentioned supramolecular features. Additionally, a steroidal compound, called cholesterol (Figure G-1(b)), is known to form helical

assemblies in the liquid-crystalline state, resulting in various attractive physical properties. These facts led us to the present thesis on helical assemblies of various organic molecules containing steroidal skeletons. This research has induced the finding of some dynamic and functional properties of the helical assemblies, which is described in this thesis in detail.

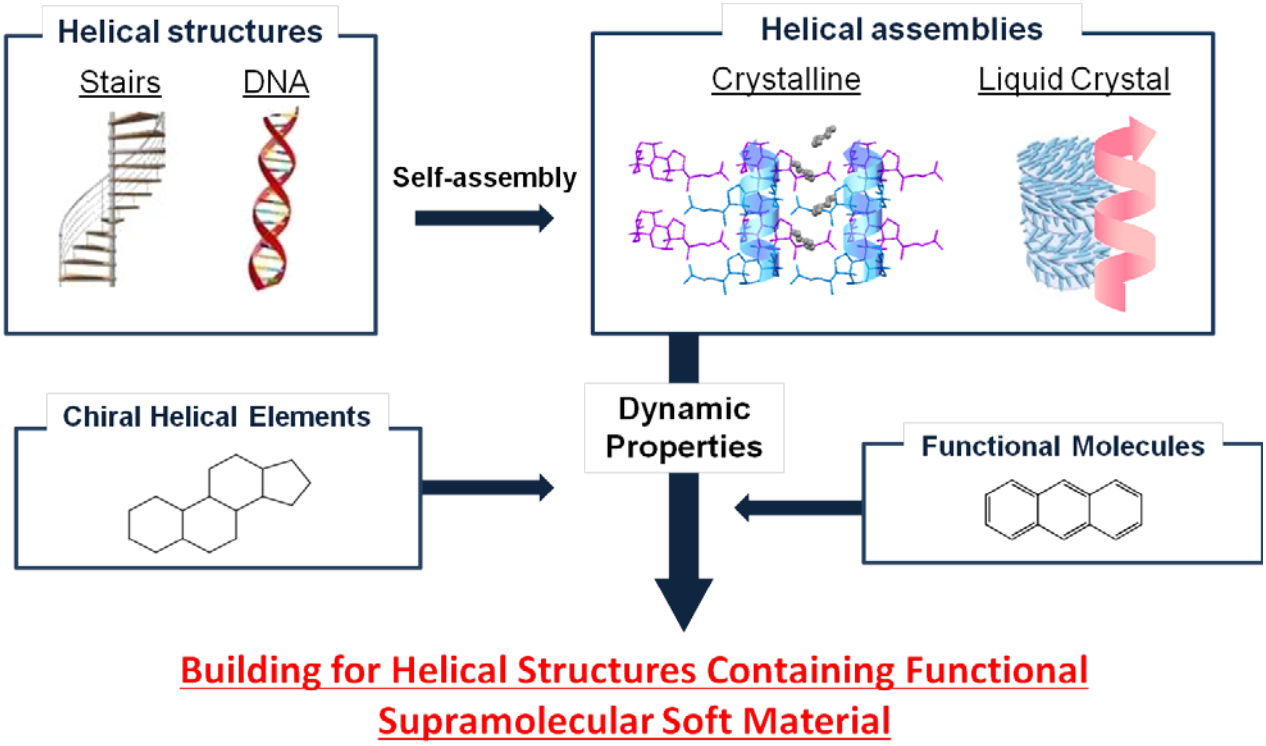

Figure G-2. Molecular assemblies containing helical structures with functional and dynamical properties.

Organic crystals as supramolecular assemblies with helicity

Gautam R. Desiraju says in his famous review as follows; "*A crystal of an organic compound is the ultimate supramolecule, and its assembly, governed by chemical and geometrical factors, from individual molecules is the perfect example of solid-state molecular recognition.*"[11] In other words, the crystal structures afford key information to understand supramolecular properties such as molecular recognition, and further to understand a mechanism of the crystal formation. In this manner, X-ray crystallographic analyses play a decisive role for making clear molecular arrangements necessary for designing the supramolecular architectures.

X-ray crystallography provides a useful method for determining atomic and molecular arrangements in crystals. In order to determine the arrangements of organic substances, single-crystal X-ray diffraction (SXRD) serves as the most common experimental method. This method is performed by analyzing the pattern of X-rays diffracted by an ordered array of single crystals. In more detail, a crystal structure is composed of a pattern, a set of atoms arranged in a particular way, and a lattice exhibiting long-range order and symmetry. Patterns are located upon the points of a lattice, which is an array of points repeating periodically in three-dimensions.

The obtained crystal structures have been saved in the Cambridge Structural Database (CSD) for the past half a century. Now the CSD is a representative repository for crystal structures of small molecules. According to the CSD data, more than 70% of the crystal structures involve helical assemblies. Moreover, helical supramolecular assemblies as well as polymers have attracted chemists because of their exotic structures and their significant properties such as anisotropic optical behaviors and optical resolution abilities. Hence, understanding of the crystalline helical assemblies would serve as a key for making the supramolecular architectures with dynamic and functional properties.

Bundling of helical assemblies in steroidal crystals

CA is a naturally-occurring steroidal bile acid and has a facially amphiphilic molecular structure. A remarkable feature is that CA forms crystalline molecular assemblies together with various organic compounds, enabling us to determine the assembling modes by X-ray crystallography. As a result, it was found that the CA crystals have the following four common features. (i)Almost all of the crystals involve 2_1-helical assemblies. (ii)The helices bundle together to form bilayer structures consist of alternative stacking of hydrophilic and lipophilic layers. (iii)The hydrophilic layers have intermolecular cyclic hydrogen bonds among the host molecules. (iv)The lipophilic layers accommodate the guest molecules in one-dimensional void spaces. In addition, the crystals change from a herringbone structure to various bilayer ones when guest molecules are included.

CA derivatives also make the bilayer structures, but display different inclusion behaviors from CA itself. For example, an amide derivative of CA includes alcoholic polar compounds, while CA mainly includes nonpolar compounds. Such a difference of the inclusion behavior is attributed to their functional groups, amide and carboxylic group, that lead to a different host–guest interaction.[12-13] While CA simply forms a closed cyclic hydrogen bond network among the host molecules, a N-H moiety of CA amide affords an additional hydrogen bond among the host and guest molecules.[14]

In order to overcome such similarity and differences, a series of studies using many steroidal derivatives reached the idea that a hierarchical interpretation is well-suited for the assembling modes of the molecules as follows (Figure G-3). Firstly, individual molecules are arranged into one-dimensional twofold helical assemblies. Secondly, the assemblies proceed to the formation of bundling of the helices. Thirdly, the resulting two-dimensional layer structures are stacked to form three-dimensional crystals. Finally, the crystals often include guest components between the layers. This hierarchical structures are alike those of proteins.

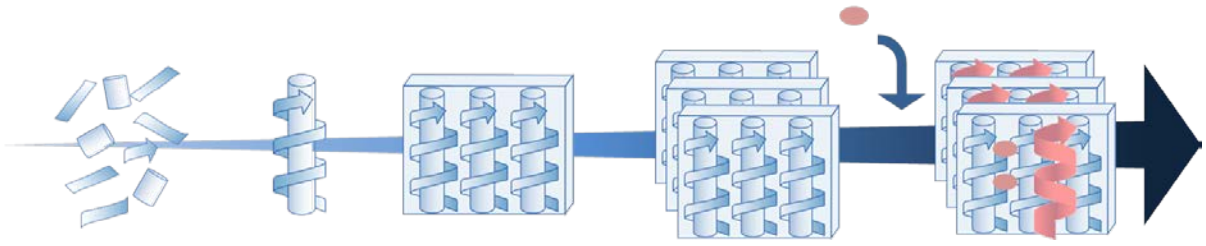

Figure G-3. Hierarchical self-assembly of CA.

Hydrogen bonds in supramolecular architectures

Supramolecular architectures are constructed with secondary interactions, such as hydrogen bonding, π-π stacking, charge transfer, hydrophobic interactions, and so on. Among them, intramolecular and/or intermolecular hydrogen bonds play a key role in the architectures. The former intramolecular hydrogen bonds are between different components of molecules with stabilized conformations. They are among the most important interactions in molecules, because they require particular molecular conformations, and when formed, they confer additional rotational stability to these conformations. In the small biological molecules, the intramolecular hydrogen bonding is observed in situations where the configuration of the molecule is such that donor and acceptor groups are in close proximity.[15] This interaction occurs frequently as the minor component of three-center hydrogen bonds. There are also circumstances where the molecules adopt a particular conformation to permit intramolecular bonding.

The hydrogen bonds help to determine the three-dimensional structures of the biological molecules, and are therefore involved in their functional aspects. The hydrogen bonds are of major importance in the globular proteins, where all the secondary and tertiary structure hydrogen bonds are of this type. Besides, carbohydrates are among the most abundant molecules in living nature, with the exception of the water molecule. They are found in wide varieties as monomers, oligomers, cyclic and linear and branched polymers. The simpler hydrogen-bonding function comes from the hydroxyl group which can have both donor and acceptor properties. They differ fundamentally from those of the polypeptides or proteins, in which the majority of hydrogen-bond groups are –NH groups, which are only hydrogen-bond donors, and the C=O groups, which can only be hydrogen-bond acceptors.

Cholic acid (CA) mostly uses the intermolecular hydrogen bonds. CA has been known to form various bilayer structures depending on the included guests. CA contains three kinds of bilayer structures which have different host frameworks and hydrogen-bonding networks. Each has cyclic hydrogen-bonding network, linear network and branched one. When guest compounds are not hydrogen-bonded to the host, the host frameworks would be determined by the size and shape of the guest compounds.[16]

Twofold helical assemblies in organic crystals and inclusion channels

A molecular assembly with a two-fold screw axis, a so-called 2_1 helical assembly, is one of the most fundamental and important motifs of organic non-centrosymmetric crystals. In crystalline state, twofold helix (2_1 helix) is particularly essential and is a universal motif, because molecules prefer to be packed with 2_1 symmetry to cancel its dipole moment and anisotropic molecular shape.[17-18] Furthermore, approximately 70% of crystals registered in the Cambridge Structural Database (CSD) contain 2_1 helical axes.[19] Hence, it is important to apprehend the mechanism of the formation of helical assemblies.

As mentioned in "*The International Table for Crystallography, Vol. A*", "In practical crystallography one wants to distinguish between right- and left-handed screws and does not want to change from a right-handed to a left-handed coordinate system."[20] Nevertheless, the handedness of 2_1 helical motifs has never been defined and never even been discussed since establishment of crystallography. This seems to be reasonable when one considers that the two-fold screw axis operation involves a 180-degree rotation, and thus, it is impossible to distinguish its handedness, i.e. right or left-handed. On the other hand, our systematic study on crystalline supramolecular assemblies of steroids enabled us to conclude that the handedness of a 2_1 helical assembly can be defined by considering the molecular shape and assembly manners, and we proposed the supramolecular-tilt-chirality method to define the handedness.

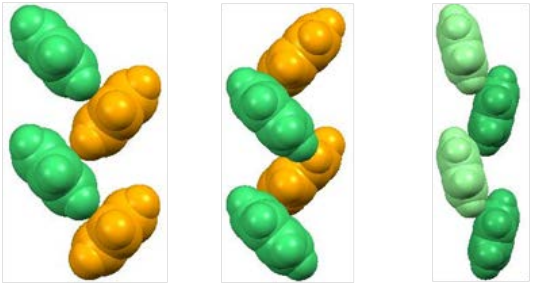

Figure G-4. 2_1 Symmetric herringbone assemblies in benzene crystals.

As mentioned above, CA has been known to form various bilayer structures depending on the included guests. In addition, CA forms one-dimensional void space runs through the lipophilic layers to accommodate the guest molecules. Interestingly, we can see benzene molecules forms 2_1 symmetric herringbone assemblies in these channels. This fact prompted us to determine handedness of twofold helices in benzene crystals (Figure G-4).

Dynamic properties of helical assemblies in cholesteric liquid crystals

Liquid crystals (LCs) are matter in a state that has properties between those of conventional liquid and those of solid crystal. Depending on molecular orientation, liquid crystals self-assemble in three main types, Nematic, Smectic, and Cholesteric. The types of LC phases can be distinguished by their different optical properties. In addition, LCs can be divided into thermotropic, lyotropic and metallotropic phases. Thermotropic and lyotropic LCs consist of organic molecules. Thermotropic LCs exhibit a phase transition into the LC phase as temperature is changed. Lyotropic LCs exhibit phase transitions as a function of both temperature and concentration of the LC molecules in a solvent (typically water). When viewed under a microscope using a polarized light source, different liquid crystal phases will appear to have distinct textures.

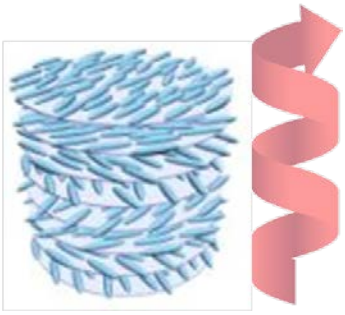

Figure G-5. Helical structure of cholesteric liquid crystal.

A cholesteric liquid crystal is a type of LC with a helical structure and which is therefore chiral (Figure G-5).[21-23] They organize in layers with no positional ordering within layers, but a director axis which varies with layers. The variation of the director axis tends to be periodic in

nature. The period of this variation (the distance over which a full rotation of 360° is completed) is known as the pitch, p. The pitch varies with temperature and it can also be affected by the boundary conditions when the cholesteric LC is sandwiched between two substrate planes. Depending on stimuli, a reversible phase change from cholesteric to other phases can be observed during heating/cooling or UV/vis light irradiation cycles. The dynamic change of cholesteric LC is mainly due to the change of molecular structure, leading to the variation of self-assembled constructions. Secondary forces between the LC molecules are considered as the main factor of the self-assembly of molecules.[24-28]

Inclusion complexes of cyclodextrin with cholesterol moiety

Various types of inclusion complex (IC) formed by noncovalent host-guest interaction have been extensively investigated and reported as useful building blocks for constructing supramolecular structures. In particular, cyclodextrins (CDs) have been the most intensively studied as host molecules, on account of their good water-solubility and ability to selectively include a wide range of guest molecules.

For the study of the hydrogen bonding, the CDs are unique in being molecules in the 1,000- to 1,300-Da range, and provide excellent quality crystals for both X-ray and neutron diffraction experiments. Their hydrogen-bonding functionality is relatively simple in that they contain only hydroxyl groups and water molecules as donors and acceptors with the sugar ring and glycosidic linkage oxygen atoms as additional acceptors.

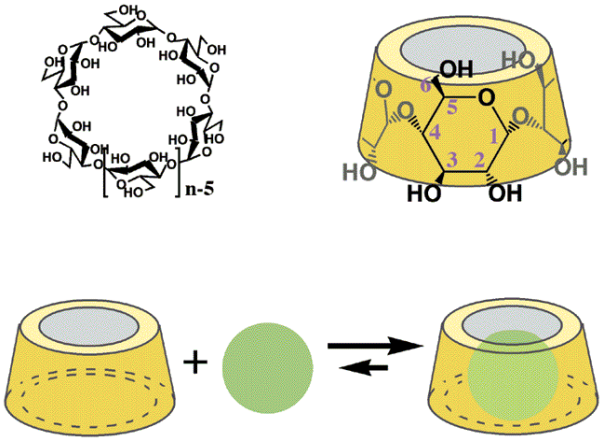

Figure G-6. Cyclodextrins: α-cyclodextrin (*n* = 6), β-cyclodextrin (*n* = 7), and γ-cyclodextrin (*n* = 8). Formation of the inclusion complex of cyclodextrin with a small guest molecule.[29]

The soluble fraction of starch consists of the linear amylases which are composed of α(1-4)-linked D-glucose units and adopt helical conformations. The primary and the secondary hydroxyl groups are located in the different side. The secondary hydroxyl groups are located at the wider side of the torus. Due to their polar hydrophilic outer shell and relatively hydrophobic cavity, they are able to build up host-guest complexes by inclusion of suitable hydrophobic molecules. The properties of the CD cavity explain some of the unusual features of these molecules. With this unique structure CDs can form “host” and “guest” complexes with very vast molecules that have a hydrophobic part and fit into the cavity of CDs.[30] Because the glucanotransferases are not very specific with respect to their cutting sites, a family of oligosaccharides are obtained with 6, 7, and 8 glucoses per annulus. These are called α-, β-, and γ-cyclodextrins (Figure G-6).

With relatively non polar cavity in comparison to polar exterior, CDs can form inclusion

compounds with hydrophobic guest molecules in aqueous solutions predominantly due to hydrophobic interactions. Then another requirement for guest molecule to form inclusion complex with CDs is that the guest molecule must be able to fit inside the cavity of the CD. Most frequently the host to guest ratio is 1:1. This is the simplest and most frequent case. However, the ratio of 2:1, 1:2, 2:2, or even more complicated associations, and higher order equilibria are also exist, almost always simultaneously.[31-37]

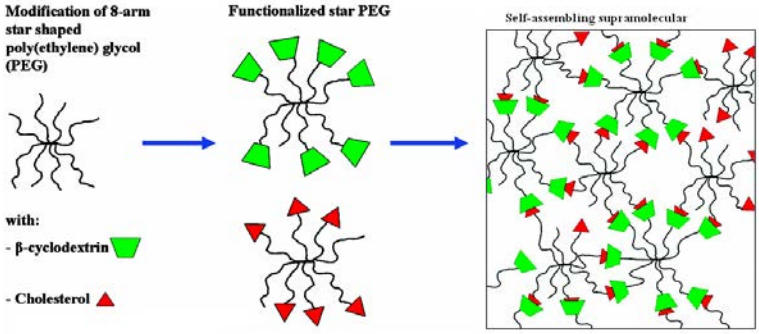

Figure G-7. Schematic illustrations of the inclusion formation of cyclodextrins and cholesterols.

CDs form inclusion complexes rather nonspecifically with a wide variety of guest molecules. Consequently, it is not surprising to find that noble gases[38], paraffins, alcohols, carboxylic acids, aromatic dyes, benzene derivatives and salts are included.[39-42]

As one of the applications, complexations of CDs are used in food formulations for flavor protection or flavor delivery. They form inclusion complexes with a variety of molecules including fats, flavors and colors. CDs are also used as process aids, for example, to remove cholesterol from products such as milk, butter and eggs (Figure G-7).[43-44] Besides, in cosmetics industries, fragrance is enclosed with the CD and the resulting inclusion compound is complexed with calcium phosphate to stabilize the fragrance in manufacturing bathing preparations and producing long-lasting fragrances.[45] In environmental science, the complexation of CD can be used to remove highly toxic substances from industrial effluent.[46]

Various types of inclusion complex (IC) formed by noncovalent host-guest interaction have been extensively investigated and reported as useful building blocks for constructing supramolecular structures. In particular, CDs have been the most intensively studied as host molecules, on account of their good water-solubility and ability to selectively include a wide range of guest molecules. Harada et al. synthesized tubes from α-CD. Their synthesis is based on a self-assembly process of CD threading on a "template polymer". After the cross-linking of the α-CD and removing the "template polymer", CD molecular tube has been achieved (Figure G-8).[47]

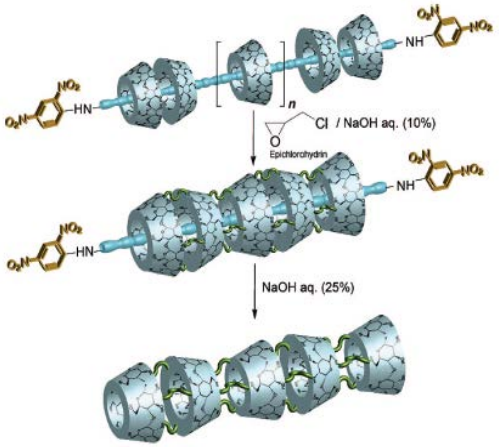

Figure G-8. Schematic illustration for the preparation of molecular tube incorporating cyclodextrin.

The two isomers of azobenzene, the trans and cis forms, can be reversibly switched to each other upon photoirradiation. Driven by hydrophobic and van der Waals interactions, trans-azobenzene can be well-recognized by α-CD, a type of CD with six glucose units. However, when trans-azobenzene is transformed to cis-azobenzene, α-CD cannot include the bulky cis form anymore because of the mismatch between the host and guest. Therefore, the host-guest assembly and disassembly between azobenzene and α-CD by external photostimuli can act as a driving force to build up molecular shuttles, motors, and machines.[48]

Besides, there have been many reports on the use of highly branched polymers as covalently bound modifiers for CDs[49-62] and on the UV-induced decomplexation of host-guest molecules that leads to the deformation of vesicles.[63-65] However, there has been no morphology study concerning photo-induced inclusion complexes prepared from monomers and CDs that are formed through non-covalent interactions.

Dynamic and optical properties of organogels with steroidal moiety

Some new naphthalene derivatives consisting of bisurea and six long alkyl chains to develop switchable fluorescent organogel systems by the cooperation of intermolecular hydrogen bonding and π-π interaction were reported. It was found that the sol-gel process and fluorescence of the system could be controlled by alternate addition of fluoride anions and protons.[66-70] However, the effect of secondary forces on helical morphology and thermo tunable fluorescence behaviors of chiral gelators are limited.

Similarly, organogels containing some steroidal moieties were synthesized and their thermo tunable properties were studied.[71-74] Organogels are formed by assembling low-molecular-weight gelators (LMWGs)[75-78] into entangled three-dimensional networks with solvent molecules entrapped through relatively strong intermolecular interactions such as hydrogen bonding and π-π stacking (Figure G-9). Accordingly, the gel-solution (gel-sol) transition for organogels is thermally reversible. It is desirable to design organogels whose gel-sol transitions can be further tuned by other physical and chemical stimuli because such external stimuli-responsive gels are highly desirable for advanced applications of organogels, such as the sol-gel process, drug delivery, sensors, and molecular logic gates.[79-88] Development of such organogels may lead to novel smart materials.

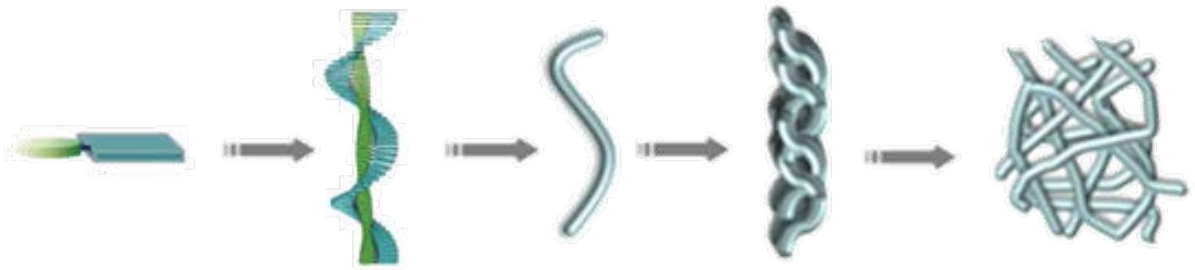

Figure G-9. Hierarchical self-assemblies of organogels from steroidal contained molecules.

Scope of this thesis

With the background mentioned above, this thesis describes dynamic properties of helical assemblies of organic chiral molecules containing steroidal skeletons (Figure G-10). So far, we have systematically researched supramolecular inclusion phenomena using steroidal crystals. Among many steroidal molecules employed previously, CA and cholamide are particularly fascinating because they can include 100 or more organic compounds.[89-100] These studies induced the two ideas as follows. The one is that twofold helical assemblies can exhibit distinguishable right- or left-handedness, prompting us to determine the handedness of twofold helical assemblies of benzene and its derivatives. The other is that the steroidal skeletons tend to form helical assemblies based on cooperative secondary forces, enabling us to construct functional supramolecular architectures with dynamical properties. By using cholesterol as one of the steroidal skeletons, we designed two chiral molecules, cholesteryl-*trans*-4-(11-acryloxyundecaloxy)cinnamate (CAUC) and cholesteryl *N*-(2-anthryl) carbamate (CAC). The former affords an inclusion assembly with β-cyclodextrin to display photoresponsive dynamical behaviors. The latter forms a supramolecular architecture with helicity, yielding organogels with significant enhanced fluorescence strength due to the aggregation-induced enhanced emission (AIEE)[101-103].

Chapter 1 describes a thermal guest-release process of CA inclusion crystals, where a structural change from a sandwich type to a bilayer type takes place.

Chapter 2 describes a hierarchical formation of 3α,7α,12α,24-tetrahydroxycholane (CAL) crystal. So far, CAL has not been confirmed to include any guest components. A slight change of the molecular structure induces a dramatic shift in molecular assemble modes, molecular recognitions and inclusion behaviors.

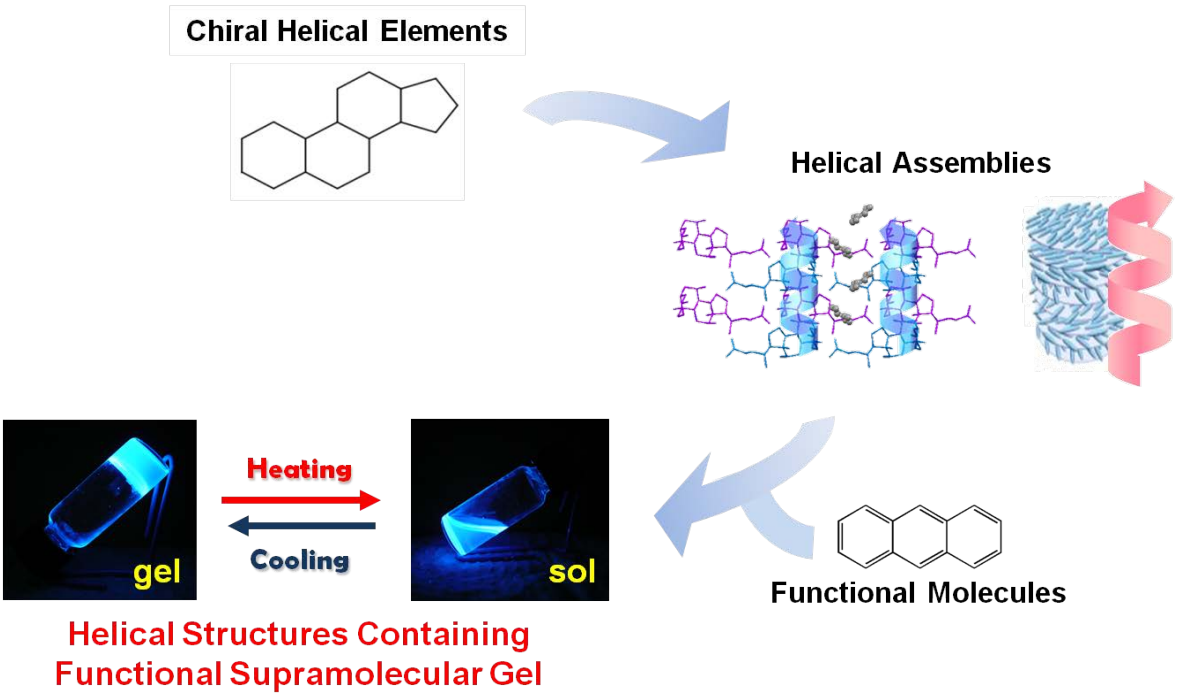

Figure G-10. Helical assemblies of organic chiral molecules containing steroidal skeletons.

Chapter 3 describes the first proposal of a universal method for distinguishing right- or left-handedness of twofold helical assemblies of planar benzene molecules. Moreover, we proposed progressive expressions on symmetry diagram, namely, the use of an enantiomeric pair of the symbols to express right- or left-handed twofold helices.

Chapter 4 describes a synthesis of a new class of chiral molecule, CAUC. After threading with β-CD, the intermolecular forces are significantly enhanced, leading to the formation of a self-assembled columnar structure. Subsequently, this chapter deals with characterization of the photo-tunable morphologies caused by UV-induced E-Z configurational isomerization.

Chapter 5 describes a synthesis of a novel chiral gelator, CAC, as well as optical behaviors and self-assembled constructions of the gelator. Formation of self-assembled constructions via secondary forces is shown through temperature dependent ^{1}H-NMR. Liquid crystalline behaviors, ^{1}H-NMR spectra at different temperature and the effect of individual secondary force on helical structure are discussed.

References

[1] S. Tung and Ting Xu, *Macromolecules*, **2009**, *42*, 761–765.

[2] J. Kao, J. Tingsanchali and T. Xu, *Macromolecules*, **2011**, *44*, 4392–4400.

[3] S. Xiao, X. Lu, Q. Lu and B. Su, *Macromolecules*, **2008**, *41*, 3884–3892.

[4] K. Inoue, K. Kato, N. Tohnai and M. Miyata, *J. Polym. Sci. Part A : Polym. Chem.*, **2004**, *42*, 4648-4655.

[5] H. Tsutsumi, M. Miyata and K. Takemoto, *J. Polym. Sci. Part A : Polym. Chem.*, **1987**, *25*, 3079-3087.

[6] O. Bortolini, G. Fantin and M. Fogagnolo, *Chirality*, **2010**, *22*, 486-494.

[7] F. Meijide, J. V. Trillo, V. H. Soto, A. Jover and J. V. Tato, *Chirality*, **2011**, *23*, 940-947.

[8] J. Yang, Q. Li, Y. Li, L. Jia, Q. Fang and A. Cao, *J. Polym. Sci. Part A : Polym. Chem.*, **2006**, *44*, 2045-2058.

[9] T. Zou, S. L. Li, X. Z. Zhang, X. J. Wu, S. X. Cheng and R. X. Zhuo, *J. Polym. Sci. Part A : Polym. Chem.*, **2007**, *45*, 5256-5265.

[10] C. C. Huval, M. J. Bailey, W. H. Braunlin, S. R. Holmes-Farley, W. H. Mandeville, J. S. Petersen, S. C. Polomoscanik, R. J. Sacchiro, X. Chen and P. K. Dhal, *Macromolecules*, **2001**, *34*, 1548–1550.

[11] G. R. Desiraju, *Angew. Chem. Int. Ed. Engl.*, **1995**, *34*, 2311-2317.

[12] K. Nakano, K. Sada and M. Miyata, *J. Chem. Soc., Chem. Commun.*, **1995**, 953-954.

[13] N. Yoswathananont, K. Sada, M. Miyata, S. Akita and K. Nakano, *Org. Biomol. Chem.*, **2003**, *1*, 210-214.

[14] K. Nakano, M. Katsuta, K. Sada and M. Miyata, *Cryst. Eng. Comm.*, **2001**, *3*, 44-45.

[15] H. A. Staab and T. Saupe , *Angew. Chem.* **1988**, *100*, 895–909.

[16] P. Dastidar, *Cryst. Eng. Comm.*, **2000**, *2*, 49-52.

[17] A. I. Kitaigorodskii, *Molecular Crystals and Molecules*, Academic Press, London, 1973.
[18] T. Matsuura and H. Koshima, *J. Photochem. Photobiol. C* 2005, **6**, 7.
[19] http://www.ccdc.cam.ac.uk/products/csd/
[20] International Tables for Crystallography, Vol. A, Space-Group Symmetry; Hahn, T., Ed.; Kluwer Academic Publishers: London, **1983**.
[21] N. Tamaoki, *Adv. Mater.*, **2001**, *13*, 1135-1147.
[22] G. Celebre, G. D. Luca, M. Maiorino, F. Iemma, A. Ferrarini, S. Pieraccini and G. P. Spada, *J. Am. Chem. Soc.*, **2005**, *127*, 11736–11744.
[23] J. Barberá, E. Cavero, M. Lehmann, J. L. Serrano, T. Sierra and J. T. Vázquez, *J. Am. Chem. Soc.*, **2003**, *125*, 4527–4533.
[24] H. Kihara, T. Kato, T. Uryu and J. M. J. Fréchet, *Chem. Mater.*, **1996**, *8*, 961–968.
[25] R. J. Davey, N. Blagden, S. Righini, H. Alison, M. J. Quayle and S. Fuller, *Crystal Growth & Design*, **2001**, *1*, 59–65.
[26] Y. Kamikawa and T. Kato, *Org. Lett.*, **2006**, *8*, 2463–2466.
[27] E. J. Foster, R. B. Jones, C. Lavigueur and V. E. Williams, *J. Am. Chem. Soc.*, **2006**, *128*, 8569–8574.
[28] M. Prehm, F. Liu, X. Zeng, G. Ungar and C. Tschierske, *J. Am. Chem. Soc.*, **2011**, *133*, 4906–4916.
[29] A. Harada, Acc. Chem. Res., **2001**, 34, 456–464.
[30] H. Ritter and M. Tabatabai, *Prog. Polym. Sci*, **2002**, *27*, 1713-1720.
[31] F. Yhaya, J. Lim, Y. Kim, M. Liang, A. M. Gregory and M. H. Stenzel, *Macromolecules*, **2011**, *44*, 8433-8445.
[32] S. Y. Cho and H. R. Allcock, *Macromolecules*, **2009**, *42*, 4484- 4490.
[33] S. Ren, D. Chen and M. Jiang, *J. Polym. Sci. Part A : Polym. Chem.*, **2009**, *47*, 4267-4278.
[34] T. E. Girardeau, T. Z. J. Leisen, H. W. Beckham and D. G. Bucknall, *Macromolecules*, **2005**, *38*, 2261-2270.
[35] Y.H. Chiu and J.H. Liu, *J. Polym. Sci. Part A : Polym. Chem.*, **2010**, *48*, 2975-2981.
[36] E. Kaya and L. J. Mathias, *J. Polym. Sci. Part A : Polym. Chem.*, **2010**, 48, *3*, 581-592.
[37] T. Costa and J. S. Seixas de Melo, *J. Polym. Sci. Part A : Polym. Chem.*, **2008,** *46*, 1402-1415.
[38] B. M. Goodson, *J. Magn. Reson*, **2002**, *155*, 157-216.
[39] T. Kida, Y. Fujino, K. Miyawaki, E. Kato and M. Akashi, *Org. Lett*, **2009**, *11*, 5282-5285.
[40] S. Chelli, M. Majdoub, S. Aeiyach and M. Jouini, *J. Polym. Sci. Part A : Polym. Chem.*, **2009**, *47*, 4391-4399.
[41] E. A. Hasan, T. Cosgrove and A. N. Round, *Macromolecules*, **2008**, *41*, 1393-1400.
[42] M. Okada, Y. Takashima and A. Harada, *Macromolecules*, **2004**, *37*, 7075–7077.
[43] J. A. Corte, K. R. Stauffer, U.S. Patent. 5560950(**1996**).
[44] F. van der Manakker, M. van der Pot, T. Vermondem, C. F. van Nostrum and W. E. Hennink, *Macromolecules*, **2008**, 41, 1766-1773.

[45] N. Prasad, D. Strauss and G. Reichart, European Patent. 1084625(**1999**).

[46] M. Arkas, R. Allabashi, D. Tsiourvas, E. M. Mattausch and R. Perfler, *Environ. Sci. Technol.*, **2006**, 40, 2771-2777.

[47] A. Harada, M. Okada, Y. Kawaguchi and M. Kamachi, *Polym. Adv. Technol.*, **1999**, *10*, 3-12.

[48] M. Jiang, J. Zou, B. Guan, *Macromolecules*, **2009**, *42*, 7465-7473.

[49] N. Prasad, D. Strauss and G. Reichart, European Patent. 1084625(**1999**).

[50] M. Arkas, R. Allabashi, D. Tsiourvas, E. M. Mattausch and R. Perfler, *Environ. Sci. Technol.*, **2006**, *40*, 2771-2777.

[51] A. Harada, A. Hashidzume, H. Yamaguchi and Y. Takashima, *Chem. Rev.*, **2009**, *109*, 5974-6023.

[52] M. Jiang, J. Zou and B. Guan, *Macromolecules*, **2009**, *42*, 7465-7473.

[53] S. Wang, X. Li, B. Chen, Q. Luo and H. Tian, *Macromol. Chem. Phys.*, **2004**, *205*, 1497-1507.

[54] J. M. Kim, *Macromol. Rapid Commun.*, **2007**, *28*, 1191-1212.

[55] H. Tian and H. Y. Tu, *Adv. Mater.*, **2000**, *12*, 1597-1600.

[56] W. Zhu, Y. Yang, R. Métivier, Q. Zhang, R. Guillot, Y. Xie, H. Tian and K. Nakatani, *Angew. Chem. Intern. Edi.*, **2011**, *50*, 10986-10990.

[57] A. Kaeser and A. P. H. J. Schenning, *Adv. Mater.*, **2010**, *22*, 2985-2997.

[58] E. Kaya and L. J. Mathias, *J. Polym. Sci. Part A : Polym. Chem.*, **2010**, *48*, 581-592.

[59] T. Nozaki, Y. Maeda and H. Kitano, *J. Polym. Sci. Part A : Polym. Chem.*, **1997**, *35*, 1535-1541.

[60] G. Gübitz and M. G. Schmid, *Biopharm. Drug Dispos.*, **2001**, *22*, 291-336.

[61] S. Daoud-Mahammed, J. L. Grossiord, T. Bergua, C. Amiel, P. Couvreur and R. Gref, *J. Polym. Sci. Part A : Polym. Chem.*, **2008**, *86A*, 736-748.

[62] C. He, X. Zhuang, Z. Tang, H. Tian and X. Chen, *Adv. Heal. Mater.*, **2012**, *1*, 48-78.

[63] E. Floor and S. E. Leeman, *J. Neurochem.*, **1988**, *50*, 1597-1604.

[64] N. Poulain and E. Nakache, *Journal of Polymer Science Part A : Polymer Chemistry*, **1998**, *36*, 3035-3043.

[65] T. Hoshino, J. Watanabe, M. Kudo, E. Sakai, S. Funyu, K. Ishitsuka and S. Okamoto, *J. Polym. Sci. Part A : Polym. Chem.*, **2012**, *50*, 1707-1716.

[66] M. Wang, J. Qiang, Y. Fang, D. Hu, Y. Cui and X. Fu, *J. Polym. Sci. Part A : Polym. Chem.*, **2000**, *38*, 474-481.

[67] T. Nozaki, Y. Maeda and H. Kitano, *J. Polym. Sci. Part A : Polym. Chem.*, **1997**, *35*, 1535-1541.

[68] Y. Ren, W. H. Kan, V. Thangadurai and T. Baumgartner, *Angew. Chem.*, **2012**, *124*, 4031-4035.

[69] J. A. Levitt, P. H. Chung, M. K. Kuimova, G. Yahioglu, Y. Wang, J. Qu and K. Suhling, *Chem. phys. chem.*, **2011**, *12*, 662-672.

[70] I. O. Shklyarevskiy, P. Jonkheijm, P. C. M. Christianen, A. P. H. J. Schenning, A. D. Guerzo, J. P. Desvergne, E. W. Meijer and J. C. Maan, *Langmuir*, **2005**, *21*, 2108–2112.

[71] L. Lu, T. M. Cocker, R. E. Bachman and R. G. Weiss, *Langmuir*, **2000**, *16*, 20–34.

[72] M. G. Page and G. G. Warr, *Langmuir*, **2009**, *25*, 8810–8816.

[73] C. W. Njauw, C. Y. Cheng, V. A. Ivanov, A. R. Khokhlov and S. H. Tung , *Langmuir*, **2013**, *29*, 3879–3888.

[74] K. Nakano, M. Katsuta, K. Sada and M. Miyata, *CrystEngComm*, **2001**, *3*, 44-45.
[75] R. Oda, I. Huc and S. J. Candau, *Angew. Chem. Int. Ed.*, **1998**, *37*, 2689-2691.
[76] K. Hanabusa, K. Hiratsuka, M. Kimura and H. Shirai, *Chem. Mater.*, **1999**, *11*, 649–655.
[77] M. Suzuki, Y. Nakajima, M. Yumoto, M. Kimura, H. Shirai and K. Hanabusa, *Langmuir*, **2003**, *19*, 8622–8624.
[78] F. Placin, J. P. Desvergne and J.C. Lassegues, *Chem. Mater.*, **2001**, *13*, 117–121.
[79] P. Dastidar, *CrystEngComm*, **2000**, *2*, 49-52.
[80] K. Kato, K. Aburaya, Y. Miyake, K. Sada, N. Tohnai and M. Miyata, *Chem. Commun.*, **2003**, 2872-2873.
[81] D. Das, T. Kar and P. K. Das, *Soft Matter*, **2012**, *8*, 2348-2365.
[82] N. Yoswathananont, K. Sada, K. Nakano, K. Aburaya, M. Shigesato, Y. Hishikawa, K. Tani, N. Tohnai and M. Miyata, *Eur. J. Org. Chem.*, **2005**, *24*, 5330-5338.
[83] P. Babu, N. M. Sangeetha and U. Maitra, *Macromol. Symp.*, **2006**, *241*, 60-67.
[84] S. Aoki, S. Suzuki, M. Kitamura, T. Haino, M. Shiro, M. Zulkefeli and E. Kimura, *Chemistry-An Asian Journal*, **2012**, *7*, 944-956.
[85] H. A. Staab and T. Saupe , *Angew. Chem.* **1988**, *100*, 895–909.
[86] A. Harada, Acc. Chem. Res., **2001**, *34*, 456–464.
[87] H. Ritter and M. Tabatabai, *Prog. Polym. Sci*, **2002**, *27*, 1713-1720.
[88] K. Aburaya, K. Nakano, K. Sada, N. Yoswathananont, M. Shigesato, I. Hisaki, N. Tohnai and M. Miyata, *Crystal Growth & Design*, **2008**, *8*, 1013-1022.
[89] N. Yoswathananont, S. Chirachanchai, K. Tashiro, K. Nakano, K. Sada and M. Miyata, *Cryst Eng Comm*, **2001**, *3*, 74-77.
[90] N. Yoswathananont, K. Sada and M. Miyata, *Mol. Cryst. Liq. Cryst.*, **2002,** *389*, 47-51.
[91] N. Yoswathananont, K. Sada, M. Miyata, S. Akita and K. Nakano, *Org. Biomol. Chem.*, **2003**, *1*, 210-214.
[92] K. Nakano, E. Mochizuki, N. Yasui, K. Morioka, Y. Yamauchi, N. Kanehisa, Y. Kai, N. Yoswathananont, N. Tohnai, K. Sada and M. Miyata, *Eur. J. Org. Chem.*, **2003**, 2428-2436.
[93] K. Nakano, K. Sada, K. Nakagawa, K. Aburaya, N. Yoswathananont, N. Tohnai and M. Miyata, *Chem. Eur. J.*, **2005**, *11*, 1725-1733.
[94] K. Nakano, K. Sada, K. Aburaya, K. Nakagawa, N. Yoswathananont, N. Tohnai and M. Miyata, *Cryst. Eng. Comm.*, **2006**, *8*, 461-467.
[95] K. Nakano, K. Sada, Y. Kurozumi and M. Miyata, *Chem. Eur. J.*, **2001**, *7*, 209-220.
[96] M. Miyata, N. Tohnai and I. Hisaki, *Acc. Chem. Res.*, **2007**, *40*, 694-702.
[97] K. Sada, T. Kondo, M. Miyata, T. Tamada and K. Miki, *J. Chem. Soc., Chem. Commun.*, **1993**, 753-755.
[98] K. Sada, T. Kondo, M. Miyata and K. Miki, *Chem. Mater.*, **1994**, *6*, 1103-1105.
[99] N. Yoswathananont, K. Sada, K. Nakano, K. Aburaya, M. Shigesato, Y. Hishikawa, K. Tani, N. Tohnai and M. Miyata, *Eur. J. Org. Chem.*, **2005**, 5330-5338.
[100] V. Bertolasi, V. Ferretti, G. Fantin and M. Fogagnolo, *Zeitschrift für Kristallographie*, **2008**, *223*, 515-523.
[101] Y. Hong, J.W.Y. Lam and B. Z. Tang, *Chem. Commun.*, **2009**, 4332-4353.
[102] W. Wu, S. Ye, L. Huang, L. Xiao, Y. Fu, Q. Huang, G. Yu, Y. Liu, J. Qin, Q. Li and Z. Li, *Chem. Commun.*, **2009**, 4332-4353.
[103] W. Tang, Y. Xiang and A. Tong, *J. Org. Chem.*, **2009**, *74*, 2163–2166.

Chapter 1

Selective Guest Retention in Thermal Guest-release Process in Sandwich-type Inclusion Crystal of Cholic Acid

Abstract

Ternary inclusion crystals of cholic acid (CA) with two aromatic compounds, *m*-fluoroaniline (**G1**) and indene (**G2**), were investigated from a viewpoint of selective incorporation and release. Recrystallization of CA from an equimolar mixture of **G1** and **G2** gave the CA crystal in a 47:53 molar ratio of **G1** to **G2**. This ternary crystal has a sandwich-type structure with a two-dimensional (2-D) host cavity consisting of two nonequivalent sites, A and B. **G1** tends to be included in the site A owing to hydrogen bonds, while **G2** in the site B. This site affinity for each guest was confirmed in a bulk crystal as well as in a single crystal of the ternary compound. Thermogravimetric analysis revealed that the two guest molecules were released at two different temperature ranges of 50-100 °C and 100-120 °C. Heat treatment of the starting crystal at 90 °C for 10 minutes yielded the expected intermediate crystal, which had a bilayer structure with a one-dimensional (1-D) cavity in a 60:40 molar ratio of **G1** to **G2**. Moreover, irrespective of the guest ratios in the starting CA crystals, **G1** was preferentially retained in the thermal guest-release process. Such preferential retention of **G1** is attributable to the host-guest hydrogen bond between CA and **G1** at the site A in the 2-D cavity.

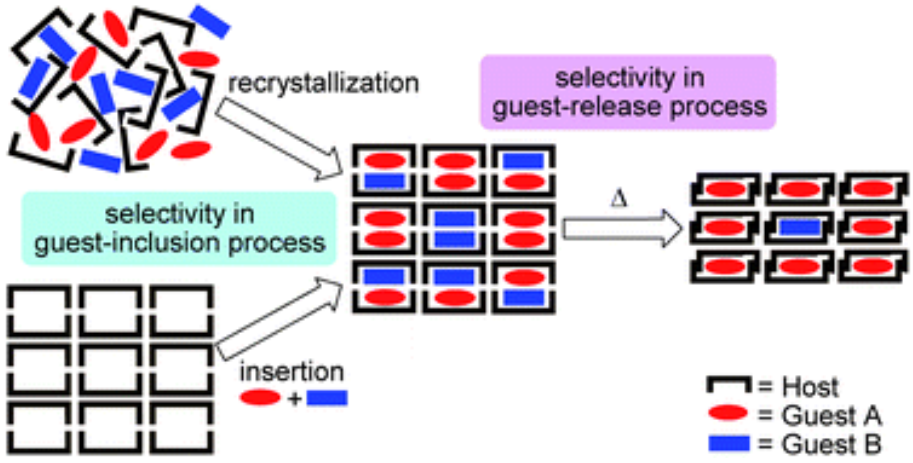

1.1 Introduction

Crystalline lattice-type inclusion compounds boast sophisticated molecular recognition for guest molecules in self-assembling.[1] Compared to macrocyclic counterparts, however, their selective inclusion mechanism is more complicated, which leads to restrictions on their industrial application. As one of rare instances, the Nurex process has long been utilized in extracting linear hydrocarbons from petroleum fractions containing branched ones, in which the objective substances are selectively included in urea crystals.[2] As excellent separation media, many researchers have created various artificial hosts, including acetylenic alcohols, bis-phenol and bis-naphthol analogues, diquinoline compounds, helical tubuland diols, xanthen alcohol, and phosphonium salt.[3-9] Furthermore, hosts based on naturally occurring compounds involving amino acids, tartarates, bile acids, and alkaloids have also been reported to show characteristic selectivities for guest compounds, taking advantage of their asymmetrical chiral structures.[3,10,11]

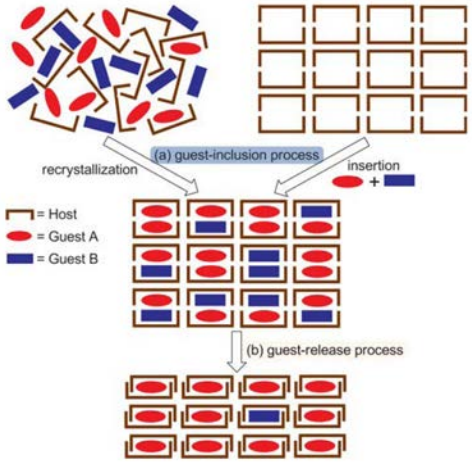

Figure 1-1. Schematic representation of guest selectivity during two processes.

The selective inclusion using these hosts has been achieved by the following two methods, as schematically shown in Figure 1-1. The one is based on recrystallization of a host compound from liquid or solid guest mixtures by adding adequate solvents. The other lies in exposure of a preformed host crystal into liquid or vapor guest mixtures, i.e. competitive insertion of guest mixtures into a host framework. In these instances, the selectivity is given for a particular guest compound in the course of including the guest into a host cavity. To our knowledge, however, no report has been conducted on the guest selectivity during the guest-release process from preformed ternary crystals consisting of guest mixtures. We have found that cholic acid (CA, Figure 1-2) provides ternary sandwitch-type crystals which are suitable for evaluating such a guest-release process.

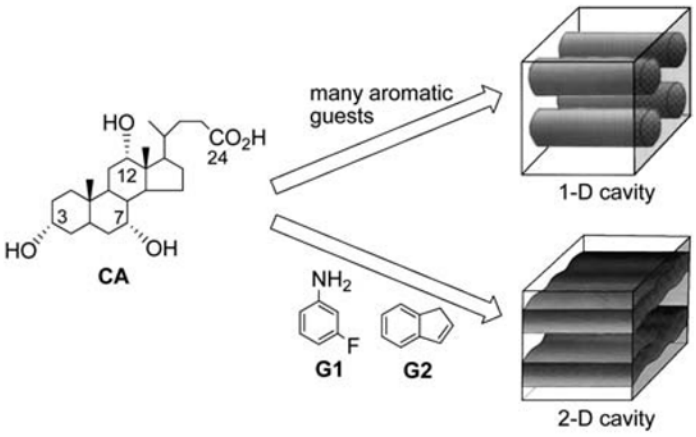

Figure 1-2. Schematic representation of 1D and 2D cavities formed by CA with guests.

1.2 Results and Discussion

1.2.1 Sandwich-type structures with 2-D cavities and guest-release process

Figure 1-3a and 1-3b show the sandwich-type structures of CA·**G1** and CA·**G2** crystals, respectively, which were already reported.[15] These two crystals have the following structural features; (i) the two crystals consist of alternative stacking of host and guest layers, and the host layer is maintained by host-host cyclic hydrogen bond networks; (ii) the guest molecules are included in 2-D cavities of two nonequivalent sites, A and B, and only the guest molecule at the site A in CA·**G1** forms a host-guest hydrogen bond network; (iii) the two crystals have different side chain conformations of the host molecules: trans-type in CA·**G1** and gauche-type in CA·**G2**.

We also reported that the two crystals show deintercalation phenomena, i.e. release of guest molecules accompanied by a structural change of the host layers.[15] When the two inclusion crystals are gradually heated, the guest molecules are released in two distinct temperature ranges. After the first range, intermediate crystals having a bilayer structure with a 1-D cavity are formed. Figure 1-3a and 1-3b show these structural changes of the two crystals: the host layers move in a direction perpendicular to the layer by releasing the guest molecules with changing the cavity dimensionality. Since the host-guest interactions are not the same at the two sites, A and B, in the 2-D cavity, the selective inclusion is expected to be performed not only in the guest-inclusion process but also in the guest-release process into/from the crystals.

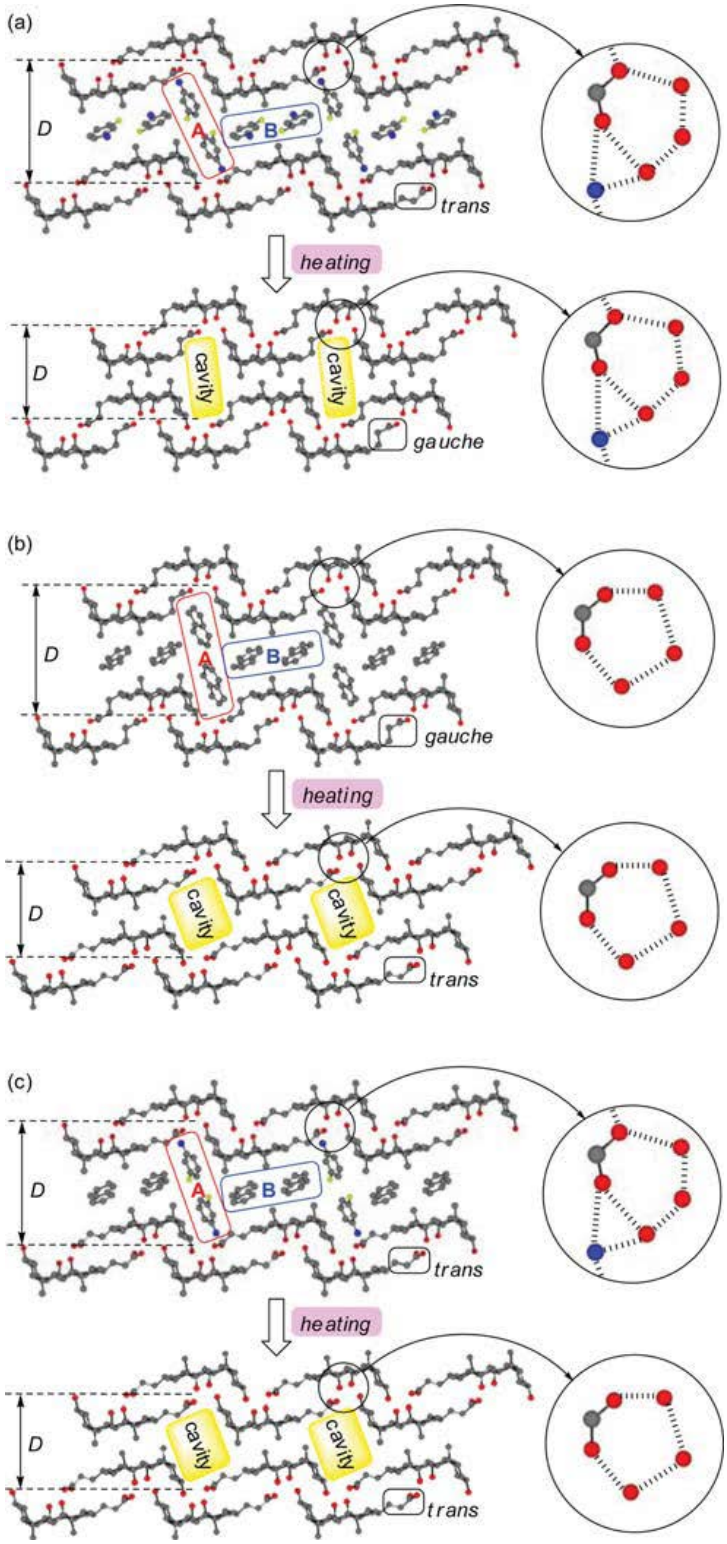

Figure 1-3. Sandwich-type crystal structures with hydrogen bond networks and structural changes of inclusion crystals by heating; (a) fromCA ·G1 to [CA·G1]Int, (b) from CA·G2 to [CA·G2]Int, and (c) from CA·(G1·G2) to [CA·(G1·G2)]Int. Gray, red, blue, light green atoms denote carbon, oxygen, nitrogen, and fluorine atoms, respectively.

1.2.2 Guest selectivity in recrystallization process

Commercially available CA was recrystallized from an equimolar mixture of **G1** and **G2**. The precipitates were similar plate crystals in appearance and had absorption bands of both guests in their IR spectra. This observation indicates formation of a ternary crystal, termed as CA·(**G1**·**G2**) hereafter, which displayed a 47:53 molar ratio of **G1** to **G2** by gas chromatography (GC), indicating no specific guest selectivity in this recrystallization system. Further thermogravimetric (TG) analyses of CA·(**G1**·**G2**) were performed. As shown in Figure 1-4a, the guest molecules were completely released up to 120 °C, and the total weight loss amounted to 36.9 %. This value is well consistent with the calculated value of 35.8 %, which is derived from a ternary inclusion crystal with a 1:2 host:guest molar ratio. Considering the GC data mentioned above, the calculated molar ratio of CA:**G1**:**G2** is 1:0.94:1.06. These results suggest that CA·(**G1**·**G2**) has a sandwich-type structure as in the cases of CA·**G1** and CA·**G2**.

In order to reveal a crystal structure of CA·(**G1**·**G2**), its X-ray powder diffraction (XRD) pattern was compared with those of CA·**G1** and CA·**G2**. It can be seen from Figure 1-5a that the XRD pattern of CA·(**G1**·**G2**) is not a mixed pattern of CA·**G1** and CA·**G2**. This suggests that the two guest molecules are included in the identical cavity of the single crystal of CA·(**G1**·**G2**), and the bulk crystal consists of homogeneous such single crystals, rather than a mixture of two distinct crystals of CA·**G1** and CA·**G2**. The main peaks of CA·(**G1**·**G2**) are similar to those of CA·**G1**, suggesting that CA·(**G1**·**G2**) has a sandwich-type structure where CA involves a side chain with a trans-type conformation.

The structural similarity between CA·(**G1**·**G2**) and CA·**G1** is supported by their IR spectra, which are interpreted on the basis of intermolecular hydrogen bond networks among host and guest molecules. As shown in Figure 1-3, both CA·**G1** and CA·**G2** have a common cyclic hydrogen bond network with a sequence of --- OH(C7) --- OH(C3) --- OH(C12) --- O=C-OH(C24) ---, consisting of four different host molecules. It is noteworthy that CA·**G1** has the site A with an additional host-guest hydrogen bond, where an amino group of the guest molecule is connected to the cyclic network. This provides a decisive difference between IR spectra of CA·**G1** and CA·**G2**, as shown in Figure 1-6a. CA·**G1** has three peaks at 3503, 3490, and 3387 cm^{-1} corresponding to O-H and/or N-H stretching band, while CA·**G2** has a peak at 3493 cm^{-1} with a shoulder around 3400 cm^{-1}. Furthermore, peaks characteristic to C=O stretching bands are given at 1687 and 1706 cm^{-1} for CA·**G1** and CA·**G2**, respectively. CA·(**G1**·**G2**) has similar peaks to CA·**G1**: three peaks at 3504, 3480, and 3389 cm^{-1} corresponding to O-H and/or N-H stretching as well as a peak at 1691 cm^{-1} corresponding to C=O stretching. These data indicate that CA·(**G1**·**G2**) and CA·**G1** have similar host-guest hydrogen bond networks.

The CA·(**G1**·**G2**) crystal contains an equal amount of **G1** and **G2** (47:53), and the host-guest hydrogen bond is apparently observed between CA and **G1**. This fact implies that **G1** and **G2** in CA·(**G1**·**G2**) are preferentially caught at the site A and B, respectively, in the 2-D cavity. In order to confirm the site affinity, X-ray crystallography for a single-crystal prepared from an equimolar mixture of **G1** and **G2** was performed. Figure 1-3c shows the crystal structure, which is a sandwich-type structure with a trans-type conformation of CA molecule. The guest molecules of **G1** and **G2** are found in the site A and B, respectively, and a host-guest hydrogen bond is observed between CA and **G1**. Namely, **G1** molecules in the site B of CA·**G1** are replaced by **G2** molecules. This result supports the idea that each guest molecule fits the corresponding site in size and shape with the host-guest interaction. The site affinity for each guest leads to a low selectivity in this recrystallization process.

1.2.3 Guest selectivity in guest-release process

TG analysis of the ternary inclusion crystal of CA·(**G1**·**G2**) revealed that the guest molecules are released in two different temperature ranges, as shown in Figure 1-4a. The first weight-loss of 27.4 % was observed at the range of 50-100 °C; the second one of 9.5 % at 100-120 °C. A similar TG curve was observed in the CA·**G2** crystal; three quarters of the initial weight were lost at the first range, and the rest at the second range.[15] In this case, the first weight-loss corresponds to a change in the host:guest molar ratio from 1:2 to 2:1, and the second one corresponds to a release to the guest-free crystal. Concerning the CA·**G1** crystal, however, each half of the weight was lost at each range, indicating a change in the host:guest ratio from 1:2 to 1:1 at the first range. In this way, the

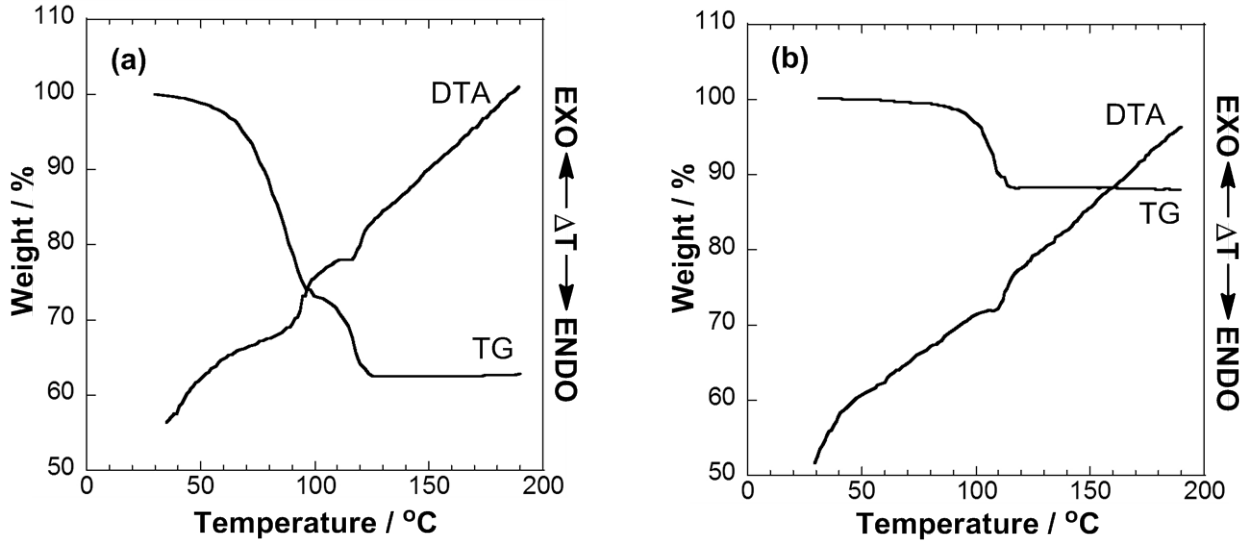

Figure 1-4. TG-DTA diagrams of (a) the original CA·(**G1**·**G2**), and (b) CA·(**G1**·**G2**) after heat treatment at 90 °C for 10 minutes.

CA·(**G1**·**G2**) crystal shows similar guest-release behavior to CA·**G2**, though they have the different crystal structure with a hydrogen bond network.

The fact that the release of guest compounds proceeds in the two ranges implies the formation of an intermediate crystal after the first range. We reported that the intermediate crystals of CA·**G1** and CA·**G2**, termed as $[CA\cdot\mathbf{G1}]_{Int}$ and $[CA\cdot\mathbf{G2}]_{Int}$, respectively, hereafter, are obtained from their sandwich-type original crystals by an adequate heat treatment, i.e. heating at a temperature of the first range.[15] Thus, a similar heat treatment was applied to CA·(**G1**·**G2**); the ternary crystal was heated at 90 °C for 10 minutes. Figure 1-4b shows the TG-DTA diagram of the CA·(**G1**·**G2**) crystal after the treatment. The total weight-loss of 12.6 % at 90-120 °C corresponds to the second weight-loss of the original crystal, indicating the formation of the intermediate crystal of CA·(**G1**·**G2**), termed as $[CA\cdot(\mathbf{G1}\cdot\mathbf{G2})]_{Int}$ hereafter. The GC results revealed that the intermediate crystal includes **G1** and **G2** at the molar ratio of 60:40, which is significantly different from the molar ratio in the original crystal of 47:53. The reason for the difference will be discussed later. The result of TG-DTA indicates that the intermediate crystal has a 2:1 host:guest ratio, i.e. the molar ratio of CA:**G1**:**G2** is 1:0.30:0.20. The inference is confirmed by the agreement between the calculated weight-loss of 12.3 %, which is based on the GC result, and the observed value.

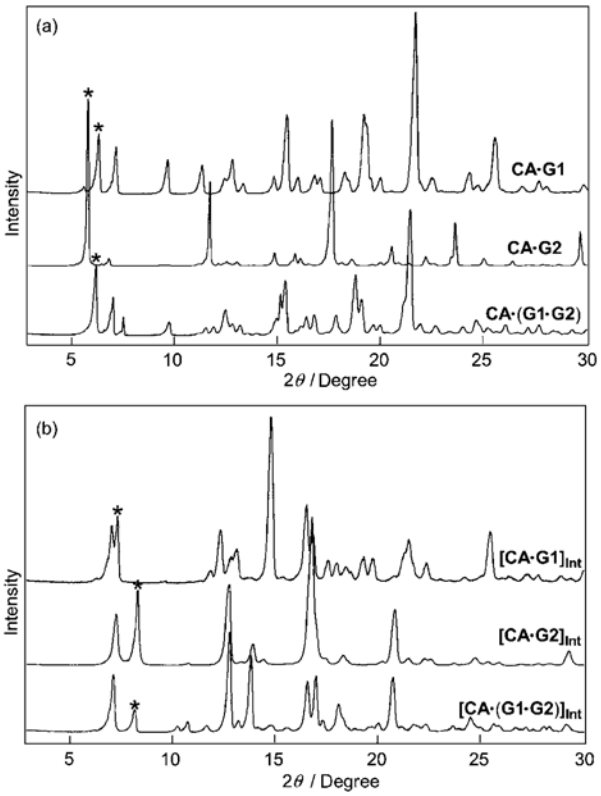

Figure 1-5. XRD patterns of (a) original and (b) intermediate crystals. Peaks corresponding to interlayer distances (*D*) are marked by asterisk.

In order to investigate the crystal structure of $[CA\cdot(\mathbf{G1}\cdot\mathbf{G2})]_{Int}$, we measured the XRD pattern, as shown in Figure 1-5b. This pattern is completely different from those of the original crystal before the heat treatment (see Figure 1-5a) and of the guest-free crystal, indicating the structure changes by the heat treatment. Compared with the XRD patterns of $[CA\cdot\mathbf{G1}]_{Int}$ and $[CA\cdot\mathbf{G2}]_{Int}$, $[CA\cdot(\mathbf{G1}\cdot\mathbf{G2})]_{Int}$ more resembles $[CA\cdot\mathbf{G2}]_{Int}$.

The structural similarity between $[CA\cdot(\mathbf{G1}\cdot\mathbf{G2})]_{Int}$ and $[CA\cdot\mathbf{G2}]_{Int}$ was also confirmed by their IR spectra, as shown in Figure 1-6b. The crystal of $[CA\cdot\mathbf{G1}]_{Int}$ displays two peaks at 3482 and 3391 cm^{-1} corresponding to O-H and/or N-H stretching band. On the other hand, $[CA\cdot\mathbf{G2}]_{Int}$ and $[CA\cdot(\mathbf{G1}\cdot\mathbf{G2})]_{Int}$ have a broad peak around 3400 cm^{-1}. The difference is attributable to the hydrogen

bond networks: [CA·**G1**]$_{Int}$ has a host-host cyclic network with an additional host-guest hydrogen bond as in the case of CA·aniline,[15,16] while [CA·**G2**]$_{Int}$ and [CA·(**G1**·**G2**)]$_{Int}$ have only a host-host network (see Figure 1-3).

The crystal of [CA·**G2**]$_{Int}$ is known to have similar structure to one of the polymorphic inclusion crystals of CA:*o*-xylene (Form II) obtained by recrystallization; the crystal has a bilayer-type structure with the 1-D cavity, in which the guest molecule is included at a 2:1 host:guest molar ratio.[21] In this crystal, there are no specific interactions between the host and guest, and the host layers are maintained by a host-host cyclic hydrogen bond network. Thus, a similar structure is formed in [CA·(**G1**·**G2**)]$_{Int}$.

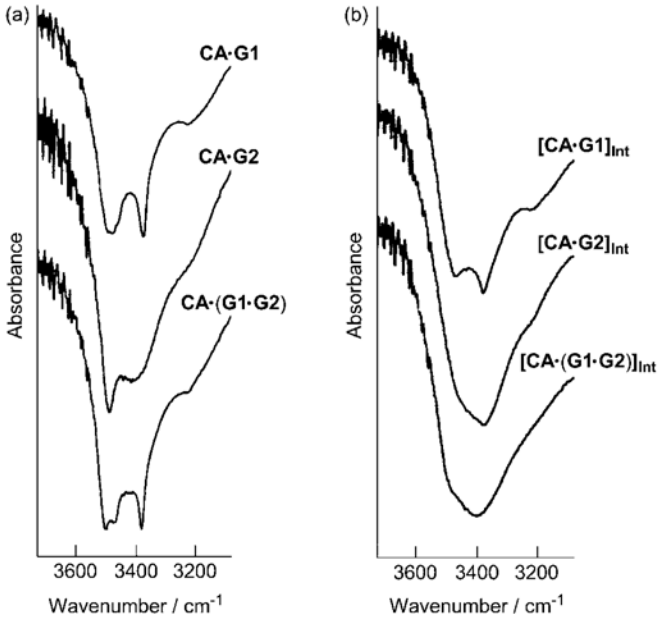

Figure 1-6. FT-IR spectra of (a) original and (b) intermediate crystals.

Figure 1-3c shows the structural change from CA·(**G1**·**G2**) to [CA·(**G1**·**G2**)]$_{Int}$ by the heat treatment; the original crystal having the sandwich-type structure like CA·**G1** converts to the bilayer structure like [CA·**G2**]$_{Int}$. As mentioned above, the two guests, **G1** and **G2,** are included preferentially in the respective site of A and B in the 2-D cavity in the original crystal. Since **G1** connects with CA through the host-guest hydrogen bond at the site A, **G1** is more tolerant of heating than **G2** and tends to retain in the 1-D cavity. In addition, since the position of site A in the 2-D cavity in the original crystal corresponds to that of the 1-D cavity in the intermediate crystal, guest compounds in site A seem to be retained in the 1-D cavity after the structural change. As a result, the molar ratio of **G1** in the intermediate crystal is higher than that in the original one.

The thermal guest-release is accompanied by the structural change as deintercalation; the host layers move perpendicular to the layer direction. The interlayer distances *D* (see Figure 1-3) correspond to the (100) plane for the crystal of CA·**G1** and CA·(**G1**·**G2**), the (001) plane for CA·**G2**, and the (10-1) plane for the bilayer-type crystals of CA.[15,17] In Figure 1-5, the XRD diffraction peaks corresponding to *D* are marked. The interlayer distances *D* of CA·(**G1**·**G2**) and [CA·(**G1**·**G2**)]$_{Int}$ are 14.3 Å based on the single-crystal X-ray crystallography data and 10.7 Å based on XRD diffraction data, respectively. Therefore, the host layers are estimated to move 3.6 Å, which is consistent with the thickness of the included aromatic guest molecules in the original crystal.

1.2.4 Guest selectivity at various molar ratios of G1 and G2

Ternary inclusion crystals of CA with **G1** and **G2** were obtained from mixed guest solutions having various molar ratios of the two guests from 1:9 to 9:1. As in the case of CA·(**G1**·**G2**) crystal obtained from an equimolar guest mixture, their intermediate crystals were found to be obtained by appropriately heating these crystals. Figure 1-7 shows the molar ratio of **G1** in the crystals, $[\mathbf{G1}]_{cry}/([\mathbf{G1}]_{cry}+[\mathbf{G2}]_{cry})$, against that in the residual solution, $[\mathbf{G1}]_{sol}/([\mathbf{G1}]_{sol}+[\mathbf{G2}]_{sol})$, in the original crystal (○) and in the intermediate crystal (●). The subscripts cry and sol denote the crystal and solution phases, respectively.

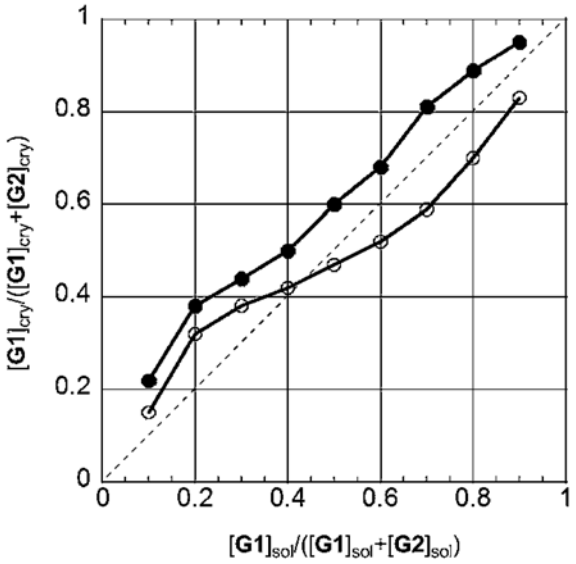

Figure 1-7. Relationship between molar ratio of two guests in crystal and in residual solution in cases of original crystals (○) and intermediate crystals (●).

As for the original crystals before the heat treatment, the ratio of **G1** in the crystal locates above the diagonal line when the ratio in the solution is less than 0.45. On the other hand, the guest preference reverses when the ratio in the solution is more than 0.45. This tendency is relevant to the each guest's preference for the sites in the 2-D cavity as mentioned above: the site A is preferable for **G1** while the site B is for **G2**. When the ratio in the crystal is less than 0.5, **G1** is preferably included in the site A over **G2** with resulting higher values in the ratio of **G1**. After the site A is occupied mostly by **G1**, i.e. the ratio in the solution is more than 0.5, competitive inclusion occurs for the site B between **G1** and **G2.** In this context, lower affinity of the site B for **G1** results in a decrease in the ratio of **G1** in the crystal.

The appropriate heat treatment of the original crystals leads to the intermediate crystals, in which the ratio of **G1** invariably exceeds that in the original ones. In other words, **G1** is preferably retained in the thermal guest-release process irrespective of the guest ratios included, and the host-guest hydrogen bond at site A is constantly effective for the guest retention. In addition, the difference in the ratio between in the original and intermediate crystals increases as the ratio in the original crystal increases over 0.5. Since the site A is occupied mostly by **G1** for higher ratios, the selective retention of **G1** due to the host-guest hydrogen bond will lead to a larger difference in the ratio.

1.3 Conclusion

We demonstrated the selective guest retention in the thermal guest-release process of the CA inclusion crystals, where the structural change of the crystals from the sandwich-type to the bilayer-type occur. By comparing the two structures of original and intermediate crystals, the selectivity was found to be attributable to the host-guest hydrogen bond at one of the two nonequivalent sites in the 2-D cavity. Unlike conventional separation in the guest-inclusion process, the present selectivity develops in the thermal guest-release process from preformed ternary inclusion compounds. We believe that this novel procedure can be applied not only to other CA inclusion compounds but also to many crystalline inclusion compounds.

1.4 Experimental Section

1.4.1 Reagents

CA and guest compounds were purchased from Wako Co. and Tokyo Kasei Co., respectively. They were of the commercially available purest grades, and were used without further purification.

1.4.2 Preparation of Inclusion Crystals

Guest mixtures were prepared by mixing two guest compounds at a predetermined molar ratio. CA (100 mg) was dissolved in the guest mixture (0.5~2 mL) by heating in a 13 ml vial, then the solution was allowed to settle overnight at 20 °C to yield crystals. Inclusion crystals thus obtained were filtered out and settled on a filter paper for some time to remove the adhering guests on the surface.

1.4.3 General Procedure

The amounts of the guests included in the crystals were determined by GC using a Shimadzu GC-14A instrument after dissolving the crystals in methanol. TG was performed on a MAC Science TG-DTA 2010S system; ca. 10 mg of the inclusion crystals was heated from 40 to 230 °C at a rate of 5 °C min^{-1}. IR spectroscopy was carried out by using JASCO FT/IR-5M. The structural types of the CA inclusion crystals were determined by XRD using a Rigaku RINT-1100 instrument.

1.4.4 Crystal Structure Determinations

Measurement was made on a Rigaku RAXIS RAPID diffractometer with an imaging plate area detector with graphite monochromated Cu-Kα radiation (λ = 1.54187 Å). Direct methods (SIR-2004) were used for the structure solution.[18] All calculations were performed with the observed reflections [$I > 2\sigma(I)$] by the program CrystalStructure crystallographic software packages[19] except for refinement, which was performed using SHELXL-97.[20] All non-hydrogen atoms were refined with anisotropic displacement parameters and hydrogen atoms were placed in idealized positions and refined as rigid atoms with the relative isotropic displacement parameters. Crystal data for CA·(**G1**·**G2**): $C_{39}H_{54}FNO_5$, Mw = 635.86 *a* = 14.8259(5) Å, *b* = 7.8389(2) Å, *c* = 16.1032(5) Å, β = 108.6510(16)°, *V* = 1773.21(9) Å^3, *T* = 273 K, monoclinic, space group $P2_1$ (No.4), *Z* = 2, μ(CuKa) = 0.6477 mm^{-1}, *Dc* = 1.191 g cm^{-3}, 20060 collected, 5641 unique (R_{int} = 0.060), reflections, the final *R*1 [$I < 2\sigma(I)$] and w*R*2 (all data) were 0.0623 and 0.1922, respectively.

1.5 References

[1] (a) *Inclusion Compound*, ed. J. L. Atwood, J. E. D. Davies, and D. D. MacNicol, Academic Press, London, 1984. vols. 1-5; (b) *Comprehensive Supramolecular Chemistry*, ed. J. -M. Lehn, J. L. Atwood, J. E. D. Davies, D. D. MacNicol, and F. Vögtle, Pergamon, Oxford, 1996; (c) *The Crystal as a Supramolecualr Entity*, ed. G. R. Desiraju, John Wiley and Sons, Chichester, 1996; (d) *Encyclopedia of Supramolecular Chemistry*, ed. J. L. Atwood and J. W. Steed, Marcel Dekker, New York, 2004; (e) F. H. Herbstein, *Crystalline Molecular Complexes and Compounds*, Oxford University Press, Oxford, 2005, vols. 1,2.

[2] K. D. M. Harris and M. D. Hollingsworth, *Comprehensive Supramolecular Chemistry: Solid State Supramolecular Chemistry*, ed. D. D. MacNicol, F. Toda, and R. Bishop, Pergamon, Oxford, 1996, vol. 6, pp. 177-237.

[3] *Perspective in Supramolecular Chemistry: Separations and Reactions in Organic Supramolecular Chemistry*, ed. F. Toda and R. Bishop, John Wiley & Sons, Chichester, 2004.

[4] L. R. Nassimbeni, *Acc. Chem. Res.*, 2003, **36**, 631-637.

[5] B. T. Ibragimov, *CrystEngComm*, 2007, **9**, 111-118.

[6] S. A. Bourne, K. C. Corin, L. R. Nassimbeni, and F. Toda, *Cryst. Growth Des.*, 2005, **5**, 379-382.

[7] T. le Roex, L. R. Nassimbeni, and E. Weber, *New J. Chem.*, 2008, **32**, 856-863.

[8] A. Jacobs, L. R. Nassimbeni, K. L. Nohako, H. Su, and J. H. Taljaard, *Cryst. Growth Des*., 2008, **8**, 1301-1305.

[9] K. Tanaka, A. Nakashima, Y. Shimada, and J. L. Scott, *Eur. J. Org. Chem*., 2006, 2423-2428.

[10] O. Bortolini, G. Fantin, and M. Fogagnolo, *Chirality*, 2005, **17**, 121-130.

[11] (a) K. Nakano, K. Aburaya, I. Hisaki, N. Tohnai, and M. Miyata, *Chem. Rec.*, 2009, **9**, 124-135; (b) M. Miyata, N. Tohnai, and I. Hisaki, *Acc. Chem. Res.*, 2007, **40**, 694-702; (c) M. Miyata, N. Tohnai, and I. Hisaki, *Molecules*, 2007, **12**, 1973-2000; (d) I. Hisaki, N. Tohnai, and M. Miyata, *Chirality*, 2008, **20**, 330-336.

[12] K. Nakano, K. Sada, Y. Kurozumi, and M. Miyata, *Chem. Eur. J.*, 2001, **7**, 209-220.

[13] K. Nakano, S. Akita, N. Yoswathananont, K. Sada, and M. Miyata, *J. Inclusion Phenom. Macrocyclic Chem.*, 2004, **48**, 181-184.

[14] N. Yoswathananont, K. Sada, M. Miyata, S. Akita, and K. Nakano, *Org. Biomol. Chem*., 2003, **1**, 210-214.

[15] K. Nakano, K. Sada, K. Nakagawa, K. Aburaya, N. Yoswathananont, N. Tohnai, and M. Miyata, *Chem. Eur. J.*, 2005, **11**, 1725-1733.

[16] M. Shibakami, M. Tamura, and A. Sekiya, *J. Inclusion Phenom.*, 1995, **22**, 299-311.

[17] K. Nakano, E. Mochizuki, N. Yasui, K. Morioka, Y. Yamauchi, N. Kanehisa, Y. Kai, N. Yoswathananont, N. Tohnai, K. Sada, and M. Miyata, *Eur. J. Org. Chem.*, 2003, 2428-2436.

[18] A. Altomare, M. Burla, M. Camalli, G. Cascarano, C. Giacovazzo, A. Guagliardi, A. Moliterni, G. Polidori, R. Spagna, *J. Appl. Crystallogr.*, **1999**, *32*, 115−119.

[19] *CrystalStructure 3.8*: Crystal Structure Analysis Package, Rigaku and Rigaku Americas (2000-2007). 9009 New Trails Dr. The Woodlands TX 77381 USA.

[20] G. M. Sheldrick, *Acta Crystallogr., Sect. A*, **2008**, *64*, 112−122.

Chapter 2

Inclusion Crystals of 3α,7α,12α,24-tetrahydroxycholane with Haloaromatic Compounds: Pitches and Stability of Herringbone Assemblies in Channels

Abstract

Design of inclusion crystals requires a comprehension of both molecular assembly modes and recognitions. This chapter describes novel inclusion crystals of 3α,7α,12α,24-tetrahydroxycholane (CAL). Formation and recognition mechanisms are considered through its hierarchical structures of the crystals. Cholic acid (CA) displays a crystal structure change from herringbone-type to bilayer-type when guest molecules are included. In contrast, CAL has similar stacked bilayers in both guest-free and inclusion crystals. The included guest molecules are accommodated on lipophilic sides of the bilayers, indicating that the inclusion induces an increase of distances between the bilayers. Pitches and stability of herringbone assemblies in channels play a big role in the formation of inclusion crystals.

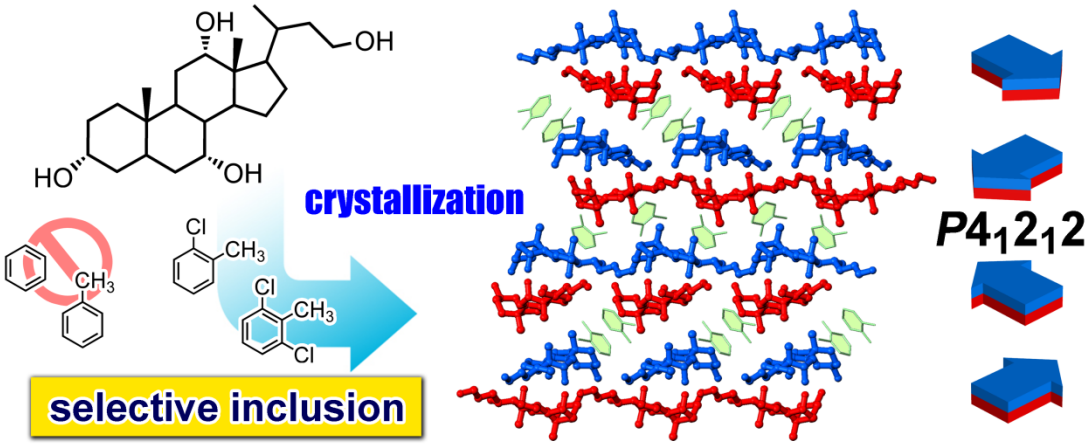

2.1 Introduction

The prediction of molecular assembly modes in organic crystals still remains unclear due to their diversity.[1] Particularly, inclusion crystals exhibit guest-dependent assembly modes, and a slight change of host and guest components brings about unexpected modes. Such diversity has fascinated us for a long time to yield comprehensive researches with many combinations of host and guest components.[2] For the past two decades, we have studied on inclusion crystals of steroidal cholic acid (CA) and its derivatives (Scheme 2-1).[3] During such a long research, it was mysterious that 3α,7α,12α,24-tetrahydroxycholane (CAL) exhibits no inclusion ability. In fact, there are no reports about the ability since the first separation of CAL from dioxane-trichloroacetic acid in 1969,[4] and our previous report was also concerned with guest-free crystal in 1994.[5] However, our latest study has induced a view that CAL has its characteristic inclusion ability. Herein, we disclose inclusion crystals of CAL with aromatic guest molecules. Moreover, comparison between inclusion crystals of CA and CAL give us valuable information about the stability of one-dimensional (1-D) assembly modes of guest components in channels.

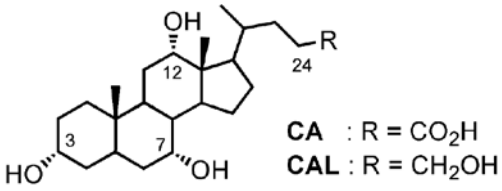

Scheme 2-1. Structures of CA and CAL.

2.2 Results and Discussion

2.2.1 Self-assembly of CAL

CAL was prepared from commercially available CA according to the literature.[6] Its inclusion ability was screened with benzene and its derivatives. CAL was recrystallized from alcoholic solutions involving guest candidates. The resulting crystals were characterized by FTIR and ^{1}H-NMR spectroscopy, X-ray diffraction as well as thermalgravimetric analyses. The following guest selectivities were observed. CA included all of benzene, mono-, di-, and tri-substituted benzenes employed. In contrast, CAL did not include benzene, toluene, 1,3- and 1,4-disubstituted benzenes, while include 1,2-di-, 1,2,3-tri-, and 1,2,6-trisubstituded benzenes. Table 2-1 shows a partial result of the screening and Table 2-2 shows the inclusion behavior of CAL toward aromatic guest molecules. We successfully obtained inclusion crystals of CAL with *o*-chlorotoluene **(1)** and 2,6-dichlorotoluene **(2)** (abriv. CAL·**1** and CAL·**2**, respectively). These results indicate that CAL exhibits remarkable guest selectivity in size and shape. It is very interesting that CAL did not include the molecules with small molecular volume.

In order to acquire an insight into this selectivity, inclusion crystals CAL·**1** and CAL·**2** were subjected to X-ray diffraction analysis, revealing that both of them exhibit the same crystalline system with the space group of $P4_12_12$,[7] which are also the same with that of the guest-free crystal of CAL (GF-CAL) (*vide infra*).

Table 2-1. Selected inclusion abilities of CA and CAL.

guest	volume ($Å^3$)	host:guest ratio*	
		CA	CAL
benzene	83.8	1:1	GF
toluene	100.6	1:1	GF
o-xylene	114.2	2:1	GF
m-xylene	117.4	1:1	GF
p-xylene	117.4	1:1	GF
o-chlorotoluene (**1**)	114.1	1:2	1:1
2,6-dichlorotoluene (**2**)	127.4	2:1	1:1

*The ratio was determined by single-crystal X-ray diffraction.

Table 2-2. Inclusion behavior of CAL toward aromatic guest molecules.[a]

Guest	volume (Å)	host:guest ratio	Guest	volume (Å)	host:guest ratio
benzene	83.8	GF[b]	*o*-xylene	117.2	GF[b]
			m-xylene	117.2	GF[b]
monosubstituted			*p*-xylene	117.2	GF[b]
fluorobenzene	89.6	GF[b]	*o*-bromotoluene	118.5	1:1
chlorobenzene	98.4	GF[b]	*o*-dibromobenzene	119.5	1:1
toluene	100.6	GF[b]	*m*-dibromobenzene	119.8	GF[b]
bromobenzene	101.8	GF[b]	*p*-dibromobenzene	119.8	GF[b]
iodobenzene	109.5	GF[b]	*o*-chloroiodobenzene	121.0	1:1
			o-iodotoluene	124.3	1:1
disubstituted			*o*-bromoiodobenzene	125.3	1:1
o-difluorobenzene	93.7	GF[b]			
o-fluorotoluene	105.5	GF[b]	**trisubstituted**		
o-dichlorobenzene	110.9	1:1	2,3-dichlorotoluene[b]	127.9	1:1
m-dichlorobenzene	110.8	GF[b]	2,4-dichlorotoluene	127.7	GF[b]
o-chlorotoluene**(1)**[b]	114.1	1:1	2,5-dichlorotoluene	127.7	GF[b]
m-chlorotoluene	114.2	GF[b]	2,6-dichlorotoluene**(2)**[b]	127.4	1:1
p-chlorotoluene	114.2	GF[b]	1-bromo-2,3-dimethylbenzene[b]	135.0	1:1

a. Guest inclusion was confirmed by powder X-ray diffraction, TG, and ^{1}H NMR analyses. *b*. Guest inclusion was confirmed by X-ray crystallographic analysis on single crystals. b. GF denotes the guest-free crystal.

Table 2-3. Crystal data of CAL inclusion crystals.

	CAL·**1**	CAL·**2**	CAL·(2,3-dichlirotoluene)
Formula	$C_{24}H_{42}O_4$·C_7H_7Cl	$C_{24}H_{42}O_4$·$C_7H_6Cl_2$	$C_{24}H_{42}O_4$·$C_7H_6Cl_2$
Fw	521.18	555.62	555.62
crystal system	tetragonal	tetragonal	tetragonal
space group	$P4_12_12$	$P4_12_12$	$P4_12_12$
a [Å]	11.7906(4)	11.8229(4)	11.8267(4)
b [Å]	11.7906(4)	11.8229(4)	11.8267(4)
c [Å]	41.8864(16)	42.2058(15)	42.3384(8)
α [°]	90	90	90
β [°]	90	90	90
γ [°]	90	90	90
V [Å]	5823.0(4)	5899.6(3)	5921.9(2)
Z	8	8	8
Dc[g cm^{-3}]	1.189	1.251	1.246
No. collected	44585	56574	46165
No. unique	5321	5403	5423
R_1/Rw	0.135 / 0.367	0.137 / 0.407	0.101 / 0.295
T [K]	123	123	123
CCDC	908618	908619	908620

[a] High R values are attributed to disorder of guest molecules.

Table 2-4. Preliminary crystal data of CAL inclusion crystal with 1-bromo-2,3-dimethylbenzene[a]

Formula	$C_{24}H_{42}O_4 \cdot C_8H_9Br$
Fw	579.66
crystal system	tetragonal
space group	$P4_12_12$
a [Å]	11.8527(4)
b [Å]	11.8527(4)
c [Å]	42.5741(8)
α [°]	90
β [°]	90
γ [°]	90
V [Å]	5981.13(19)
Z	8
Dc[g cm^{-3}]	1.287
No. collected	40938
No. unique	5471
R_1/Rw	0.208 / 0.505
T [K]	123

[a] High R values are attributed to disorder of guest molecules.

Figure 2-1 shows a crystal structure of CAL·**1**. The molecules form a dimer with C_2 symmetry through self-complementary hydrogen bonds involving the hydroxyl groups (O12···O7a···O7···O12a and O3···O3a). The dimer aligns to form a bilayer, which subsequently stacks with right-handed 4_1-helical symmetry along the *c* axis to give the crystal structure. In the crystal, 2_1-helical symmetric 1-D channels are formed to accommodate guest molecules.

Figure 2-2 shows the molecular arrangements of the bilayers relating to the hydrophilic and hydrophobic interfaces, respectively. The former is based on sheet-like structure composed of the dimers hydrogen-bonded through their side-chains (O12d···O24b···O3···O3a···O24c···O12e) (Figure 2-2b). The latter is based on an arrangement with 2_1-helical symmetry through van der Waals contacts (Figure 2-2c). The periodic pitch of the CAL helix is synchronized with that of **1** (11.8 Å) (Figure 2-2c).

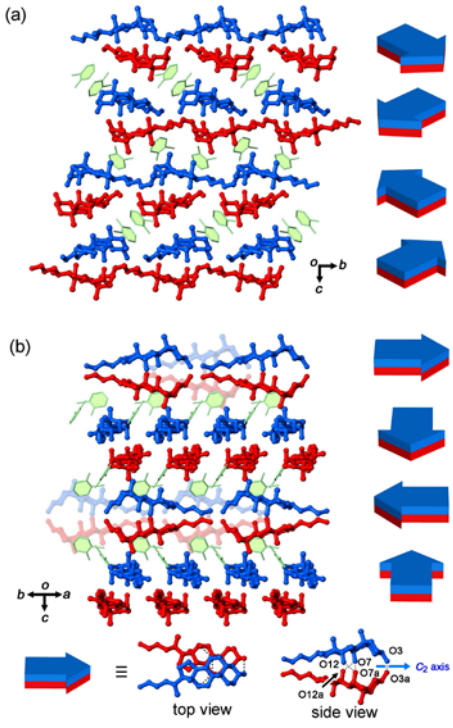

Figure 2-1. Packing diagrams of CAL·**1** viewed down from (a) the *a* axis and (b) the diagonal axis of the *ab* plane, along with schematic representation of 4_1 helical arrangements of CAL molecules.

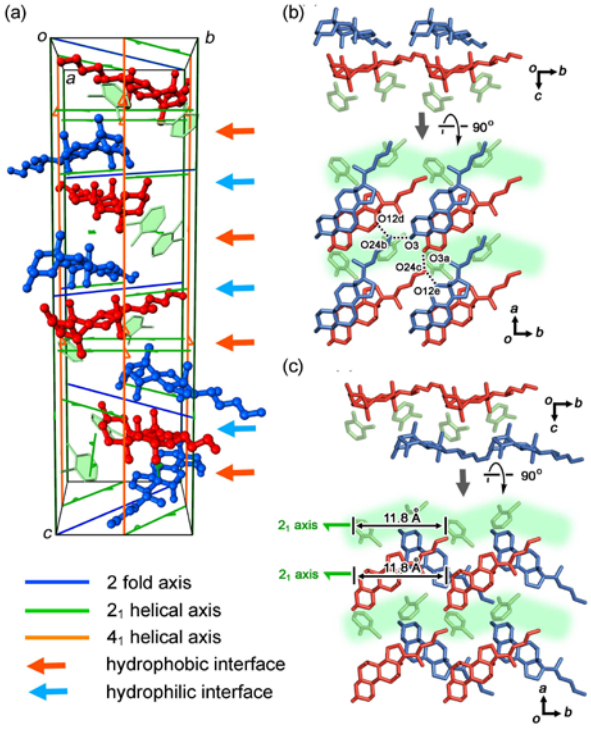

Figure 2-2. (a) The unit cell of CAL·**1** with the symmetry axes. (b) Molecular assembly of CAL relating with the hydrophilic interface. (c) Molecular assembly of CAL relating with the hydrophobic interface.

2.2.2 Molecular Recognitions of CAL

For structural comparison of GF-CAL and CAL·**1**, their packing diagrams are shown in Figure 2-3 together with hierarchical formation of the sheet motif. Interestingly, CAL forms almost identical sheet motifs laid on the *ab* plane and the bilayer structures in both crystals. This is greatly different from the case of CA.[8] However, the guest inclusion of CAL·**1** provided an expansion of the *c* axis (i.e. bilayer distances) from 8.0 Å to 10.5 Å, although significant changes were not observed for both the *a* and *b* axes (11.8 Å). In Figure 2-3c, inclusion channels of CAL·**1** are visualized with a green surface, showing that the channels have 2_1 symmetric zigzag shape with a dimension of 9.5 Å × 4.7 Å and a periodic distance (pitch) of 11.8 Å, and are located along the *a* and *b* axes perpendicularly.

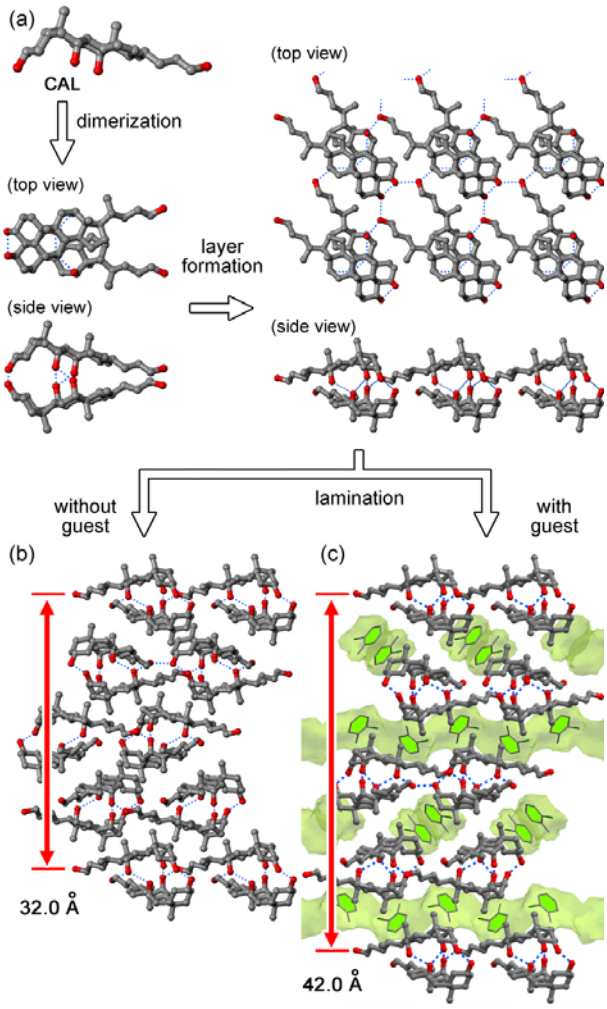

Figure 2-3. Comparison for the periodic distance of stacked bilayers of CAL. (a) Hierarchical interpretation for formation of sheet motifs of CAL via dimerization. (b) A packing diagram of GF-CAL with periodic distance of 32.0 Å. (c) A packing diagram of inclusion crystal CAL·**1** with periodic distance of 42.0 Å. Surfaces of the guest-included channels are colored with green.

In connection with the guest selectivity of CAL, differences in pitches of the channels between of CA and CAL led us to the idea that the intrinsic pitches of inclusion channels provided by host molecules are closely related to the guest selectivity of hosts. Figure 2-4 shows the crystallographically-determined alignments of guest molecules in the CA and CAL channels,[9] exhibiting the following three significant features. Firstly, benzene and toluene molecules form 2_1 helices with a pitch of about 7.9 Å in CA channels (Figure 2-4a),[10-11] while these are not included into CAL channels. This result indicates that the 2_1-helical arrangements of benzene and toluene are not stabilized in the CAL channel because of its pitch longer than that of CA (7.9 Å). In fact, there are no reports that these guest molecules are included in a host framework with such long pitches. Secondly, **1** forms 2_1 helices with a pitch of 7.9 Å and 11.8 Å in CA·**1** (Figure 2-4b) and CAL·**1** (Figure 2-4c) crystals, respectively. It is noteworthy that CA·**1** exhibits the former guest alignment only with a 1:2 host:guest. This crystal looses the

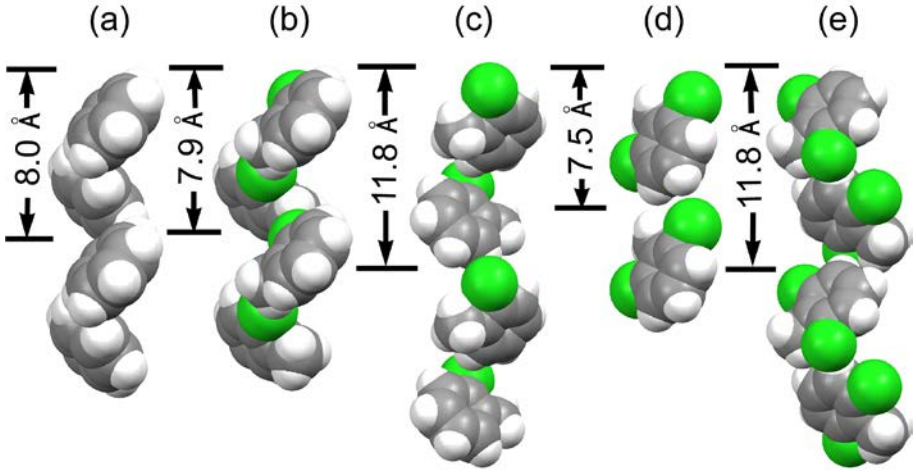

Figure 2-4. 2_1 Helical 1-D arrangements of guest molecules in channels and their periodic lengths (a) CA·benzene, (b) CA·**1** (c) CAL·**1**, (d) CA·**2**, and (e) CAL·**2**.

guest under heating to yield the crystal with a 2:1 host:guest ratio,[12] indicating relatively less stability of CAL·**1**. Thirdly, molecules of **2** forms a translational 1D column in CA·**2** with a 2:1 host:guest ratio, while a 2_1 helical column in CAL·**2** with 1:1 host:guest ratio. This difference in the inclusion ratio indicates that the pitch of the channel in CA·**2** is too short to make a 2_1-helical assembly, but is suitable to make a parallel 1-D assembly. On the other hand, the pitch in CAL·**2** is suitable to make a 2_1-helical assembly. These results suggest that a relation between the guest molecules and the helical pitches play an important role for stabilization of herringbone assemblies with 2_1 symmetry in the channels. Furthermore, the fact that CAL includes no molecules of *o*-xylene but those of **1**, despite of their similar size and shape, indicates that halogen interactions also contribute to stabilization of the inclusion crystals, as observed in a number of crystalline systems.[13,14]

2.2.3 Hydrogen bonding

Furthermore, we believe that hydrogen bonding is a key point for the formation of inclusion crystals. To compare with CA, one hydrogen bonding site of CAL on 24th hydroxyl group was decreased. It is known that the distance for forming hydrogen bonding is about 3.0Å. However, the distance between 12th and 24th hydroxyl group of CAL is 4.2Å. For this reason, it was considered that formation of hydrogen bonding here is impossible. Instead of cyclic hydrogen bonding, CAL formed hydrogen bonding in helical fashion. Consequently, hydrogen bonding pattern makes a great impact for molecular assembly and recognition.

2.3 Conclusion

Due to a small change of molecular structure, both molecular assemblies and recognition are all different. Furthermore, from the investigation of molecular assembly, formation of supramolecular chirality is expected to be clarified through such investigation. We have demonstrated that various slight variations of host and guest molecules in size, shape and polarity induce drastic changes in arrangements and stability of inclusion crystals. Further detailed investigations on the variations are expected to deliver valuable information on hierarchical structures as well as supramolecular chirality of host-guest assemblies in the crystalline state.

2.4 Experimental Section

2.4.1 General Methods

All chemicals and solvents were commercially available and used without purification.

2.4.2 Synthesis of CAL

・Methyl esterification of CA

Commercially available CA 5g (1.22x10mmol) was dissolved in 60ml methanol, 3ml hydrogen chloride was added dropwise. The mixture was then stirred at 70^{o}C for 2 hours. After completion of reaction, the mixture was cooled down to room temperature, diluted with distilled water. Ethyl acetate was used to extract products. The separated organic phase was washed thoroughly with saturated sodium hydrocarbonate aqueous solution. The separated organic phase was dried over anhydrous sodium sulfate. Finally, after removing of solvent, 3.91g products were obtained.

・Reduction reaction

1g (2.37mmol) CA-Ester synthesized in last step was dissolved in 30 ml THF. The solution was added dropwise in 20 min into a prepared solution in which 0.27g (7.11mmol) $LiAlH_4$ was dissolved in 40 ml THF. The mixture was then stirred at room temperature for 39 hours. After completion of reaction, 200ml methanol and 50ml 10% hydrogen chloride were added. After filtration with Celite, the filtrate was extracted with diethylether. The separated organic phase was washed thoroughly with saturated sodium chloride aqueous solution, dried over anhydrous magnesium sulfate. Removing of solvent via evaporator, dried in vacuum, and recrystallized in methanol. Finally, 0.3g CA-ol was obtained.

2.4.3 Preparation of Single Crystals

The host molecules (CA and CAL) were dissolved in methanol, and then various guest molecules were added to the solution. Slow evaporation of the solvent at room temperature gave single crystals of all the host molecules.

2.4.4 Crystal Structure Determinations

X-ray diffraction data were collected on a Rigaku R-AXIS RAPID diffractometer with a 2D area detector by using graphite-monochromatized $Cu_{K\alpha}$ radiation (λ = 1.54178Å). Direct methods (SIR-2004) were used to solve the structure. All calculations were performed with the observed reflections [$I > 2\sigma(I)$] by using the CrystalStructure crystallographic software package, except for refinement, which was performed using SHELXL-97. All non-hydrogen atoms were refined with anisotropic displacement parameters, and they were placed in idealized positions and refined as rigid atoms with the relative isotropic displacement parameters.

2.5 References

[1] (a) G. R. Desiraju, *Nature Mater.*, **2002**, *1*, 77. (b) J. D. Dunitz, A. Gavezzotti, *Angew. Chem. Int. Ed.*, **2005**, *44*, 1766. (c) J. Bernstein, "*Polymorphism in Molecular Crystals*", Oxford Science Publications, **2002.**

[2] (a) E. Giglio, "*Inclusion Compounds*," edited by J. L. Atwood, J. E. D. Davies, D. D. MacNicol, Academic Press, London, **1984**, Vol.2 (b) D. D. Macnicol, F. Toda, R. Bishop, "*Comprehensive Supramolecular Chemistry*", Pergamon, **1996**, Vol.6. (c) F. H. Herbstein, "*Crystalline Molecular Complexes and Compounds*", Oxford Science Publications, **2005**, Vol.1-2.

[3] (a) M. Miyata, N. Tohnai, I. Hisaki, *Acc. Chem. Res.*, **2007,** *40*, 694. (b) M. Miyata, N. Tohnai, I. Hisaki, *Molecules*, **2007**, *12*, 1973. (c) K. Nakano, K. Aburaya, I. Hisaki, N. Tohnai, M. Miyata, *Chem. Record*, **2009**, 9, 124.

[4] G. A. D. Haslewood, L. Tokes, *Biochem. J.*, **1969**, *114*, 179.

[5] (a) M. Miyata, K. Sada, Y. Yasuda, *Mol. Cryst. Liq. Cryst.*, **1994**, *240*, 183. (b) K.Sada, T. Kondo, Y. Yasuda, M. Miyata, K. Miki, *Chem. Lett.*, **1994**, 727.

[6] (a) X. Zhu, E. Amouzou, S. Mclean, *Can. J. Chem.*, **1987**, *65*, 2447. (b) H. Li, L. X. Wang, *Org. Biomol. Chem.*, **2003**, *1*, 3507.

[7] Crysta data for **CAL·1**: $C_{31}H_{49}ClO_4$, Mw = 521.18, $a = b$ = 11.7906(4) Å, c = 41.8864(16) Å, V = 5823.0(4) Å^3, T = 123 K, *tetragonal*, space group $P4_12_12$ (No. 92), Z = 8, d_{calcd} = 1.198 g/cm^3, 44585 collected, 5321 unique (R_{int} = 0.296) reflections, the final $R1$ and w$R2$ values 0.135 (I > 2.0σ(I)) and 0.367 (all data), respectively. Crysta data for **CAL·2**: $C_{31}H_{48}Cl_2O_4$, Mw = 555.62, $a = b$ = 11.8229(4) Å, c = 42.2058(15) Å, V = 5899.6(3) Å^3, T = 123 K, *tetragonal*, space group $P4_12_12$ (No. 92), Z = 8, d_{calcd} = 1.251 g/cm^3, 56574 collected, 5403 unique (R_{int} = 0.263) reflections, the final $R1$ and w$R2$ values 0.137 (I > 2.0σ(I)) and 0.407 (all data), respectively. CCDCs 908618 and 908619 contains the supplementary crystallographic data for this paper. These data can be obtained free of charge from The Cambridge Crystallographic Data Centre via www.ccdc.cam.ac.uk/data_request/cif.

[8] **CA** exhibits a structural change from herringbone-type for guest-free crystals to bilayer-type for inclusion crystals, see for example: M. Miyata, M. Shibakami, S. Chirachanchai, K. Takemoto, N. Kasai, K. Miki, *Nature*, **1990**, *343*, 446.

[9] Although thermal ellipsoids of guest molecules are extended aniotropically in CAL·2, the molecular arrangement of the guest in the channel is creditable.

[10] K. Nakano, K. Sada, M. Miyata, *Chem. Lett.* **1994**, 137–140.

[11] For supramolecular chirality of 2_1 helical assemblies of benzene, see: (a) A. Tanaka, I. Hisaki, N. Tohnai, M. Miyata, *Chem. Asian J.*, **2007**, *2*, 230. (b) I. Hisaki, T. Sasaki, K. Sakaguchi, W.-T.

Liu, N. Tohnai, M. Miyata, *ChemComm*, **2012**, 48, 2219. (c) I. Hisaki, T. Sasaki, N. Tohnai, M. Miyata, *Chem. Eur. J.*, **2012**, *18*, 10066.

[12] (a) K. Nakano, K. Sada, K. Nakagawa, K. Aburaya, N. Yoswathananont, N. Tohnai, M. Miyata, *Chem. Eur. J.*, **2005**, *11(6)*, 1725. (b) K. Nakano, S. Akita, T. Murai, W. T. Liu, I. Hisaki, N. Tohnai, M. Miyata, *CrystEngComm*, **2010**, *12*, 1461.

[13] (a) *Halogen Bonding: Fundamentals and Applications*, *Structure and Bonding*, edited by P. Metrangolo and G. Resnati, Springer, Berlin, **2007**. (b) P. Metrangolo, H. Neukirch, T. Pilati and G. Resnati, *Acc. Chem. Res.*, **2005**, *38*, 386. (c) E. Parisini, P. Metrangolo, T. Pilati, G. Resnati and G. Terraneo, *Chem. Soc. Rev.*, **2011**, *40*, 2267. (d) J. W. Lauher, F. W. Fowler and N. S. Goroff, *Acc. Chem. Res.*, **2008**, *41*, 1215; (h) K. Merz and V. Vasylyeva, *CrystEngComm*, **2010**, *12*, 3989.

[14] T. Sasaki, I. Hisaki, S. Tsuzuki, N. Tohania, M. Miyata, *CrystEngComm*, **2012**, 14, 5749.

Chapter 3

Right- and Left-handedness of 2_1 Symmetrical Herringbone Assemblies of Benzene

Abstract

A molecular assembly with a two-fold screw axis, a so-called 2_1 helical assembly, is one of the most fundamental and important motifs of organic non-centrosymmetric crystals, since over 70% of crystals registered in the Cambridge Structural Database (CSD) contain 2_1 helical axes. To understand the mechanism of formation of 2_1 helical assemblies is important for the study of dynamic properties of helical assemblies.

A universal method to determine handedness of 2_1 helical assemblies composed of planar aromatic molecules is proposed and demonstrated with taking $P2_1/c$ and *Pbca* crystals of benzene, the simplest aromatic molecule, as examples.

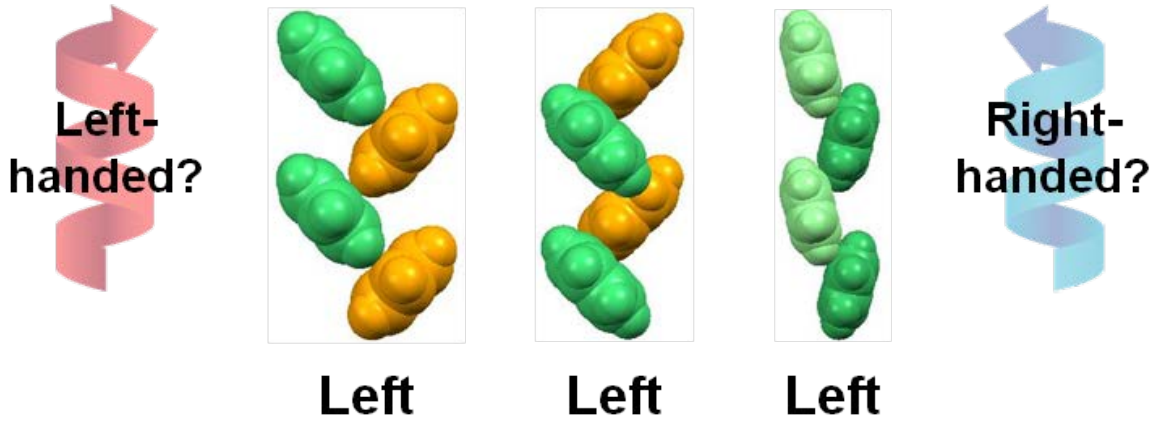

3.1 Introduction

Helical polymers and supramolecular assemblies have attracted chemists not only because of their beautiful and exotic structures, but their significant properties such as anisotropic optical behaviors and optical resolution abilities. To date a number of helical structures have been achieved in various scales and phases.[1-7]

In crystalline state, two-fold helix (2_1 helix) is particularly essential and is a universal motif, because molecules prefer to be packed with 2_1 symmetry to cancel their dipole moment and anisotropic molecular shape.[8-9] Indeed, approximately 70% of crystals registered in the Cambridge Structural Database (CSD) contain 2_1 helical axes.[10] The definition of supramolecualr chirality of 2_1 helices, however, is still incomplete: namely, handedness of 2_1 helical assemblies has not been distinguished yet. This arises from the fact that crystallography describes a molecule as a point and a crystal as a set of points related by symmetry operations, and thus, there is no need to consider a molecular shape (one-point model, see Figure 3-1a).

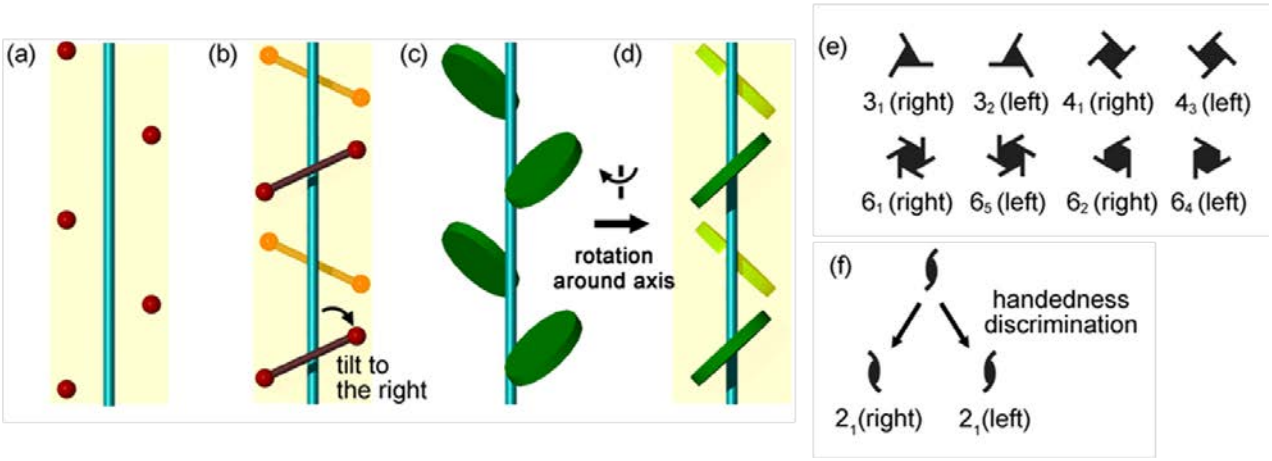

Figure 3-1. 2_1 Helical assembles composed of (a) points (one-point model), (b) line segments (two-point model) where the segments are located in front of or behind the helical axis, and (c) planar molecules, whose tilt can be distinguished as in the case of the two-point model when the assembly is projected from a certain direction as shown in (d). Symbols expressing helical screw axis: (e) 3-, 4-, and 6-fold screw axis operations, and (f) our proposed 2_1 screw axis operation distinguishing right- or left-handedness. Handedness of a 2_1 helical assembly expressed by the two-point model can be determined on the basis of the molecular tilt against the helical axis (supramolecular tilt chirality method), for example: right-handed for (b). Blue bars denote helical axes.

In contrary to this, we have proposed the supramolecular tilt chirality method to define the handedness of 2_1 helical assemblies.[11-15] In this concept, molecules are approximated by two points connected with a line segment (two-point model). As shown in Figure 3-1b, given the segments in front of a 2_1 screw axis inclined to the right, the assemblies can be defined to be right-handed (vice versa).[11-15] This method has been particularly suitable to describe chirality of 2_1 helices composed of molecules with slender skeletons.[16-17] However, how does it work for 2_1 helices composed of other types of molecules such as planar aromatic compounds? In connection with this, we noticed that projection of the planes from a certain direction can express its tilt as in the case of the two-point model (Figure 3-1c,d).

Herein, we first propose a more universal method to distinguish right- or left-handedness of 2_1 helical assemblies of planar molecules. The method can be applied not only for side-to-side, but also for slipped herringbone arrangements with 2_1 symmetry (vide infra). Based on the method, we demonstrate what types of geometry and chirailty are achieved in 2_1 helices of benzene, the simplest planar molecule, in its monoclinic crystal with space group $P2_1/c$ and orthorhombic with *Pbca*. Moreover, we propose progressive expression on the symmetry diagram, namely, the use of the enantiomeric pair of the symbol to express right- or left-handed 2_1 helical axes. In *The International Table for Crystallography,* enantiomeric pairs of screw axes such as 3_1–3_2, 4_1–4_3, 6_1–6_5, 6_2–6_4 are described with enantiomeric pairs of the corresponding symbols (Figure 3-1e).[18] For the 2_1 screw axis, on the other hand, only one symbol has been used because of the reason we describe above. However, we now can distinguish helical sense of the 2_1 helix, allowing us to use an enantiomeric pair of the symbols as shown in Figure 3-1f.

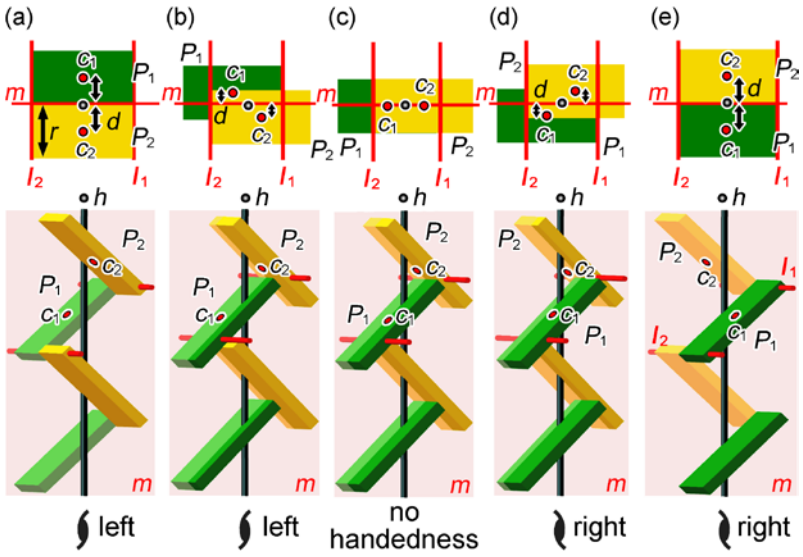

Figure 3-2. Schematic representation of 2_1 symmetric columns of planar molecules assembled in ways of (a and e) side-to-side, (b and d) slipped herringbone, and (c) perfect herringbone. $\boldsymbol{P_1}$ and $\boldsymbol{P_2}$: green and yellow plates related by 2_1 symmetry operation. ***h***: the helical axis. $\boldsymbol{c_1}$ and $\boldsymbol{c_2}$: centroids of the $\boldsymbol{P_1}$ and $\boldsymbol{P_2}$ plates, respectively. $\boldsymbol{l_1}$ and $\boldsymbol{l_2}$: intersection lines of the planes on which the plates $\boldsymbol{P_1}$ and $\boldsymbol{P_2}$ are laid. ***m***: a plane perpendicularly intersecting the axes ***h***, $\boldsymbol{l_1}$ and $\boldsymbol{l_2}$. ***r***: the width of the plate. ***d***: the distance between the $\boldsymbol{c_n}$ (n = 1 or 2) and axis ***h***. The side-to-side, slipped herringbone, and perfect herringbone structures have relationships of $\boldsymbol{d} \approx \boldsymbol{r}/2$, $0 < \boldsymbol{d} < \boldsymbol{r}/2$, and $\boldsymbol{d} = 0$, respectively. The structures in (a and b) exhibit left-handedness, while (d and e) right-handedness. No handedness can be determined for (c).

3.2 Results and Discussion

3.2.1 2_1 symmetric columns of planar molecules assemblies

Typical five orientations of plates in 2_1 helices are schematically described in Figure 3-2. In the case of the side-to-side arrangements (a) and (e), one can viscerally and easily recognize the assemblies as left- and right-handed helices, respectively. The side-to-side arrangement, however, is just one case of 2_1 helices of planar aromatic compounds,[13] and many of the others have a herringbone arrangement because of favorable edge-to-face (CH/π) interaction of aromatic rings.[19–25] Although many of the herringbone arrangements contain 2_1 helical axes, their handedness has never been discussed probably because their appearances are far from a helix. Even in such cases, however, one can distinguish plates in front of the ***h*** axis from those behind the axis when the centroids $\boldsymbol{c_1}$ and $\boldsymbol{c_2}$ are not on the plane ***m***, and therefore, the helical handedness can be determined by the tilt of the molecules at the front according to the two-point model. For example, in the case of model (b), the centroids $\boldsymbol{c_1}$ and $\boldsymbol{c_2}$ are apart from the plane ***m*** though the distance ***d*** is much shorter than that of the model (a), capable of discriminating the planes (colored in yellow) in front of the ***h*** axis from those (colored in green) behind the axis. When focusing on the molecular tilt, the yellow plates incline to the left, resulting in the decision that the 2_1 helical assembly is left-handed. The perfect herringbone model (c), on the other hand, has the centroids which are laid on the palne ***m***. Therefore, the relative location of the plates cannot be determined as inthe former cases.

3.2.2 2_1 Helicity inhering in the $P2_1/c$ crystal of benzene

We demonstrate determination of the handedness of 2_1 helical arrangements of benzene molecules formed in the monoclinic and orthorhombic crystals with the $P2_1/c$ and *Pbca* space groups, respectively. Figure 3-3a shows the *b* axis projection of the $P2_1/c$ crystal of benzene reported in 1969.[26]

The molecules are colored in green or orange for clarity. The crystal contains totally four helices (Figure 3-3b): two enantiomeric pairs of the side-to-side arrangements A–B and A–C, and the slipped herringbone arrangements A–E and A–D. On the basis of the method described above, the helices A–B and A–C show left- and right-handedness, respectively. Similarly, the helices A–E and A–D show left- and right-handedness, respectively. Since the inverted centers are laid between the 2_1 screw axes, the adjacent helices, *i.e.* A–B and A–C, or A–D and A–E, have opposite handedness, making the crystal structure achiral. This fact is also unambiguous from the essential nature of the space group $P2_1/c$.

To add information of helicity and assembly type of 2_1 helical arrangements into the symmetry diagram, here we propose progressive expression by using enantiomeric symbols as well as subscripted Roman numbers. Enantiomeric symbols are applied to express their handedness. Assembly types are distinguished by using subscripted Roman numbers such as I, II, and III, depending on the numbers of assembly manners. For example, the conventional diagram of the $P2_1/c$ space group has been described as shown in Figure 3-3c(left), in which 2_1 helices are unclear concerning helical senses and types, while the proposed diagram can be easily recognized concerning them [Figure 3-3c(right)].

3.2.3 2_1 Helicity inhering in the *Pbca* crystal of benzene

2_1 Helices in the *Pbca* crystal of benzene, reported in 1964,[27] are also analyzed as shown in Figure 3-4. In contrary to the $P2_1/c$ crystal which has 2_1 helical axes only along the *b* axis, the *Pbca* crystal has 2_1 helical axes as well as inversion centers along the *a*, *c*, and *b* axes. Therefore, the *Pbca* crystal includes three sets of enantiomeric paired 2_1 helices, totally six helices. The motifs of these helices are shown in Figure 3-4b: left- and rignt-handed helices (A–B and A–C) running along the *a* axis have the side-to-side arrangement, those along the *c* axis (D–E and D–F) and the *b* axis (G–I and G–H) have the slipped herringbone arrangements. At a glance, it seems to be difficult for a herringbone arrangement, particularly in the case of D–E and D–F, to distinguish the relative location of the benzene rings. However, the centroids of the benzene are obviously apart from the ***m*** plane, even with a subtle distance of ***d***, and therefore, the handedness can be determined clearly. The symmetry diagram of the *Pbca* space group with the progressive symbols are shown in Figure 3-4c. Each diagram projected from *a*, *c*, or *b* involves one enantiomeric pair of the helices I, II, and III.

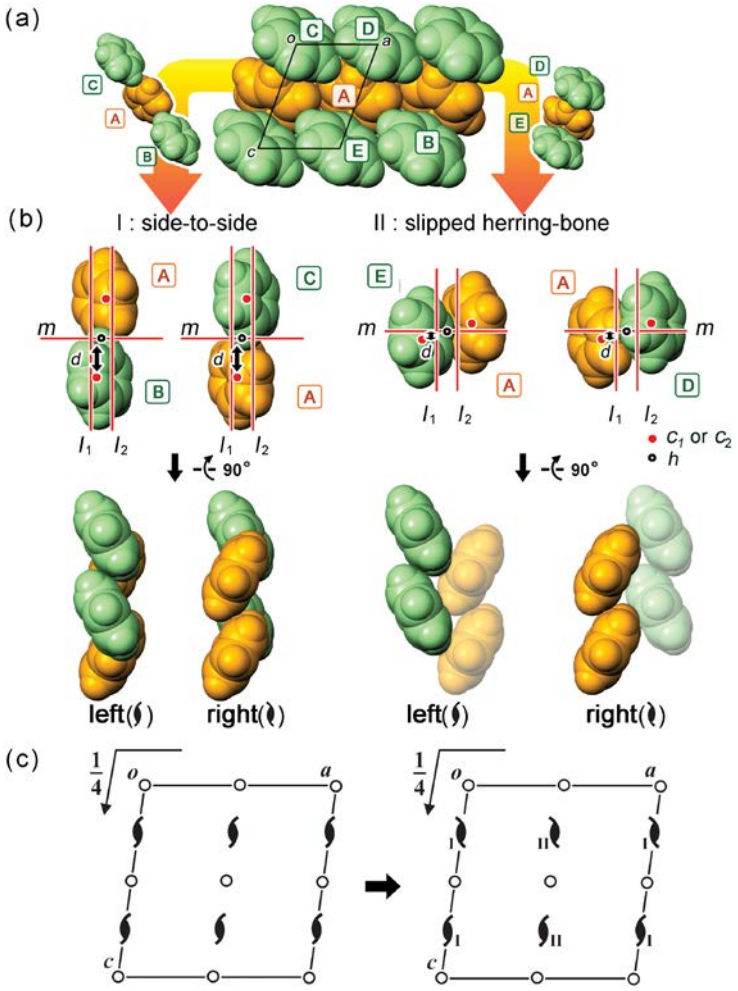

Figure 3-3. 2_1 Helicity inhering in the $P2_1/c$ crystal of benzene. (a) Packing diagram. (b) Two sets of 2_1 helices composed of molecules A, B and C arranged in a side-to-side manner (left), and of A, E, and D arranged in a slipped herringbone manner (right). (c) Conventional (left) and newly-proposed (right) symmetry diagrams of the $P2_1/c$ space group, where the conventional symbols of the two-fold screw axes were changed so as to distinguish the handedness and type of helical motifs. The geometrical symbols, $\boldsymbol{l_1}$, $\boldsymbol{l_2}$, $\boldsymbol{c_1}$, $\boldsymbol{c_2}$, $\boldsymbol{h}$, and ***m*** are conformed with those in Figure 2.

3.3 Conclusion

In summary, we first proposed a universal method to distinguish right- or left-handedness of 2_1 helical assembly of planar molecules, and demonstrated determination of helical handedness for the $P2_1/c$ and *Pbca* crystals of benzene. The method can be applied not only for side-to-side, but also for slipped herringbone arrangements, the latter of which is abundantly observed in the crystalline state due to favorable CH/π interactions. Moreover, we proposed progressive expressions on the symmetry diagram, namely, the use of the enantiomeric pair of the symbol to express right- or left-handed 2_1 helical axes.

The idea described here can be widely extended to crystals of other planar polycyclic aromatic hydrocarbons such as naphthalene and anthracene, enabling one to design molecular arrangements in crystalline states toward functional materials, as well as to thoroughly understand crystal structures.

3.4 Experimental Section

3.4.1 Computer data analysis

The crystal structures were calculated by using Mercury program. Crystal structures of benzene belonging to space groups $P2_1/c$ (refcode: BENZEN03)[26] and *Pbca* (refcode: BENZEN)[27] were retrieved from Cambridge Structural Database.

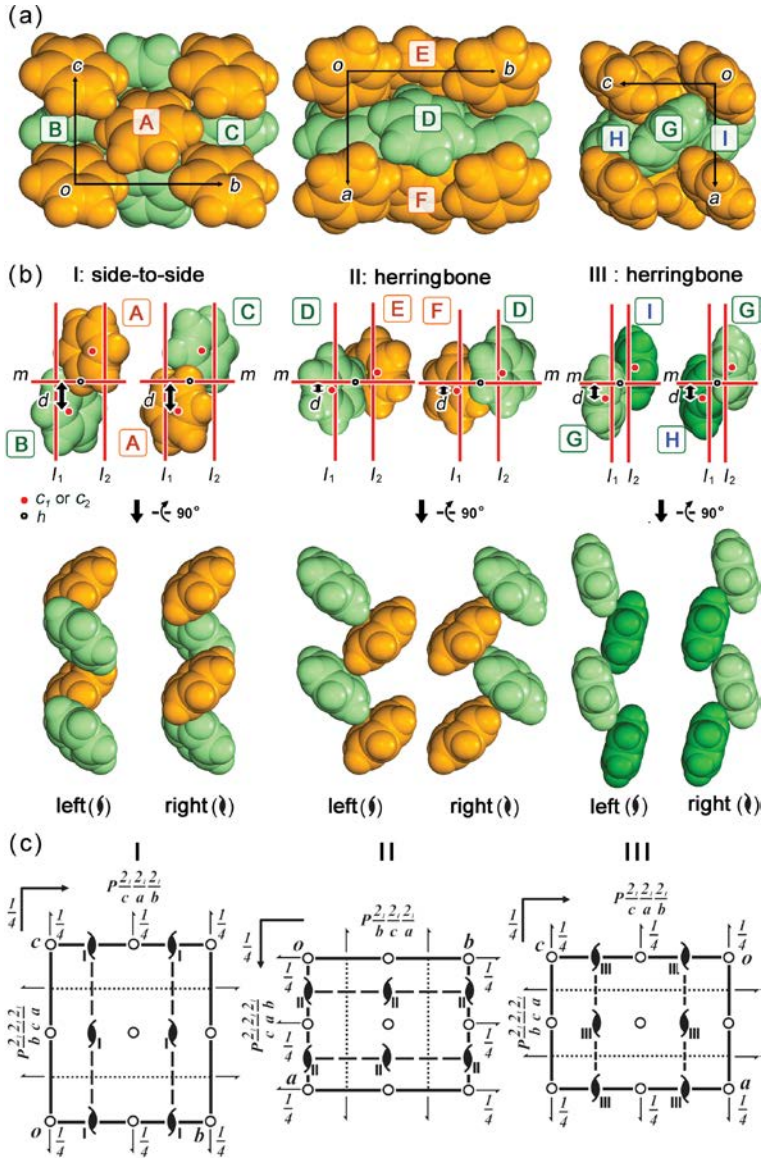

Figure 3-4. 2_1 Helicity inhering in the *Pbca* crystal of benzene. (a) Packing diagram. (b) Three sets of 2_1 helices with molecules A, B, and C in a side-to-side manner (left), D, E, and F in a slipped herringbone manner (center), and G, H, and I in a slipped herringbone manner (right). (c) Proposed symmetry diagrams of the *Pbca* space group, where the conventional symbols of the 2_1 screw axes are changed so as to distinguish the handedness and type of helical motifs (I, II, or III). The geometrical symbols, $\boldsymbol{l}_1$, $\boldsymbol{l}_2$, $\boldsymbol{c}_1$, $\boldsymbol{c}_2$, $\boldsymbol{h}$, and $\boldsymbol{m}$ are conformed with those in Figure 2.

3.5 References

[1] E. Yashima, K. Maeda, H. Iida, Y. Furusho and K. Nagai, *Chem. Rev.*, **2009**, *109*, 6102-6211.

[2] J. Kumaki, S. Sakuraiya and E. Yashima, *Chem. Soc. Rev*., **2009**, *38*, 737-746.

[3] K. Akagi, *Chem. Rev*., **2009**, *109*, 5354-5401.

[4] D. J. Hill, M. J. Mio, R. B. Prince, T. S. Hughes and J. S. Moore, *Chem. Rev.*, **2001**, *101*, 3893-4011.

[5] C. Piguet, G. Bernardinelli and G. Hopfgartner, *Chem. Rev.*, **1997**, *97*, 2005-2062.

[6] M. Albrecht, *Chem. Rev*., **2001**, *101*, 3457-3497.

[7] T. Shimizu, M. Masuda and H. Minamikawa, *Chem. Rev*., **2005**, *105*, 1401-1444.

[8] A. I. Kitaigorodskii, *Molecular Crystals and Molecules*, Academic Press, London, **1973**.

[9] T. Matsuura and H. Koshima, *J. Photochem. Photobiol. C: Photochem. Rev.*, **2005**, *6*, 7-24.

[10] http://www.ccdc.cam.ac.uk/products/csd/

[11] M. Miyata, N. Tohnai and I. Hisaki, *Acc. Chem. Res.*, **2007**, *40*, 694-702.

[12] I. Hisaki, N. Tohnai and M. Miyata, *Chirality*, **2008**, *20*, 330-336.

[13] A. Tanaka, I. Hisaki, N. Tohnai and M. Miyata, *Chem. Asian J.*, **2007**, *2*, 230-238.

[14] T. Yuge, T. Sakai, N. Kai, I. Hisaki, M. Miyata and N. Tohnai, *Chem. Eur. J.*, **2008**, *14*, 2984-2993.

[15] I. Hisaki, N. Shizuki, T. Sasaki, Y. Ito, N. Tohnai and M. Miyata, *Cryst. Growth Des.*, **2010**, *10*, 5262-5269.

[16] I. Hisaki, N. Shizuki, K. Aburaya, M. Katsuta, N. Tohnai and M. Miyata, *Cryst. Grwoth Des.*, **2009**, *9*, 1280-1283.

[17] T. Watabe, K. Kobayashi, I. Hisaki, N. Tohnai and M. Miyata, *Bull. Chem. Soc. Jpn.*, **2007**, *80*, 464-475.

[18] *International Tables for Crystallography, Vol. A, Space-Group Symmetry*; Hahn, T., Ed.; Kluwer Academic Publishers: London, **1983**.

[19] G. R. Desiraju and A. Gavezzotti, *Acta Crystallogr. Sect. B*, **1989**, *45*, 473-482.

[20] G. R. Desiraju and T. Steiner, *The Weak Hydrogen Bond in Structural Chemistry and Biology,* Oxford University Press, Oxford, **1999**.

[21] M. Nishio, *CrystEngComm*, **2004**, *6*, 130-158.

[22] S. Tsuzuki, K. Honda, T. Uchimaru, M. Mikami and K. Tanabe, *J. Phys. Chem. A*, **1999**, *103*, 8265-8271.

[23] S. Tsuzuki, K. Honda, T. Uchimaru, M. Mikami and K. Tanabe, *J. Am. Chem. Soc.*, **2000**, *122*, 3746-3753.

[24] K. Shibasaki, A. Fujii, M. Mikami and S. Tsuzuki, *J. Phys. Chem. A*, **2007**, *111*, 753-758.

[25] S. Tsuzuki and A. Fujii, *Phys. Chem. Chem. Phys*., **2008**, *10*, 2584-2594.

[26] G. J. Piermarini, A. D. Mighell, C. E. Weir and S. Block, *Science*, **1969**, *165*, 1250-1255.

[27] G. E. Bacon, N. A. Curry and S. A. Wilson, *Proc. R. Soc. London, Ser. A*, **1964**, *279*, 98-110.

[28] G. J. Piermarini, A. D. Mighell, C. E. Weir and S. Block, *Science*, **1969**, *165*, 1250.

Chapter 4

Photo-Tunable Morphologies of β-Cyclodextrin-Threaded Inclusion Complexes Containing a Terminal Cholesteryl Group

Abstract

Threading of cyclodextrin (CD) to convert from intramolecular to intermolecular hydrogen bonding leads to the self-assembly of an inclusion complex (IC). A chiral cholesteryl-*E*-4-(11-acryloxy-undecaloxy)-cinnamate (CAUC) monomer containing a photoisomerizable C=C bond and a cholesteryl terminal group was synthesized and threaded with β-CD to form an inclusion complex. The synthesized IC forms a rod-like construction because of the enhanced intermolecular hydrogen bonding. After UV irradiation, the self-assembled rod structure changed to a spherical structure because of the change in the molecular polarity and intermolecular forces. The bent structure of Z-CAUC may release some of the threaded CDs and lead to a decrease in intermolecular forces. The E-Z configurational photoisomerization of CAUC is irreversible.

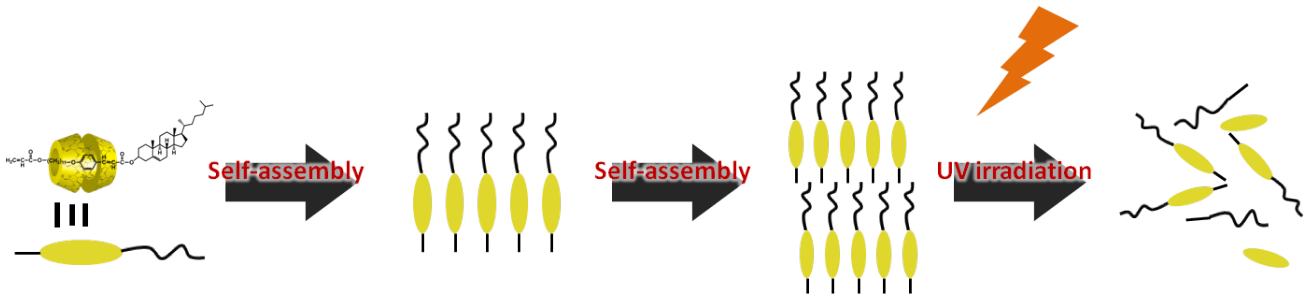

4.1 Introduction

Generally, hydrogen bonding and dipole-dipole interactions are expected to predominate over the highly ordered multipolar and inductive interactions when anisotropy and ordering in liquid crystals and inclusion complexes is being established. The most commonly accepted hypothesis is that the anisotropic phase is generated because of the anisotropy of the polarizability that results from the conjugated core units.[1-6] In our previous report, a new class of highly conjugated liquid crystalline molecules and inclusion complexes with a highly conjugated arm was prepared. Because of the highly conjugated side group, the synthesized liquid crystal (LC) revealed smectic phases. In dilute systems, the self-assembly of the LCs formed a football-shaped construction.[7]

It is well known that CDs can form inclusion complexes with a wide variety of low molecular weight compounds, including both inorganic and organic molecules. The low solubility of CDs in water confirms the formation of intramolecular hydrogen bonds. After the threading of host molecules, intramolecular forces become disturbed, and the change to intermolecular forces leads to the formation of self-assembled constructions.[8-12] Molecular size and physical properties of CDs are submitted as Table 4-1. Unlike molecular chemistry, which is based on covalent bonds,

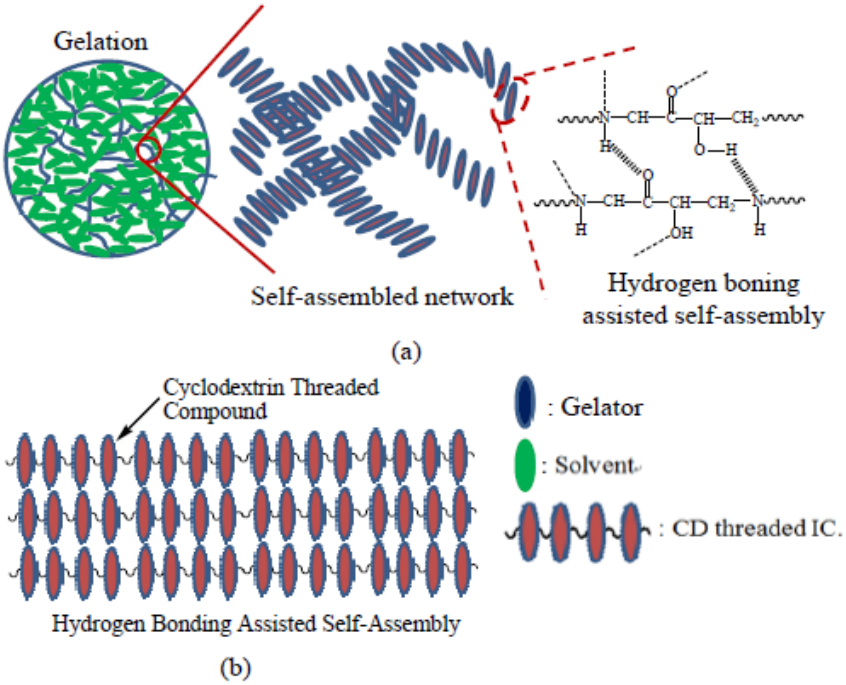

Figure 4-1. Self-assembly of (a) gelators in solvents and (b) CD threaded molecules.

supramolecular chemistry aims at developing highly complex chemical systems from components that interact through non-covalent intermolecular forces.[13-16] In recent years, the use of molecular recognition in the design of self-assembling systems that consist of cyclodextrins and guest molecules has attracted increasing attention. Most investigations have focused on the preparation and characterization of both main-chain and side-chain polyrotaxanes in which the polymeric guests pass through a number of CDs to form the inclusion complexes.[17-20] As shown in Figure 4-1(a), both polar interaction and hydrogen bonding lead to the self-assembly of molecules to form gels. Furthermore, highly branched polymers with threaded CDs form columnar constructions, as shown in Figure 4-1(b). Moreover, the inclusion complexes are often synthesized using star-shaped polymers and CDs[21-24]. Supramolecular arrangements as shown in Figures 4-1(a) and 4-1(b) are primarily caused by the secondary forces between the molecules.

Table 4-1. Physical properties of the three kinds of cyclodextrin.

Property	α-cyclodextrin	β-cyclodextrin	ϒ-cyclodextrin
Number of gulucose units	6	7	8
Molecular weight (g mol^{-1})	972	1,135	1,279
Water solubility (g/100 ml) at 25 °C	14.5	1.85	23.2
Specific rotation	150.5±0.5	162.5±0.5	177.4±0.5
Internal diameter (Å)	4.9	6.2	7.9
External diameter (Å)	14.6	15.4	17.5
Height cone (Å)	7.9	7.9	7.9
Cavity volume ($Å^3$)	176	346	510

There have been many reports on the use of highly branched polymers as covalently bound modifiers for CDs[25-28] and on the UV-induced decomplexation of host-guest molecules that leads to the deformation of vesicles[29-31]. However, there has been no morphology study concerning photo-induced inclusion complexes prepared from monomers and CDs that are formed through non-covalent interactions. In the present work, a new class of chiral molecule, cholesteryl-*E*-4-(11-acryloxy-undecaloxy)-cinnamate (CAUC), was synthesized. After threading with β-CD, the intermolecular forces were significantly enhanced, which led to the formation of a self-assembled columnar structure. The photo-tunable morphologies of the synthesized IC caused by UV-induced E-Z configurational isomerization were characterized.

4.2 Results and Discussion

4.2.1 Synthesis of β-CD threaded complexes

To investigate the effect of UV irradiation on the self-assembly of molecules, a chiral monomer of CAUC was synthesized. The synthesized products were characterized by ^{1}H-NMR, FTIR, and elemental analysis. Figure 4-2(a) shows the ^{1}H-NMR spectrum of CAUC. Specific protons of the synthesized CAUC are assigned on the spectrum. The cholesteryl group shows complicated absorption peaks between 0.7 to 2.4 ppm. Cholesterol is a chiral moiety that is used for the induction of helical structures in the cholesteric phases of liquid crystals and for the induction of helical constructions of self-assembled compounds. In addition, this cholesteryl group was used as a blocking terminal group to prevent the release of threaded CDs, as shown in Scheme 4-1.

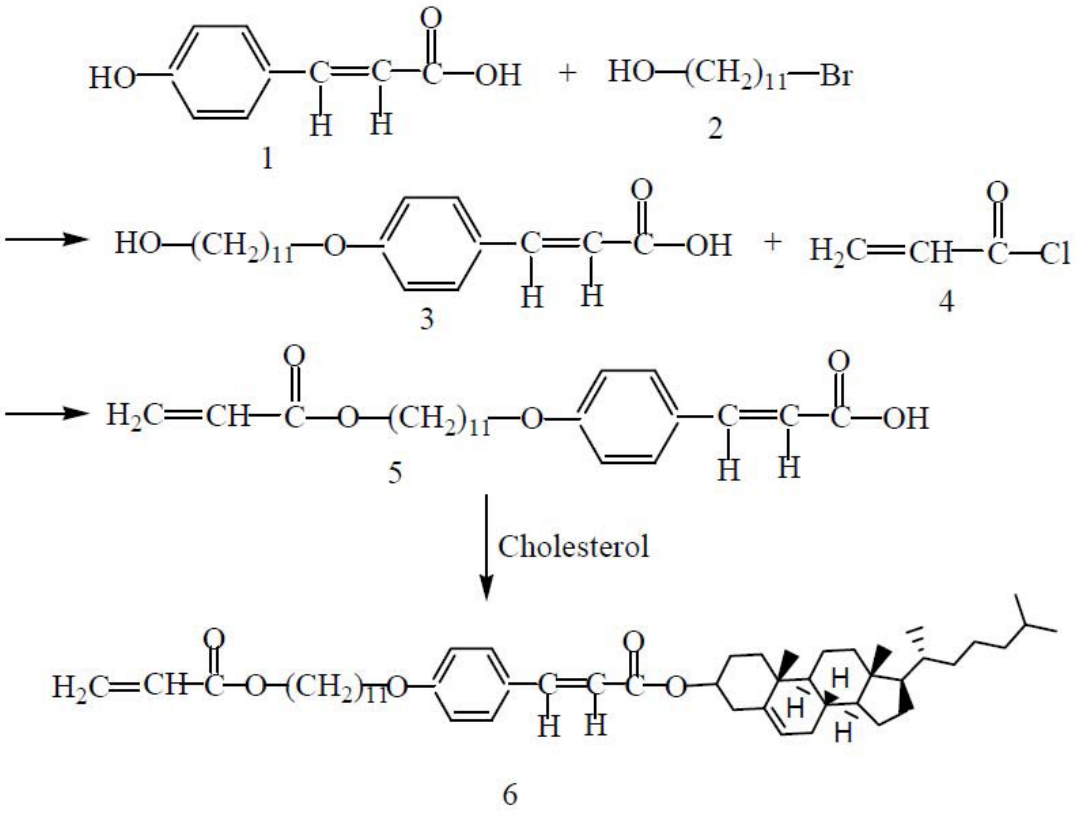

Scheme 4-1. Synthesis of CAUC.

Our analysis showed that the inclusion complex (IC) of CAUC threaded with β-cyclodextrin was synthesized successfully. As shown in Scheme 4-2, after ultrasonic agitation, the precipitated synthetic inclusion complex was collected. The collected sample powder was thoroughly washed with THF and water. Theoretically, the unreacted monomers and *β*-cyclodextrins were removed by washing. As described in our report, the number of *β*-CDs threaded onto the synthesized IC was analyzed with ^{1}H-NMR.

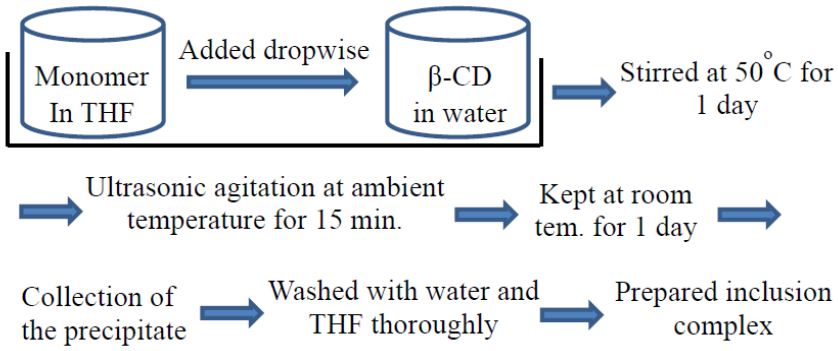

Scheme 4-2. Preparation of inclusion complex (IC).

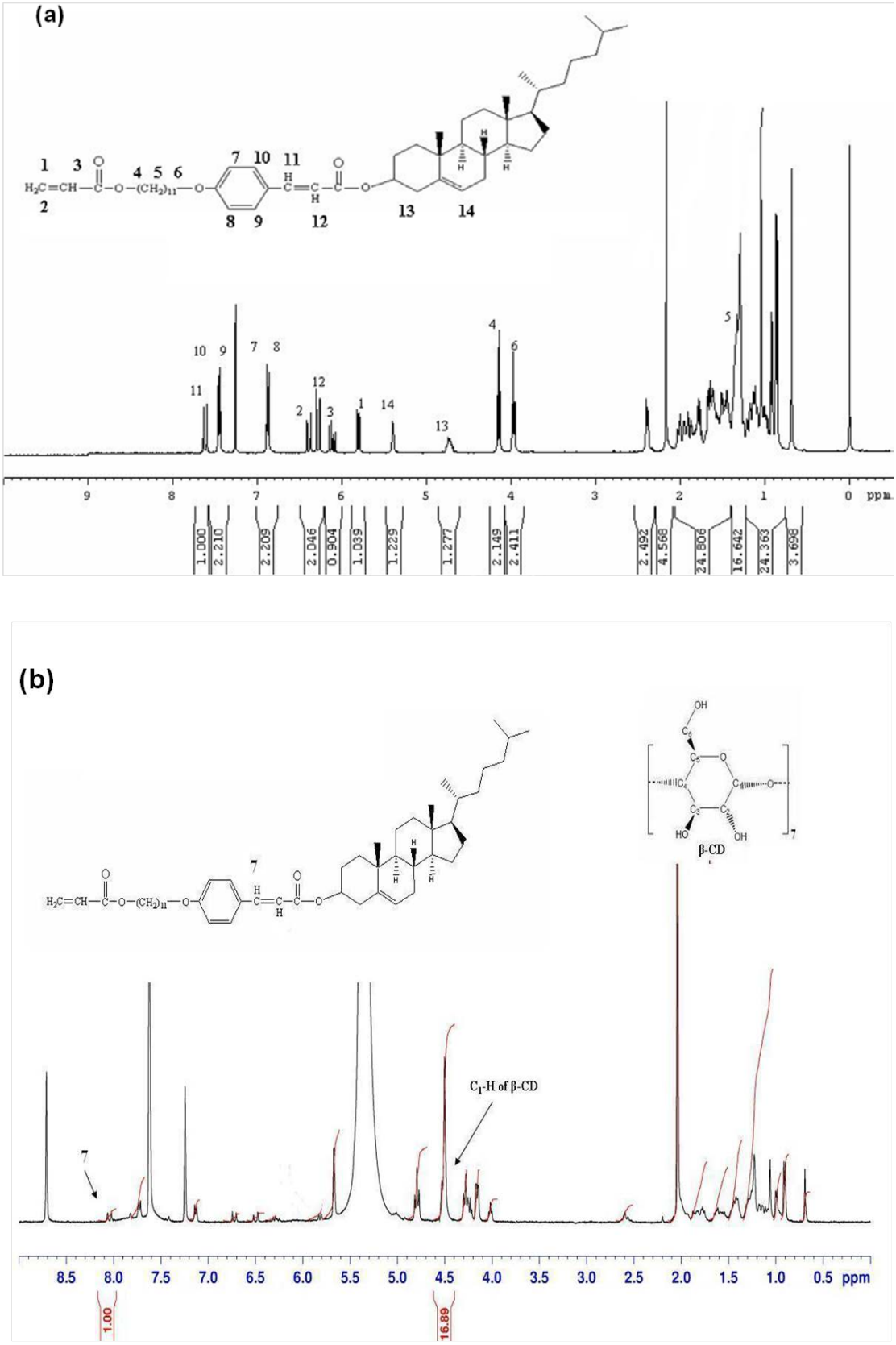

Figure 4-2. ^{1}H-NMR of the synthesized (a) CAUC monomer, and (b) inclusion complex IC.

The ^{1}H-NMR spectrum of the synthesized IC is shown in Figure 4-2(b). As can be seen, for C_1 of glucose in CD molecule, the peak area is 16.89. Each *β*-CD consists of 7 glucoses. Absorption peak around 8.0 ppm is calculated as 0.87. Accordingly, 16.89/7:0.87 = 2.8:1. From the area of the protons, the number of threaded *β*-CDs was calculated to be 2.8. This result suggests that two to three *β*-CDs were threaded onto CAUC to form the inclusion complex. Scheme 4-3 shows a model of the inclusion complex. As shown in this scheme, the intramolecular hydrogen bonds of CD after threading should be converted to intermolecular forces. In such situations, the relatively stronger intermolecular forces are expected to predominate. Comparison of the FTIR spectra from monomeric CAUC, *β*-CD and IC is offered as supplementary information.

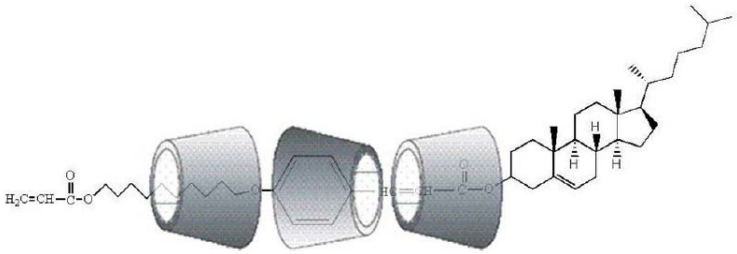

Scheme 4-3. Molecular structure of inclusion complex (IC)

4.2.2 Identification of the synthesized compounds

To identify the formation of the IC, ^{1}H-NMR, FTIR and DSC analysis were performed. Figure 4-3 shows the results from the FTIR analysis of the IC and *β*-CD. A significant absorption of a carbonyl group (C=O) is observed at approximately 1700 cm^{-1}. Absorption peaks around 3400 cm^{-1} and 1640 cm^{-1} are ascribed to OH and C=C groups, respectively. Some other absorption peaks are observed in the fingerprint region. Furthermore, totally different scanning curves were observed as shown in Figure 4-4(a). The monomer CAUC shows a melting point at approximately 70 °C. Enthalpy of the DSC peaks were calculated. From the DSC analysis, CAUC may reveal

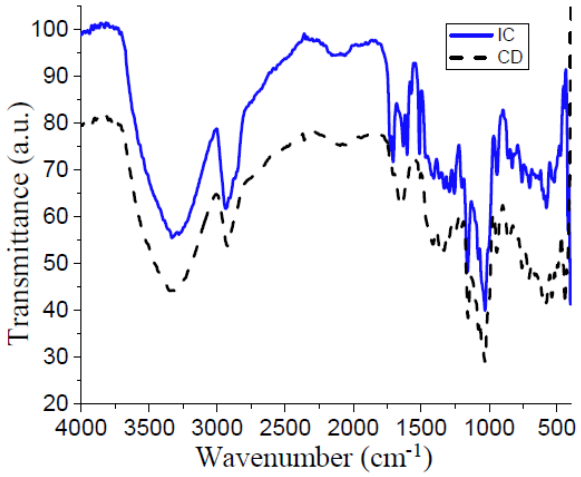

Figure 4-3. FTIR spectra of the IC and CD.

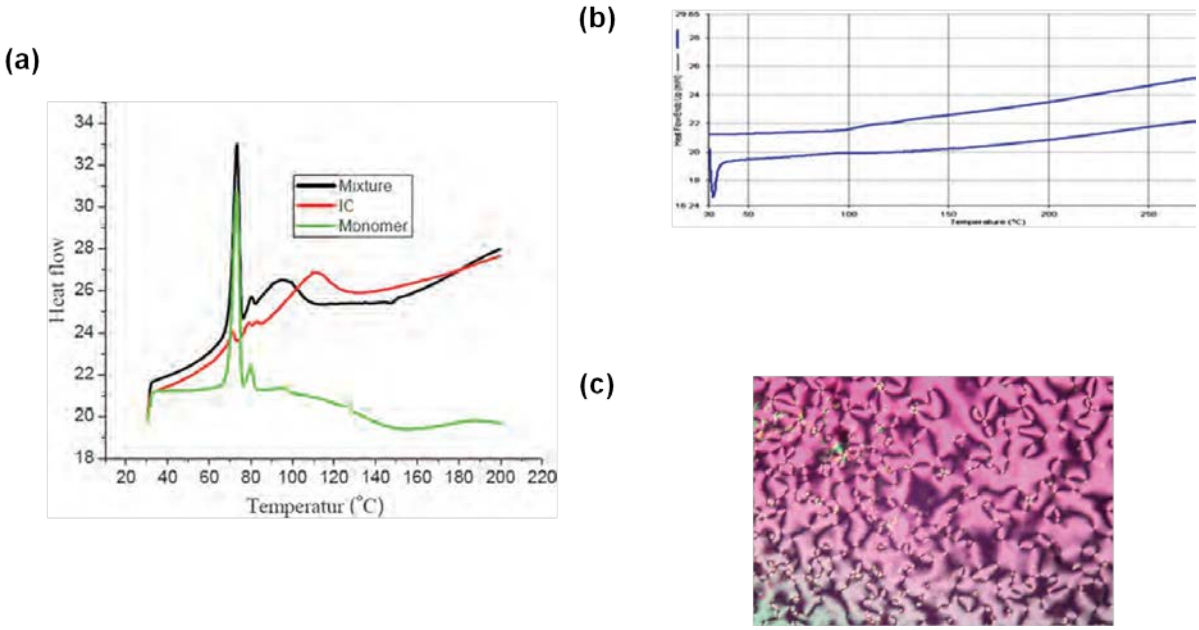

Figure 4-4. (a) DSC heating cycle of the monomer, the IC, and the mixture of monomer and CD, (b) DSC cooling cycle and second scanning of the IC, and (c) POM texture of CAUC at 78.2°C.

a mesophase although the temperature range is quite limited. For the mixture of *β*-CD and CAUC monomer, a broad peak is observed at approximately 100 °C. This is ascribed to the escape of water from the cavity of *β*-CD. In the case of the IC, escape of water was observed at approximately 110 °C. This is caused by the escape of water from the cavity of the *β*-CD that is in the IC. This result suggests that water is strongly held in the confined space of the IC.

Theoretically, the threaded *β*-CD has a smaller cavity because of the existence of the threaded monomer. However, the stronger intermolecular hydrogen bonding may strengthen the interaction between the IC and embedded water molecules, which leads to a shift of the peak to a higher temperature. Once the IC is formed in solution, some self-assembly of the IC is expected. The entrapped water between the ICs should have difficulty escaping as well. Figure 4-4(b) shows the cooling cycle and the second scanning of the IC. As shown in Figure 4-4(b), no significant peaks were observed. The results suggest that water embedded inside the CD cavity was removed thoroughly.

Furthermore, TGA analysis of *β*-CD was performed. A significant weight decrease is observed around 100 °C. The result consists with the phenomena shown in Figure 4-4(a). It is ascribed to the escape of water from CDs. In order to investigate the mesophase of CAUC, texture analysis using

POM equipped with a heating stage was carried out. The result is shown in Figure 4-4(c), an anisotropic mesophase texture was observed. The result suggests that CAUC reveals thermotropic liquid crystalline phases in case of neat materials.

4.2.3 Self-assembly of CAUC

The self-assembly of CAUC was investigated, and the results are shown in Figure 4-5. As shown in Figure 4-5(a) and (b), both rod and needle-like constructions were observed. The sharp terminal structure may be caused by a defect in the self-assembly of ICs. The balance of intramolecular forces and surrounding surface tension determines the final construction. In addition, as shown in Figure 4-5(c), a colorful texture was observed under POM. Figure 4-5(d) shows the cross-section of the self-assembled ICs. This result shows that the self-assembled construction possesses a highly ordered arrangement. Notably, in the absence of threading with β-CD, CAUC does not undergo self-assembly in solvents. From DSC of neat CAUC, it shows thermotropic liquid crystalline phases. Of course, liquid crystal is a kind of self-assembly of molecules. However, in solvent, the secondary force interaction between CAUC molecules is too weak to form self-assembled construction.

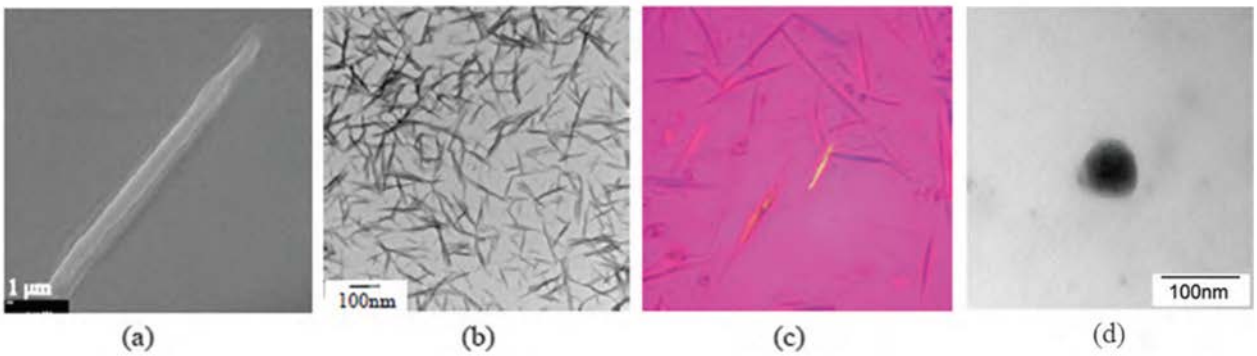

Figure 4-5. Results of the (a) SEM, (b) TEM, and (c) POM texture, and (d) TEM cross-section analyses of IC.

4.2.4 Photoisomerization of CAUC

CAUC contains a photoisomerizable C=C bond. The optical properties of both CAUC and IC were investigated. CAUC in solvent was irradiated with a UVP-lamp (6 W, available wavelength ranged from 250 to 320 nm) without wavelength filter. The results are summarized in Figure 4-6. As shown in Figure 4-6(a), a UV irradiation decreases the absorption at approximately 320 nm. This absorption is caused by the photo-induced isomerization of the C=C bond. The isomerization of CAUC from an *E* to a *Z* configuration may alter the electronic environment and lead to the decrease in UV absorption. Figure 4-6(b) shows the result of UV irradiation of the IC. One additional absorption peak appears at approximately 410 nm. This peak is caused by the threaded β-CD. An increase in UV irradiation decreases the 320 nm absorption peak, but increases the 410 nm peak. These results suggest that photoirradiation significantly alters the molecular structures of CAUC and the IC.

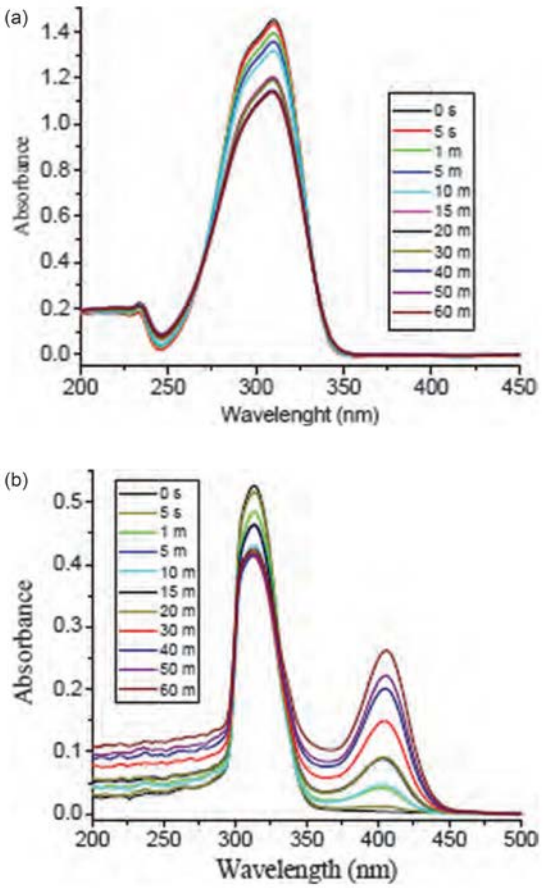

Figure 4-6. UV-vis spectra of (a) CAUC and (b) IC.

4.2.5 Photo-induced morphology change

To investigate the effect of *E*-*Z* isomerization of the IC on molecular interaction, self-assembly of the IC in DMSO (dimethyl sulfoxide) was performed. Figure 4-7 shows the results. Before UV irradiation, self-assembly of the IC forms a rod-like structure as shown in Figure 4-7(a). Interestingly, after UV irradiation, the self-assembled construction forms a ball-like structure as shown in Figure 4-7(b). These results suggest that the ICs self-assemble in a highly ordered manner because of the stronger intermolecular hydrogen bonds. After UV-induced isomerization, CAUC converts from the *E* to the *Z* configuration, which leads to a change in the molecular polarity. During this time, β-CD may de-thread from CAUC, which decreases both the intermolecular hydrogen bonding and molecular polarity. Figure 4-8 shows a schematic representation of the formation of the self-assembled constructions with different levels of molecular interaction. As shown in Figure 4-8(a), before UV irradiation the threaded β-CDs have relatively stronger intermolecular hydrogen bonding that leads to the formation of a rod structure. However, a random system usually forms a spherical construction because of the weak molecular interaction, as shown in Figure 4-8(b). The balance of intermolecular forces, surface tension and system stability causes the formation of the final spherical structure. Isomerization of CAUC from *E* to *Z* is irreversible. After UV irradiation, the spherical construction did not return to a

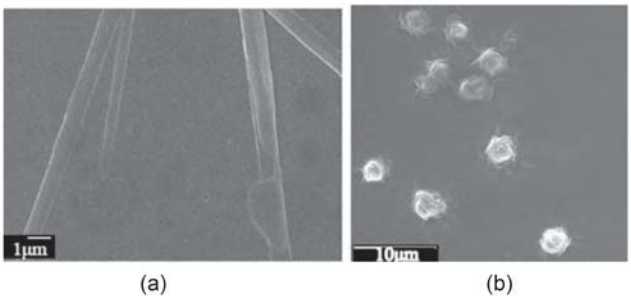

Figure 4-7. SEM images of self-assembled IC (a) before and (b) after UV irradiation.

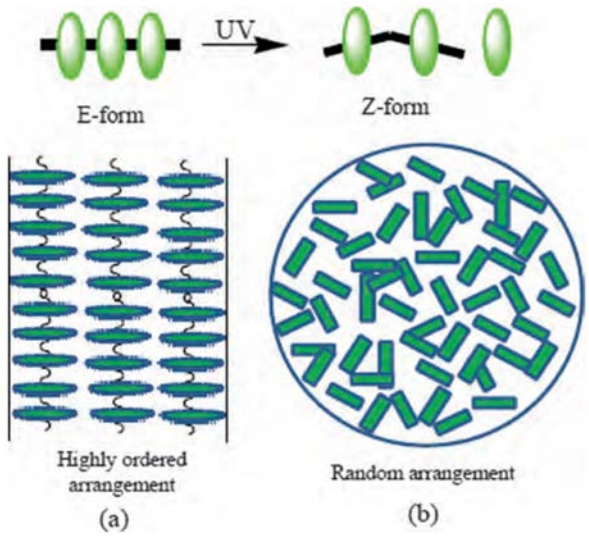

Figure 4-8. Schematic representation of IC (a) before and (b) after UV irradiation.

rod structure even after heating in DMSO at 80°C for 2 hours. In addition, free-radical polymerization of the synthesized IC with ethylene glycol dimethacrylate (EGDMA) was confirmed. The FTIR absorption from the C=C bond at approximately 1650 cm^{-1} disappeared after polymerization. Unlike neat compounds, threaded β-CD and bonded monomers may interact with each other leads to the shift of peaks. After polymerization, the broad peak around 1700 cm^{-1} is ascribed to the absorption of C=O groups in IC polymer. These results suggest that the fabricated rod-like self-assembled construction can be used to strengthen the physical properties of polymer films, such as those in fiber reinforced plastic (FRP) systems. Theoretically, this material would be available for micro-electromechanical systems (MEMS).

4.3 Conclusion

Chiral CAUC with a photoisomerizable C=C bond and a cholesteryl terminal group was synthesized. After threading with β-CDs, the synthesized IC possesses a stronger intermolecular hydrogen bonding potential that leads to the formation of a rod construction. After UV irradiation, CAUC configurationally isomerizes from E to Z, which decreases the strength of the intermolecular forces. Therefore, this self-assembled structure changes from a rod-shaped to a spherical morphology. This variation is irreversible even after heating at 80°C for 2 hours. UV induced isomerization may de-thread CDs from CAUC, resulting in the weakening of intermolecular forces which causes the changes in morphology.

4.4 Experimental Section

4.4.1 Materials characterization

The Fourier Transform Infrared Spectroscopy (FTIR) spectra were recorded on a Jasco VALOR III Fourier transform infrared spectrophotometer. Nuclear magnetic resonance (NMR) spectra were obtained using a Bruker AMX-400 high-resolution NMR spectrometer. Differential scanning calorimetry (DSC) was conducted on a Perkin-Elmer DSC 7 in a nitrogen atmosphere with the heating and cooling rates of +5 °C min^{-1} and −5 °C min^{-1}, respectively. A thermogravimetric

analyzer (TGA-7) from Perkin Elmer was used to record the temperature of thermal decomposition at a heating rate of +40 K min^{-1} under a nitrogen atmosphere. The cross-sectional morphology of the samples was characterized by transmission electron microscopy (TEM) using a JEOL JEM-1200CX-II microscope with a Cu-grid substrate. The anisotropic properties of the highly ordered, self-assembled samples were investigated using an Olympus BH-2 polarized light microscope (POM) equipped with a Mettler hot stage FP-82, and the temperature scanning rate was determined to be 10 °C min^{-1}. Furthermore, for POM analysis of ICs, a few drops of self-assembled *β*-cyclodextrin-liquid crystal ICs in pyridine were placed on a substrate. After drying, the samples were analyzed using POM instruments.

4.4.2 Materials

- **Synthesis of E-4'-(6-hydroxyhexyloxy)-cinnamic acid (1)**

E-4'-Hydroxycinnamic acid (3 g, 18.3 mmol) and a catalytic amount of potassium iodide were dissolved in ethanol (50 ml). Potassium hydroxide (3.08 g, 55 mmol) in water (40 ml) was subsequently added drop-wise. Next, 11-bromo-1-undecanol (5.6 g, 21 mmol) was added, and the mixture was heated at reflux for two days. The resulting mixture was cooled to ambient temperature and poured into a large amount of ice water. Dilute hydrogen chloride was then added drop-wise until a solid precipitate was formed (pH=3). The white precipitate was collected, washed several times with water and dried under vacuum, providing a 90% yield. For aqueous solution, Milli-Q water was used in this investigation.

- **Synthesis of E-4'-(6-acryloxyhexyloxy) cinnamic acid (2)**

Compound 1 (1 g, 3 mmol) and a catalytic amount of 2,6-di-tert-butyl-4-methylphenol were dissolved in distilled 1,4-dioxane (40 ml). A solution of N,N-dimethylaniline in 1,4-dioxane (10 ml) was added drop-wise. The solution was cooled in an ice bath, and a solution of acryloyl chloride (0.6 ml, 6.6 mmol) in 1,4-dioxane (10 ml) was slowly added with vigorous stirring. After stirring at room temperature for 2 h, the mixture was heated to 60°C for 3 h. The mixture was cooled to room

temperature and poured into a large amount of ice water. The white precipitate was collected, washed several times with water, and dried in vacuum to give a yield of approximately 90%.

・Synthesis of Cholesteryl-E-4’-(6-acryloyloxyhexyloxy)-cinnamate (CAUC)

Compound 2 (2 g, 5.2 mmol), cholesterol (2.2 g, 5.7 mmol), and 4-dimethylaminopyridine (DMAP) (0.13 g, 1 mmol) were dissolved in dry dichloromethane (30 ml) at 30^{o}C. The solution was cooled in an ice bath under nitrogen atmosphere. N,N’-Dicyclohexylcarbodiimide (DCC) (1.3 g, 6.2 mmol) was dissolved in CH_2Cl_2 (10 ml) and added to the mixture. The mixture was stirred at 30^{o}C for 48 h. The resulting solution was filtered and washed with an aqueous potassium hydroxide solution (5 % w/v), 1 M hydrogen chloride, and saturated $NaHCO_3$. After evaporation, the crude product was recrystallized from ethyl acetate to give a yield of approximately 45%. ^{1}H-NMR ($CDCl_3$, δ ppm): 0.73 (*s*, 3H, −CH_3), 0.85–1.02 (*m*, 12H, −CH_3), 1.03–2.51 (*m*, 46H, −CH_2**)**, 3.91–4.02 (*t*, 2H, CH_2O), 4.13–4.21 (*t*, 2H, −OCH_2), 4.68–4.82 (*m*, 1H, OCH in chol.), 5.43 (*t*, 1H, CH_2=C in chol.), 5.81–5.85 (dd, *J* = 1.66 Hz, 1H, H2C=C), 6.09–6.18 (*dd*, *J* = 10.32 Hz, 1H, C=CH–C), 6.29–6.34 (*d*, *J* = 15.8 Hz, 1H, Ph-C=CH), 6.42–6.48 (*dd*, *J* = 1.66 Hz, 1H, H_2C=C), 6.85–6.87 (*d*, *J* =8.5 Hz, 2H, aromatic), 7.42–7.44 (*d*, *J* =8.5 Hz, 2H, aromatic), 7.62–7.66 (*d*, *J* = 15.8 Hz, 1H, Ph–CH=C). Molecular formula: $C_{50}H_{76}O_5$: Calcd. C, 79.37; H, 10.05. Found C, 79.01; H, 10.15.

・Synthesis of inclusion complex

β-Cyclodextrin (*β*-CD) (3 g, 2.6 mmol) was dissolved in water (3 ml) at 60 °C. CAUC (0.5 g, 0.7 mmol) was dissolved in tetrahydrofuran (THF) (10 ml) and added to the *β*-CD solution. The reaction mixture was stirred at 50 °C for 24 h. The turbid solution was agitated ultrasonically at room temperature for 15 min, and the clear solution was allowed to stand at room temperature for 1 day. The precipitate was collected and washed thoroughly with THF to remove the residual CAUC. The collected precipitate was subsequently washed with water to remove residual *β*-CD. After 3 washes, the precipitate was dried under vacuum. ^{1}H-NMR ($CDCl_3$, δ in ppm): 4.12–4.18 (*t*, 2H, CH_2O), 4.25–4.31 (*t*, 2H, −OCH_2), 4.52 (*m*, 7H, C_1–H of *β*-CD), 4.77–4.85 (*m*, 1H, OCH in chol.), 5.65 (*t*, 1H, CH_2= C in chol.), 5.79–5.82 (*dd*, *J* =1.66 Hz, 1H, H_2C= C), 6.32–6.36 (*dd*, *J* =10.32 Hz, 1H,

C=CH–C), 6.49–6.54 (*d*, *J* = 15.8 Hz, 1H, Ph-C=CH), 6.70–6.75 (*dd*, *J* = 1.66 Hz, 1H, H_2C=C), 7.12–7.15 (*d*, *J* = 8.5 Hz, 2H, aromatic), 7.71–7.73 (*d*, *J* = 8.5 Hz, 2H, aromatic), 8.02–8.08 (*d*, *J* = 15.8 Hz, 1H, Ph–CH=C).

4.5 References

[1] Cai H, Yang R, Yang G, Huang H and Nie F, *Nanotechnology*, **2011**, *22*, 305602.

[2] Huang R, Su R, Qi W, Zhao J and He Z, *Nanotechnology*, **2011**, *22*, 245609.

[3] Evan M Smoak, Andrew D Carlo, Catherine C Fowles and Ipsita A Banerjee, *Nanotechnology*, **2010**, *21*, 025603.

[4] Liu J H and Chiu Y H, *J. Polym. Sci. Part A*, **2010**, *48*, 1142.

[5] Zhang W, Yuan J, Weiss S, Ye X, Li C and Muller AH E, *Macromolecules*, **2011**, *44*, 6891.

[6] Wang W, Li T, Yu T and Zhu F M, *Macromolecules*, **2008**, *41*, 9750.

[7] Niknam Jahromi M J and Liu J H, Soft Materials **2011**, DOI:10.1080/1539445X.2011.633149.

[8] Frasconi M and Mazzei F, *Nanotechnology*, **2009**, *20*, 285502.

[9] Lee K P, Gopalan A I, Lee S H and Kim M S, *Nanotechnology*, **2006**, *17*, 375.

[10] Chiu Y H and Liu J H, *J. Polym. Sci., Part A*, **2010**, *48*, 3368.

[11] Yhaya F, Lim J, Kim Y, Liang M, Gregory A M and Stenzel M H, *Macromolecules*, **2011**, 44, 8433.

[12] Okada M, Takashima Y and Harada A, *Macromolecules*, **2004**, *37*, 7075.

[13] Zhao M, Jiang P, Deng K, Xie S S, Ge G L and Jiang C, *Nanotechnology*, **2009**, *20*, 425301.

[14] Ugur S S, Sariisik M and Aktas A H, *Nanotechnology*, **2010**, *21*, 325603.

[15] Liu J H. Chiu Y H and Chiu T H, *Macromolecules*, **2009**, *42*, 3715.

[16] Cheng H, Yuan X, Sun X, Li K, Zhou Y and Yan D, *Macromolecules*, **2010**, *43*, 1143.

[17] Pirnau A, Bogdan M and Floare C G, *J. Phys.: Conf. Ser.* , **2009**, *182*, 012013.

[18] Kawauchi T, Kawauchi M, Kodama Y and Takeichi T, *Macromolecules*, **2011**, *44*, 3452.

[19] Hasan E A, Cosgrove T and Round A N, *Macromolecules*, **2008**, *41*, 1393.

[20] Yuan W and Ren J, *J. Polym. Sci., Part A*, **2009**, *47*, 2754.

[21] Kim T G, Ragupathy D, Gopalan A I and Lee K P, *Nanotechnology*, **2010**, *21*, 134021.

[22] Mic M, Cruickshank D and Turcu I, *J. Phys.: Conf. Ser.* , **2009**, *182*, 012011.

[23] Cai H, Yang R, Yang G, Huang H and Nie F, *Nanotechnology*, **2011**, *22*, 305602.

[24] Xue J, Jia Z, Jiang X, Wang Y, Chen L, Zhou L, He P, Zhu X and Yan D, *Macromolecules*, **2006**, *39*, 8905.

[25] Tsai C C, Leng S, Jeong K U, Horn R M V, Wang C L, Zhang W B, Graham M J, Huang J, Ho R M, Chen Y, Lotz B and Stephen Cheng S Z D, *Macromolecules*, **2010**, *43*, 9454.

[26] Wang L, Wang J L and Dong C M, *J. Polym. Sci., Part A*, **2005**, *43*, 4721.

[27] Manakker F, Pot M, Vermonden T, Nostrum C F and Hennink W E, *Macromolecules*, **2008**, *41*, 1766.

[28] Voit B, *J. Polym. Sci., Part A*, **2000**, *38*, 2505.

[29] Zou J, Guan B, Liao X, Jiang M and Tao F, *Macromolecules*, **2009**, *42*, 7465.

[30] Xie D, Jiang M, Zhang G Z and Chen D Y, *Chem. Eur. J.* , **2007**, *13*, 3346.

[31] Moughton A O, O'Reilly R K, *J. Am. Chem. Soc.* , **2008**, *130*, 8714.

Chapter 5

Thermo-Switchable Fluorescence Organogels Based on Hydrogen Bond-Assisted Chiral Gelators

Abstract

To clarify the individual effect of secondary forces on the self-assembly of molecules, a chiral cholesteryl *N*-(2-anthryl) carbamate (CAC) consisting of anthryl, carbamate and cholesteryl groups was synthesized. From the results of the temperature-dependent ^{1}H-NMR, the hydrogen bond-assisted π-π interaction was found to maintain the growth of the axis of the self-assembled structure, and the three-dimensional effect from the cholesteryl group induces the rotational structure.

Fluorescence behavior of the CAC molecules with and without assistance of secondary forces was investigated. Thermo-switchable fluorescence of gelators was observed. Supramolecular organogels reveal significant enhanced fluorescence strength due to the aggregation-induced enhanced emission (AIEE) of the CAC molecules.

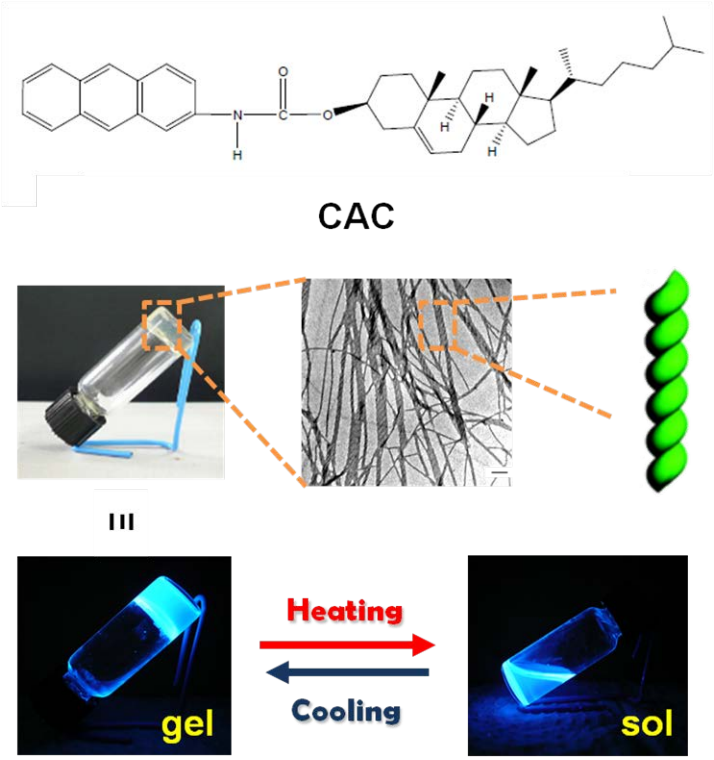

5.1 Introduction

Molecular gels have been the subject of increasing attention in recent years due to their unique structures and wide range of potential applications.[1-5] Molecular gels are entangled three dimensional networks with solvent molecules entrapped inside. Self-assembled fibers formed by hydrogen bonds are one promising candidate to produce molecular gels because of their strength, directionality, reversibility, and selectivity. A wide range of different types of organic molecules has been investigated as low molecular weight organogelators, including saccharides, peptides, amides, ureas, nucleobases, steroid derivatives and others.[6-9] Many of these organogelators self-assemble utilizing hydrogen bonds and/or π-π interactions to form the corresponding gels.[10-13]

Many research groups have reported that the presence of at least one stereoasymmetric center in the structure of a small molecule gelator determines its ability to form gels in organic solvents or in water.[14-17] Molecular chirality thus seems to promote the growth of assemblies with high aspect ratios that entrap the solvent in which they form, leading to the simple empirical (though not general) rule that a molecule has a better chance to be a good gelator if it is chiral. However, these observations remain, for the most part, difficult to explain.[18-21]

Twin-dendritic or organogelators self-assemble in bulk to form self-organized arrays and in solution to gel organic solvents are reported.[22–26] The self-organization of polymers jacketed with self-assembling dendrons to elucidate how primary structure determines the adopted conformation and fold, how the supramolecules associate, and their resulting functions were investigated.[27–29] Helical self-assembly and helical supramolecular polymerization or self-assembly were advanced to take place via two different mechanisms. Either a nonchiral structure self-assembles directly into a racemic helical structure containing both helical senses and the incorporation of a stereocenter selects the handedness of the structure, or a nonchiral structure self-assembles into a nonhelical structure and the helicity of this structure is induced by the incorporation of a stereocenter in the structure. All evidence from the reported reviews and many other publications favor the first mechanism.[30–34]

A multiple switching system responding to light, thermal stimuli, fluoride anions, and protons by using a photochromic fluorescent organogel based on bisthienylethene-bridged naphthalimides was investigated.[35-39] Some new naphthalene derivatives consisting of bisurea and six long alkyl chains to develop switchable fluorescent organogel systems by the coordination of intermolecular hydrogen bonding and π-π interactions were reported. The sol-gel process and the fluorescence of the systems could be controlled by alternate addition of fluoride anions and protons.[40-44] In our previous report, photo-tunable morphologies of inclusion complexes were achieved due to the dramatic interaction between threaded β-cyclodextrins.[45] The effect of secondary forces on helical morphology and thermotunable fluorescence behaviors of chiral gelators is limited. In this chapter, we report the

synthesis of a chiral gelator as well as optical behaviors and self-assembled construction of the gelator. Formation of self-assembled constructions via secondary forces was investigated through temperature-dependent ^{1}H-NMR. Liquid crystalline behavior, ^{1}H-NMR spectra at different temperatures and the effect of individual secondary forces on helical structures are also discussed.

5.2 Results and Discussion

5.2.1 Synthesis of Cholesteryl *N*-(2-anthryl) carbamate (CAC)

Cholesteryl *N*-(2-anthryl) carbamate (CAC) was synthesized via carbamation. The synthetic process and molecular structures are shown in Scheme 5-1. As shown in the scheme, the anthryl group conjugated with the neighboring carbamate attached to the cholesteryl group forms CAC. The synthesized molecular structure was confirmed using both ^{1}H-NMR and FTIR. The ^{1}H-NMR and FTIR spectra are shown in Figure 5-1(a) and (b), respectively. The related functional groups and protons are noted in the spectra. In Figure 5-1(a), most protons on the cholesteryl group and aromatic ring protons appeared between 0.8 and 2.5 ppm, and 7.2 and 8.5 ppm, respectively. Moreover, the presence of both amine and carbonyl groups in CAC in Figure 5-1(b) was confirmed. From the results of NMR, FTIR and elemental analysis, the synthesized CAC was identified.

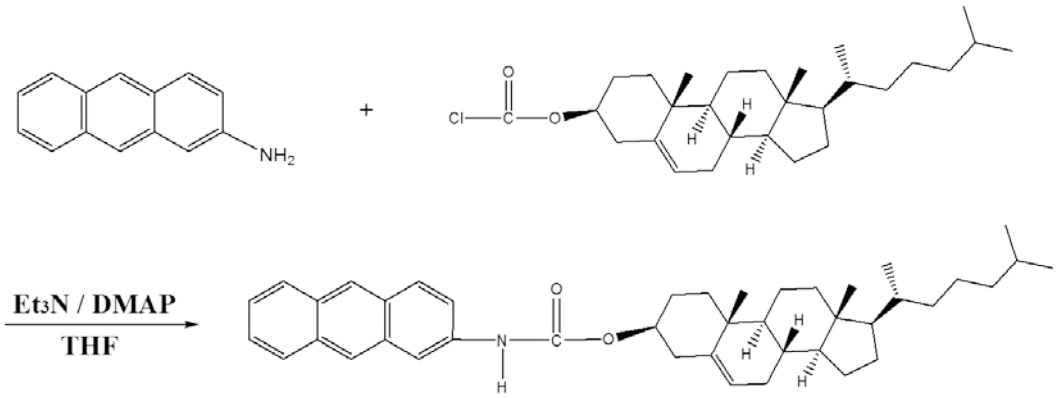

Scheme 5-1. Synthesis of cholesteryl *N*-(2-anthryl) carbamate (CAC).

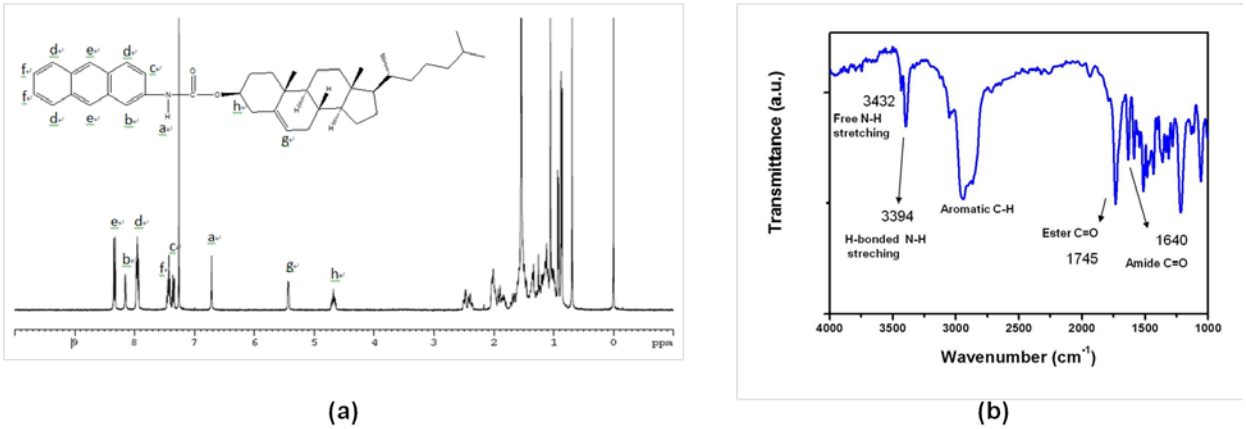

Figure 5-1. (a) ^{1}H-NMR spectrum and (b) FTIR spectrum of **CAC**.

5.2.2 Optical and Thermal Properties of CAC

The liquid crystalline phases were confirmed using both DSC and POM analysis. The DSC thermogram of CAC is shown in Figure 5-2(a). From the DSC analysis, T_{Ch-I} values (phase transition temperatures from cholesteric to isotropic) in heating and cooling cycles were calculated as 273°C and 222°C, respectively. In addition, Figure 5-2(b) shows the cholesteric liquid crystalline phase of CAC at 210°C under POM. The results of thermal analysis suggest that the interaction between neat CAC molecules is high enough to form the liquid crystalline phases. From the molecular structure, formation of the liquid crystalline phases could be due to the presence of hydrogen bonding and polar-polar interaction between CAC molecules. Cholesteryl derivatives usually reveal liquid crystalline properties due to the van der Waals interactions between cholesteryl groups.[33-35]

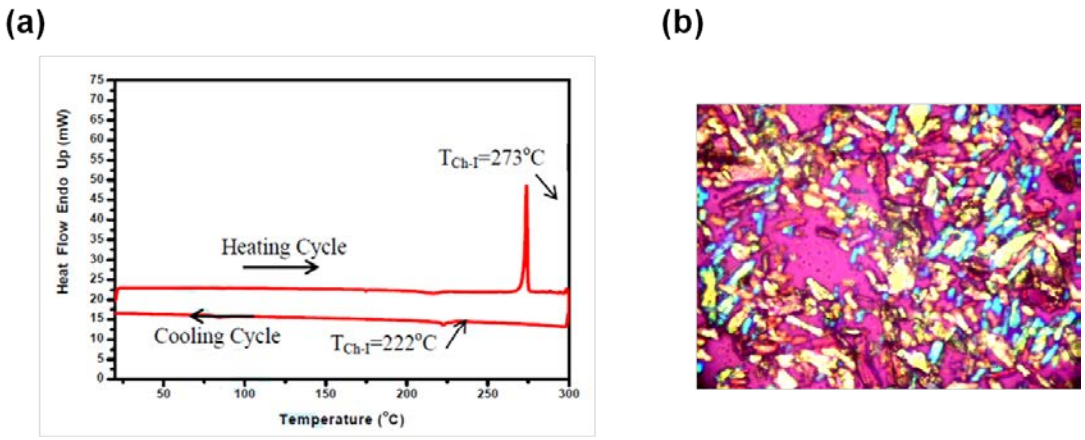

Figure 5-2. (a) DSC thermogram of neat of CAC and (b) POM texture of neat CAC at 210°C.

5.2.3 Gelatinous Self-assembly of CAC

To investigate the self-assembly of CAC molecules in solvents, a series of gelation experiments in solvents was carried out. The results are summarized in Table 5-1. Gelation of CAC was observed in both mixed and pure solvents. The critical gelation concentration of the systems was calculated, and both good and poor solvents for the CAC compound were determined. A schematic representation of the molecular interaction between CAC molecules is shown in Figure 5-3.

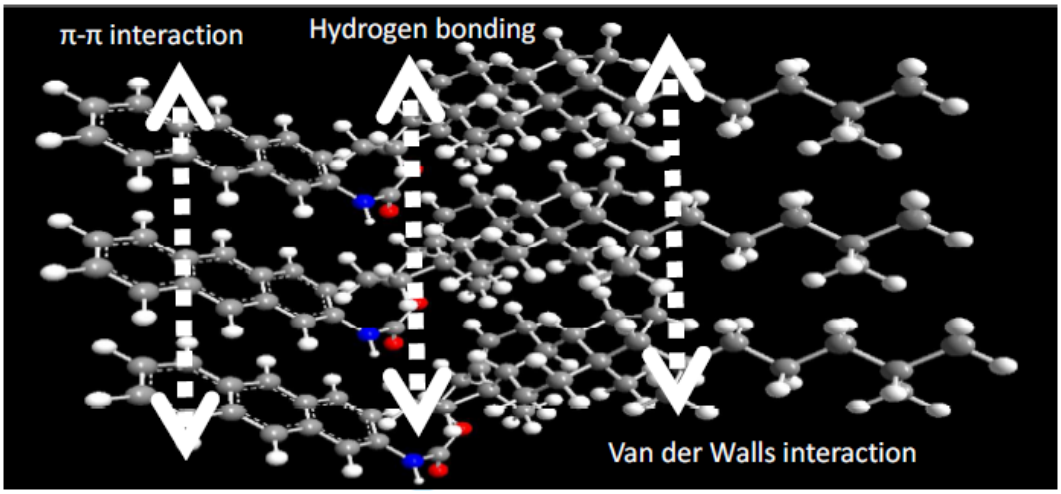

Figure 5-3. Schematic representation of the molecular interaction between CAC molecules through π-π interaction, hydrogen bonding and van der Waal forces.

Formation of supramolecular gels is due mainly to the existence of the secondary forces. Figure 5-4 shows the real images of the reversible transition between gel and solution states. Heat energy overcomes the secondary forces between CAC molecules and solvents and leads to the formation of the liquid phase. The cooling process causes the formation of the gels. The heating and cooling cycles are reversible.

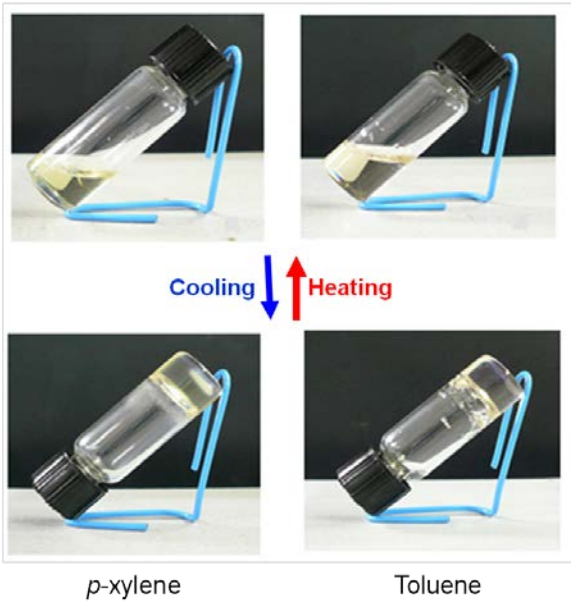

Figure 5-4. Real images of the revisable transition of gel-solution states in *p*-xylene and toluene.

To investigate the molecular interaction between CAC molecules in the gel state, temperature-dependent ^{1}H-NMR analysis was performed. Figure 5-5 shows the thermal effect on the stacking of aromatic rings. As shown in Figure 5-8, because of the induced magnetic field, protons on aromatic rings will be shifted when molecules are in close proximity.

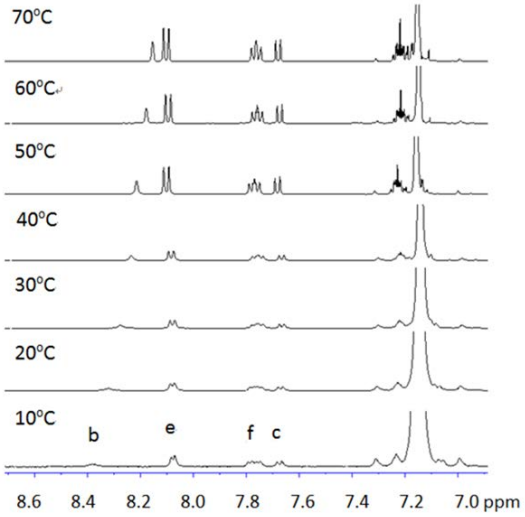

Figure 5-5. Temperature dependent ^{1}H-NMR spectrum of the anthryl group of CAC.

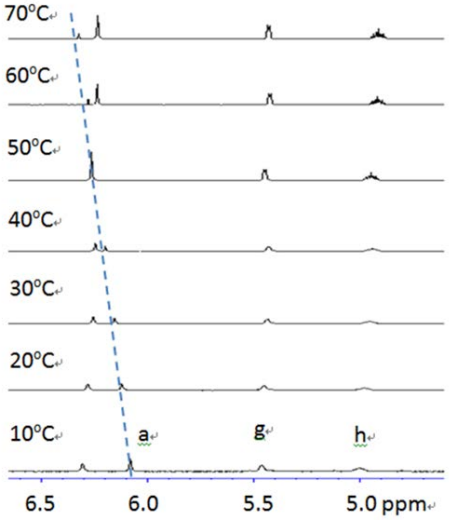

Figure 5-6. Temperature dependent ^{1}H-NMR spectrum of the carbamate group of CAC.

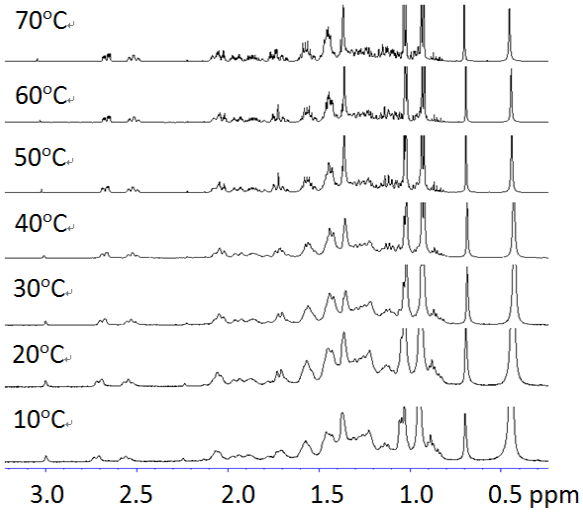

Figure 5-7. Temperature dependent ^{1}H-NMR spectrum of cholesteryl group of CAC.

Depending on the location of protons, upfield and downfield shifts are expected. As shown in Figure 5-5, with an increase in temperature, a significant upfield shift is observed. At lower temperatures, gelation brings aromatic rings close together and leads to a significant induced field effect. Increases in temperature decrease the supramolecular arrangement and the effect of secondary forces. In the heating cycle, upfield shift is ascribed to the release of intermolecular forces between CAC molecules.

Formation of a hydrogen bond is expected because of the existence of carbomate in the CAC molecule. Figure 5-6 shows the thermal effect on the ^{1}H-NMR spectrum. The downfield shift is ascribed to the release of hydrogen bonding because of the deformation of self-assembled gels when temperature is increased. A signal shift ~5.0 ppm is due to the van der Waals interaction with the cholesteryl group. Some further shifts from van der Waals interactions were observed, as shown in Figure 5-7. Although the shift of peaks around the area is not clear, this shift is ascribed to the supramolecular interaction from the cholesteryl groups. In the cooling cycle, self-assembled molecules reveal some van der Waals interaction leading to the variation in spectra. In the case of chiral groups, theoretically, some specific steric effects may be revealed due to the steric hindrance.

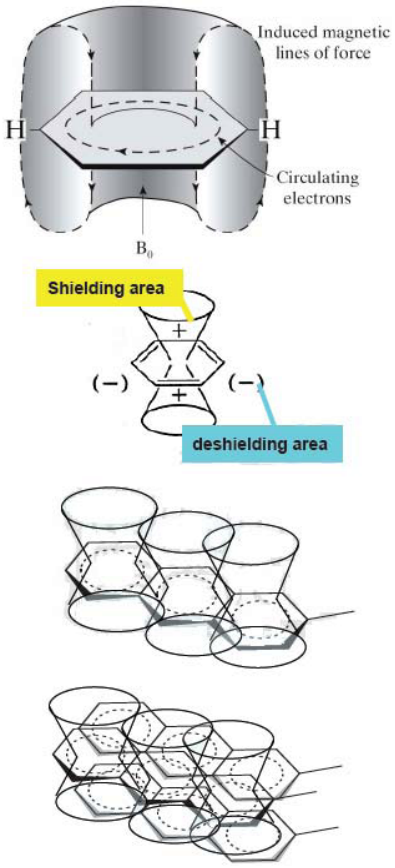

Figure 5-8. Schematic representation of magnetic anisotropy in aromatic ring system via induced magnetic field.

Table 5-1 Gelation of CAC in various organic solvents.

Solvent	Gelation[a]
$CHCl_3/CH_3OH$ (3:1)	G (7.5)[b]
CH_2Cl_2/CH_3OH (3:1)	G (5.0)
$CHCl_3$/*n*-hexane (1:1)	G (5.0)
CH_2Cl_2 (1:1)	G (3.4)
Benzene	G (3.0)
Toluene	G (6.0)
p-Xylene	G (10.0)
MEK	G (10.0)
THF, 1,4-dioxane, NMP, pyridine, CH_2Cl_2, $CHCl_3$	S
Hexane, H_2O, diethyl ether, methanol, ethanol, acetone, DMSO, DMF, acetonitrile	I

[a] G= gel formed at room temperature, S= soluble, I= insoluble. [b] Critical gelation concentration (g/L).

5.2.4 Helical Supramolecular Architectures in Gelled CAC

As the TEM images of the zero-gels show in Figure 5-9, the self-assembled CAC molecules form helical structures. The sample gel was prepared from CAC in benzene at the critical concentration of 3 g/L. The appearance of the structure suggests a right-handed helical structure. From the results shown in Figures 5-7, the central axis of the self-assembled structure is ascribed to the interaction between aromatic rings. The aromatic ring interaction shown in Figure 5-5 is much stronger than the interaction in Figure 5-7 due to the van der Waals forces from cholesteryl groups. As shown in Figure 5-6, a significant shift of the hydrogen bond from 6.1 to 6.4 ppm is observed with an increase in temperature. These results indicate that self-assembly is assisted by the hydrogen bonding. Thus, a higher thermal effect is ascribed to the stronger interaction between the CAC molecules.

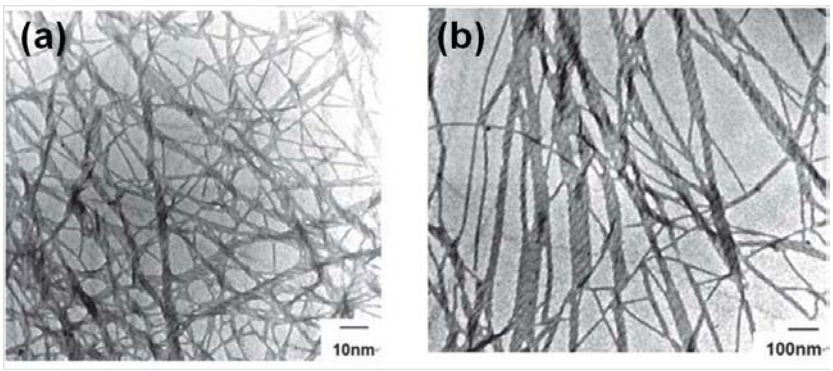

Figure 5-9. (a) TEM image of gels prepared from CAC in benzene at critical concentration of 3 g/L, and (b) an enlarged image of (a).

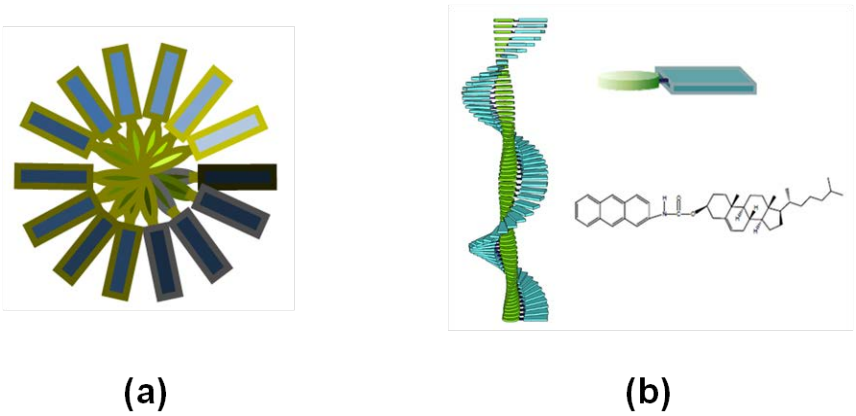

Figure 5-10. Schematic representations of the self-assembly of the CAC molecules: (a) top view, and (b) side view of the helical construction.

A schematic representation of the self-assembly of the CAC molecules is shown in Figure 5-10. Interaction of aromatic rings maintains the growth of the axis of the self-assembled structures via the assistance of hydrogen bonding. Steric hindrance usually causes a nonlinear arrangement leading to the formation of the helical construction. The results of temperature-dependent NMR suggest that the chiral effect from cholesteryl groups leads to the formation of a right-handed structure.

Induction of helical structures via chiral segments has been extensively reported in the literature. Theoretically, aggregation of self-assembled helical constructions forms bundles and then three-dimensional networks. Figure 5-11 shows a schematic representation of the aggregation of bundles and the formation of organogels.

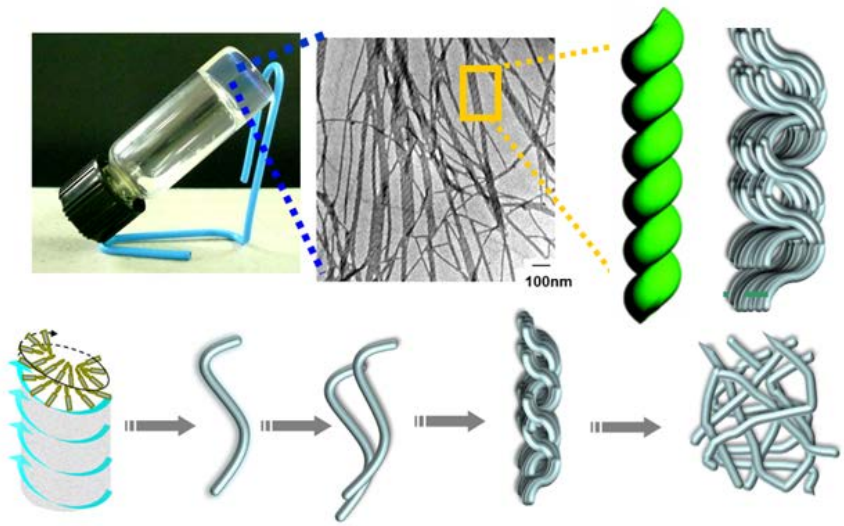

Figure 5-11. Schematic representations of the aggregation of bundles and the formation of organogels.

5.2.5 Optical Properties of Gelled CAC

Because the synthesized CAC contains a chromophoric aromatic ring, the optical behavior of CAC in the gel status was investigated. Figure 5-12 shows the results of the fluorescence of CAC in various solvents such as benzene, toluene, $CHCl_3$/hexane and $CHCl_3$/methanol. In the gel state at low temperatures, CAC molecules self-assemble and form supramolecular gels. The λmax values for the gel state in various solvents are quite similar and the λmax is much stronger than in the liquid state. The enhanced fluorescence strength is ascribed to the AIEE. Due to the stronger secondary forces between CAC molecules, the nonradiative relaxation is inhibited. However, at high temperatures in the solution state, the λmax values of the systems are different, possibly due to the different levels of interaction of solvents on CAC. The excited species may also release energy via vibrations leading to the decrease in fluorescence intensity.

To evaluate the gelation effect on the luminance of fluorescence, UV (λmax= 400 nm) irradiation of CAC in benzene was performed. Figures 5-13(a) and (b) show the fluorescence of CAC in the gel state and the solution state, respectively. The red shift shown in Figure 5-13(a) is ascribed to the interaction between CAC molecules through secondary forces. Without supramolecular interactions, as shown in Figure 5-13(b), an increase in temperature from 25 to 80°C shows only a small variation in fluorescence. These results suggest that self-assembly of CAC produces a significant effect on the increase in fluorescence. Figure 5-13(c) shows the real image of the fluorescence luminance of gel and solution. The phenomenon of photo-induced fluorescence is reversible.

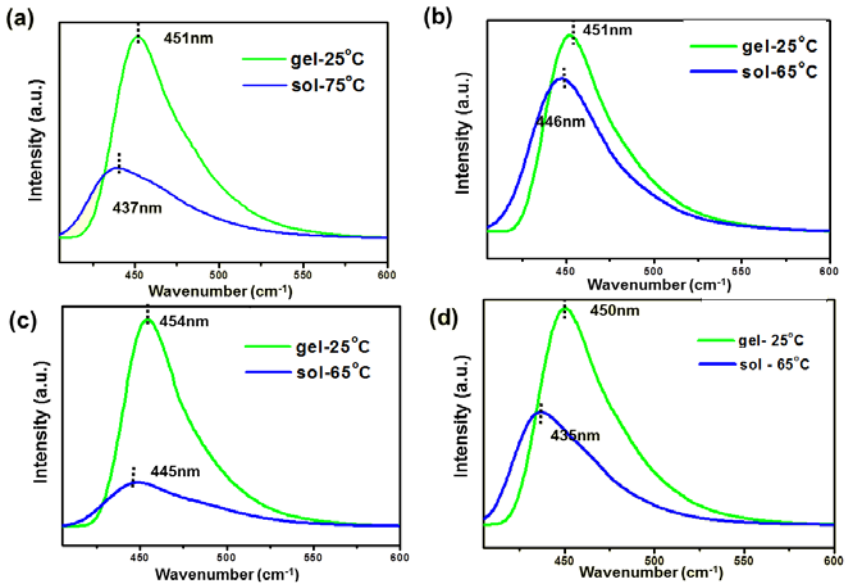

Figure 5-12. Fluorescence spectra of CAC in (a) benzene (3 g/L), (b) $CHCl_3$/hexane= 1:1 (5 g/L), (c) $CHCl_3$/methanol= 3:1 (7.5 g/L), and (d) toluene (6 g/L).

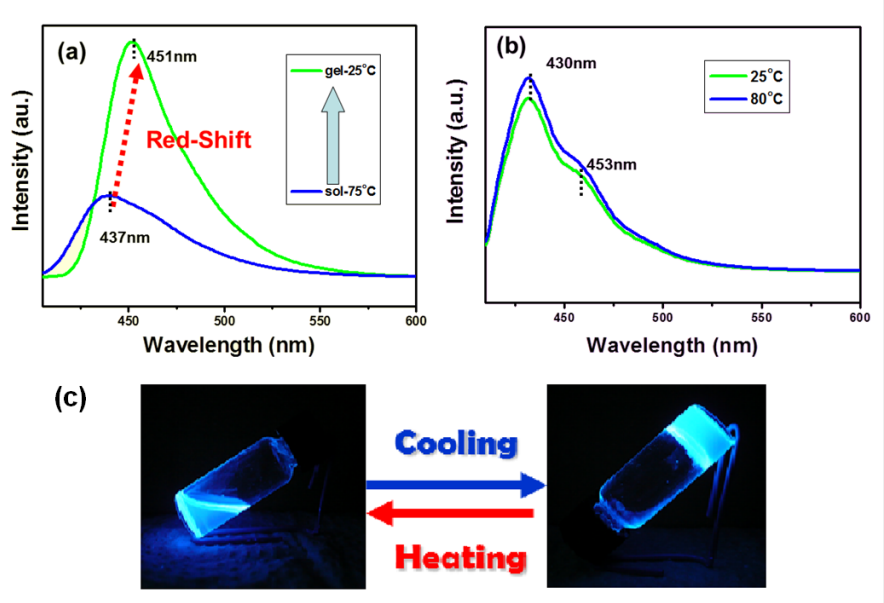

Figure 5-13. Thermal effects on fluorescence of CAC in (a) gel, and (b) solution state, (c) real image of florescence of CAC gel and solution.

5.3 Conclusion

A chiral gelator consisting of anthryl, carbamate and cholesteryl groups was synthesized. The effect of secondary forces on the formation of a self-assembled helical structure was studied via temperature-dependent ^{1}H-NMR. The results show that hydrogen bond-assisted π-π interaction maintains the growing of the axis in the self-assembled construction, and the three dimensional effect from the cholesteryl group induces the rotational structure. In the gel state, significant enhanced fluorescence strength is observed due to the AIEE of CAC molecules.

5.4 Experimental Section

5.4.1 Materials characterization

The Fourier transform infrared spectroscopy (FTIR) spectra were recorded on a Jasco VALOR III Fourier transform infrared spectrophotometer. Nuclear magnetic resonance (NMR) spectra were obtained using a Bruker AMX-400 high-resolution NMR spectrometer. Differential scanning calorimetry (DSC) was conducted on a Perkin-Elmer DSC 7 in a nitrogen atmosphere with heating and cooling rates of +5 and -5 °Cmin^{-1}, respectively. The morphology of the samples was characterized by transmission electron microscopy (TEM) using a JEOL JEM-1200CX-II microscope with a Cu-grid substrate. The anisotropic properties of the highly ordered selfassembled samples were investigated using an Olympus BH-2 polarized light microscope (POM) equipped with a Mettler hot stage FP-82, and the temperature scanning rate was determined to be 10 °C min^{-1}. Fluorescence emission intensities were measured using a North Dalian BF-72 fluorescence microscope.

5.4.2 Materials

• Synthesis of Cholesteryl N-(2-Anthryl) Carbamate (CAC)

Tetrahydrofuran (THF) was purified via distillation in the presence of sodium wire. A mixture of 2-aminoanthracene (1 g), dimethylaminopyridine DMAP (one drop), and trimethylamine (0.6 g) in THF was stirred for 30 min at 0°C in a nitrogen atmosphere. Cholesteryl chloroformate (2.09 g) was added dropwise. After completion of the addition, the ice bath was removed. The mixture was stirred at 25°C for 6 hours. After the reaction, the precipitated salt was filtered and THF was removed using a rotary evaporator. The crude solid product was dissolved in dichloromethane and washed with water. After drying over magnesium sulfate, dichloromethane was removed using a rotary evaporator. The product was then purified using silica gel chromatography with ethyl acetate/*n*-hexane (1:4) as a mobile phase. Yield = 62%.

FTIR (KBr, cm^{-1}): 3432 (free N-H), 3394 (hydrogen bonded N-H), 3051 (sp^2 C-H), 2939 (C-H in Ar), 2807 (sp^3 C-H), 1745, 1640 (C=O), 1063 (COC), ^{1}H-NMR ($CDCl_3$, δ in ppm): 4.61-4.74 (m, 1H, COOCH), 5.43 (m, 1H, C=CH), 6.71 (s, 1H, CONH), 7.33-7.36 (m, 1H, Ar-H), 7.40-7.44 (m, 2H, Ar-H), 7.93-7.96 (m, 3H, Ar-H), 8.14 (s, Ar-H), 8.31-8.34 (d, 2H, Ar-H). Elemental analysis: $C_{42}H_{55}NO_2$ (605): Calcd. C, 83.3; H, 9.1; N, 2.3. Found: C, 83.7; H, 8.8; N, 2.4.

5.5 References

[1] T. Nakano, Y. Satoh, Y. Okamoto, *Macromolecules*, **2001**, *34*, 2405.

[2] Y. Shen, S. Zhu, F. Zeng, R. H. Pelton, *Macromolecules*, **2000**, *33*, 5427-.

[3] D. K. Wang, D. J. T. Hill, F. A. Rasoul, A. K. Whittaker, *J Polym Sci Part A: Polym Chem*, **2012**, *50*, 1143.

[4] H. Kawasaki, S. Sasaki, H. Maeda, *Langmuir*, **1998**, *14*, 773.

[5] M. J. Song, D. S. Lee, J. H. Ahn, D. J. Kim, S. C. Kim, *J Polym Sci Part A: Polym Chem*, **2004**, *42*, 772.

[6] J. Tu, L. Chen, Y. Fang, C. F. Wang, S. Chen, *J Polym Sci Part A: Polym Chem*, **2010**, *48*, 823.

[7] X. Chen, K. Liu, P. He, H. Zhang, Y. Fang, *Langmuir*, **2012**, *28*, 9275.

[8] I. Villuendas, J. I. Iribarren, S. Muñoz-Guerra, *Macromolecules*, **1999**, *32*, 8015.

[9] Y. Akiyama, Y. Shinohara, Y. Hasegawa, A. Kikuchi, T. Okano, *J Polym Sci Part A: Polym Chem*, **2008**, *46*, 5471.

[10] T. Kishida, N. Fujita, K. Sada, S. Shinkai, *Langmuir*, **2005**, *21*, 9432.

[11] J. Tritt-Goc, M. Bielejewski, R. Luboradzki, A. Łapiński, *Langmuir*, **2008**, *24*, 534.

[12] H. Tetsuka, Y. Doi, H. Abe, *Macromolecules*, **2006**, *39*, 9071.

[13] J. Yang, Q. Li, Y. Li, L. Jia, Q. Fang, A. Cao, *J Polym Sci Part A: Polym Chem*, **2006**, *44*, 2045.

[14] P. Chen, R. Lu, P. Xue, T. Xu, G. Chen, Y.Zhao, *Langmuir*, **2009**, *25*, 8395.

[15] L. Li, H. Seino, K. Yonetake, M. Ueda, *Macromolecules*, **1999**, *32*, 3851.

[16] M. Kumoda, M. Watanabe, Y. Takeoka, *Langmuir*, **2006**, *22*, 4403.

[17] H. Tetsuka, Y. Doi, H. Abe, *Macromolecules*, **2006**, *39*, 2875.

[18] M. Suzuki, R. Yanagida, C. Setoguchi, H. Shirai, K. Hanabusa, *J Polym Sci Part A: Polym Chem*, **2008**, *46*, 353.

[19] X. Dai, S. A. Knupp, Q. Xu, *Langmuir*, **2012**, *28*, 2960.

[20] M. M. Alam, K. Aramaki, *Langmuir*, **2008**, *24*, 12253.

[21] J. Thuillez, F. Thouraud, E. Fleury, *J Polym Sci Part A: Polym Chem*, **2008**, *46*, 4122.

[22] V. Percec, M. Peterca, M. E. Yurchenko, J. G. Rudick, P. A. Heiney, *Chem. Eur. J.*, **2008**, *14*, 909.

[23] B. M. Rosen, C. J. Wilson, D. A. Wilson, M. Peterca, M. R. Imam, V. Percec, *Chem. Rev.*, **2009**, *109*, 6275.

[24] J. G. Rudick, V. Percec, *Acc. Chem. Res.*, **2008**, *41*, 1641.

[25] J. G. Rudick, V. Percec, *New J. Chem.*, **2007**, *31*, 1083.

[26] V. Percec, P. Leowanawat, *Israel J. Chem.*, **2011**, *51*, 1107.

[27] V. Percec, M. R. Imam, M. Peterca, P. Leowanawat, *J. Am. Chem. Soc.*, **2012**, *134*, 4408.

[28] V. Percec, S. D. Hudson, M. Peterca, P. Leowanawat, E. Aqad, R. Graf, H. W. Spiess, X. Zeng, G. Ungar, P. A. Heiney, *J. Am. Chem. Soc.*, **2011**, *133*, 18479.

[29] V. Percec, M. Peterca, T. Tadjiev, X. Zeng, G. Ungar, P. Leo wanawat, E. Aqad, M. R. Imam, B. M. Rosen, U. Akbey, R. Graf, S. Sekharan, D. Sebastiani, H. W. Spiess, P. A. Heiney, S. D. Hudson, *J. Am. Chem. Soc.*, **2011**, *133*, 12197.

[30] B. M. Rosen, M. Peterca, K. Morimitsu, A. E. Dulcey, P. Leo wanawat, A. M. Resmerita, M. R. Imam, V. Percec, *J. Am. Chem. Soc.*, **2011**, *133*, 5135.

[31] M. Peterca, M. R. Imam, C. H. Ahn, V. S. K. Balagurusamy, D. A. Wilson, B. M. Rosen, V. Percec, *J. Am. Chem. Soc.*, **2011**, *133*, 2311.

[32] B. M. Rosen, D. A. Wilson, C. J. Wilson, M. Peterca, B. C. Won, C. Huang, L. R. Lipski, X. Zeng, G. Ungar, P. A. Heiney, V. Percec, *J. Am. Chem. Soc.*, 2**009**, *131*, 17500.

[33] M. Peterca, V. Percec, M. R. Imam, P. Leowanawat, K. Morimitsu, P. A. Heiney, *J. Am. Chem. Soc.*, **2008**, 1*30*, 14840.

[34] V. Percec, B. C. Won, M. Peterca, P. A. Heiney, *J. Am. Chem. Soc.*, **2007**, *129*, 11265.

[35] N. Malic, R. A. Evans, *J Polym Sci Part A: Polym Chem*, **2012**, *50*, 1434.

[36] S. Karthikeyan, R. P. Sijbesma, *Macromolecules*, **2009**, *42*, 5175.

[37] Y. Doi, M. Tokita, *Langmuir*, **2005**, *21*, 9420.

[38] R. J. Day, I. M. Robinson, M. Zakikhani, R. Young, *J Polym Sci Part A: Polym Chem*, **1987**, *28*, 1833-1840.

[39] C. Galiotis, I. M. Robinson, R. J. Young, B. J. E. Smith, D. N. Batchelder, *Polym Commun*, **1985**, *26*, 354

[40] H. Jeong, W. E. Lee, G. Kwak, *Macromolecules*, **2010**, *43*, 1152.

[41] I. M. Robinson, M. Zakikhani, R. J. Day, R. J. Young, C. Galiotis, *J Mater Sci Lett*, **1987**, *6*, 1212.

[42] G. Hungerford, A. Rei, M. I. C. Ferreira, C. Tregidgo, K. Suhling, *Photochem Photobiol Sci*, **2007**, *6*, 825.

[43] H. Itagaki, I. Takahashi, *Macromolecules*, **1995**, *28*, 5477.

[44] T. Fujii, H. Yamamoto, K. Oki, *J Mater Chem*, **1994**, *4*, 635.

[45] W. T. Liu, N. Tohnai, I. Hisaki, M. Miyata, D. Steven, Y. H. Chiu, J. H. Liu, *Sci Adv Mater*, **2012**, *4*, 1.

Summary

This thesis has described the dynamic properties and synthesis of helical assembly of organic molecules containing steroidal moieties via secondary forces. As is well known, asymmetric structures can only be induced in chiral environment. Some helical construction and some interesting phenomena were observed in this thesis via self-assembly of chiral compounds containing cholesteryl group.

In **chapter 1**, the author described the selective guest retention in the thermal guest-release process of the cholic acid (CA) inclusion crystals. The selectivity was found to be attributable to the host-guest hydrogen bond at one of the two nonequivalent sites in the 2-D cavity when the structural change of the crystals from the sandwich-type to the bilayer-type occurs. The present selectivity develops in the thermal guest-release process from preformed ternary inclusion compounds.

In **chapter 2**, the molecular recognition mechanism of 3α,7α,12α,24-tetrahydroxycholane (CAL) were investigated. From the investigation of molecular assembly, formation of supramolecular chirality is expected to be clarified through such investigation. We have demonstrated that various slight variations of host and guest molecules in size, shape and polarity induce drastic changes in arrangements and stability of inclusion crystals. Further detailed investigations on the variations are expected to deliver valuable information on hierarchical structures as well as supramolecular chirality of host-guest assemblies in the crystalline state.

In **chapter 3**, a universal method to determine handedness of 2_1 helical assemblies composed of planar aromatic molecules is proposed and demonstrated with taking $P2_1/c$ and *Pbca* crystals of benzene, the simplest aromatic molecule, as examples. The 2_1 helical assembly is one of the most fundamental and important motifs of organic non-centrosymmetric crystals. Over 70% of crystals registered in the Cambridge Structural Database (CSD) contain 2_1 helical axes.

In **chapter 4**, the synthesis and the characterization of chiral cholesteryl-*E*-4-(11-acryloxy-undecaloxy)-cinnamate (CAUC) were carried out. Chiral CAUC with a photoisomerizable C=C bond and a cholesteryl terminal group was synthesized. After threading with β-CDs, the synthesized IC possesses a stronger intermolecular hydrogen bonding potential that leads to the formation of a rod construction. After UV irradiation, CAUC configurationally isomerizes from E to Z, which decreases the strength of the intermolecular forces. Therefore, this self-assembled structure changes from a rod-shaped to a spherical morphology. UV induced isomerization may de-thread CDs from CAUC, resulting in the weakening of intermolecular forces which causes the changes in morphology.

In **chapter 5**, cholesteryl *N*-(2-anthryl) carbamate (CAC), consisting of anthryl, carbamate and cholesteryl groups was synthesized. The effect of secondary forces on the formation of a self-assembled helical structure was studied via temperature-dependent ^{1}H-NMR. The results show that hydrogen bond-assisted π-π interaction maintains the growing of the axis in the self-assembled construction, and the three dimensional effect from the cholesteryl group induces the rotational structure. In the gel state, significant enhanced fluorescence strength is observed due to the AIEE of CAC molecules.

As a conclusion, we have investigated dynamic properties of self-assembly of chiral organic

molecules containing steroidal moieties via a series of X-ray structural analysis. A systematic study on the steroidal assemblies would clarify any relations between organic molecules and their assemblies through cooperative interactions, bridging the gap between small molecules and biopolymers. Furthermore, we used not only the solid crystal structures but also the liquid crystals containing steroidal moieties. According to the experiment data of spectral and microscopy analysis, we confirmed the formation of helical structures due to the steroidal moieties.

In this thesis, we designed and synthesized supramolecular soft material containing helical structures successfully.

General Introduction **:** The background and scope of this thesis

Chapter 1. Selective Guest Retention in Thermal Guest-release Process in Sandwich-type Inclusion Crystal of Cholic Acid

(***Paper1.*** *Chem.Eng.Comm.*, **2010**, *12*, 1461-1466.)

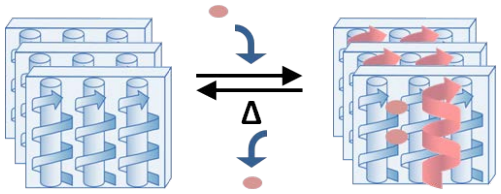

Dynamics

Bundle of helices

Chapter 2. Inclusion Crystals of 3α,7α,12α,24-tetrahydroxycholane with Haloaromatic Compounds : Pitches and Stability of Herringbone Assemblies in Channels

(***Paper4.*** *Chem. Lett* . **2013**, *42*, 143-145.)

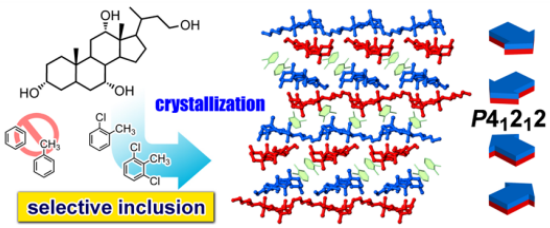

Handedness determination

Chapter 3. Right- and Left-handedness of 2_1 Symmetrical Herringbone Assemblies of Benzene

(***Paper2.*** *Chem.Comm.*, **2012**, *48*, 2219-2221.)

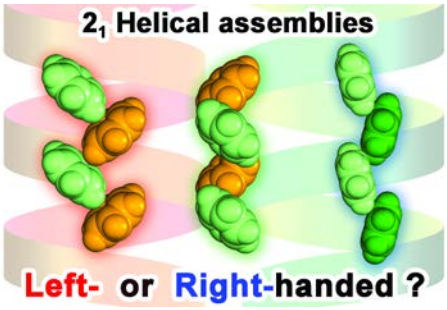

Molecular design with steroidal moieties

Chapter 4. Photo-Tunable Morphologies of β-Cyclodextrin-Threaded Inclusion Complexes Containing a Terminal Cholesteryl Group

(***Paper3.*** *Sci. Adv. Mater.*, **2012**, *4*, 1031-1038.)

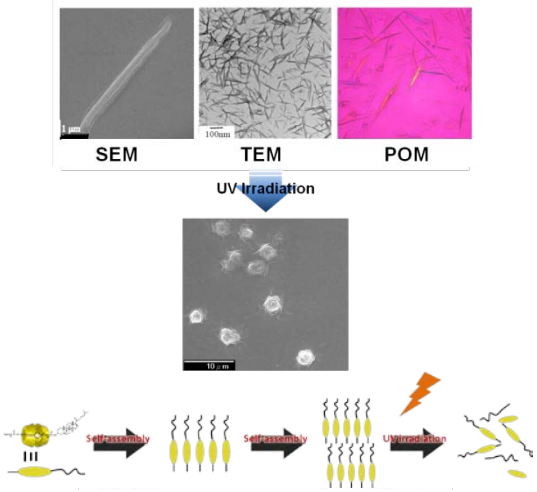

Chapter 5. Thermo-Switchable Fluorescence Organogels Based on Hydrogen Bond-Assisted Chiral Gelators

(***Paper5.*** *J.Polym. Sci.PART A: Polym. Chem.*, **2013**, *51*, 793-800.)

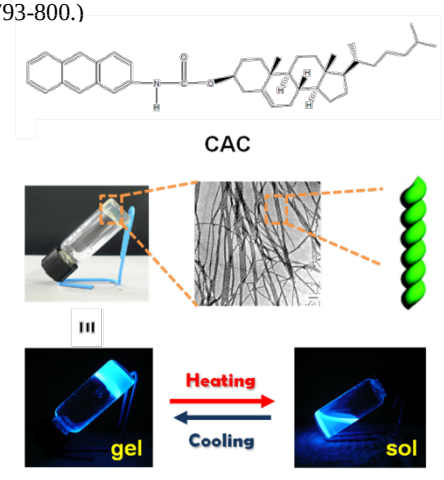

Summary **:** Summary in each chapter and perspective

List of Publications

[1] Selective Guest Retention in Thermal Guest-release Process in Sandwich-type Inclusion Crystal of Cholic Acid
Kazunori Nakano, Shigendo Akita, Taketoshi Murai, Wen-Tzu Liu, Ichiro Hisaki, Norimitsu Tohnai and Mikiji Miyata
ChemEngComm, **2010**, *12*, 1461-1466.

[2] Right- and Left-Handedness of 2_1Symmetrical Herringbone Assemblies of Benzene
Ichiro Hisaki, Toshiyuki Sasaki, Kazuaki Sakaguchi, Wen-Tzu Liu, Norimitsu Tohnai and Mikiji Miyata
Chem.Comm., **2012**, *48*, 2219-2221.

[3] Photo-Tunable Morphologies of β-Cyclodextrin - Threaded Inclusion Complexes Containing a Terminal Cholesteryl Group
Wen-Tzu Liu, Norimitsu Tohnai, Ichiro Hisaki, Mikiji Miyata, Dolok Steven, Yi-Hong Chiu and Jui-Hsiang Liu
Sci. Adv. Mater., **2012**, *4(10),* 1031-1038.

[4] Inclusion Crystals of 3α,7α,12α,24-tetrahydroxycholane with Aromatic Compounds : Pitches and Stability of Herringbone Assemblies in Channels
Wen-Tzu Liu, Yute Kin, Kazunori Nakano, Ichiro Hisaki, Norimitsu Tohnai and Mikiji Miyata
Chem. Lett., **2013**, *42*, 143-145.

[5] Thermo-Switchable Fluorescence Organogels Based on Hydrogen Bond-Assisted Chiral Gelators
Wen-Tzu Liu, Norimitsu Tohnai, Ichiro Hisaki, Jui-Hsiang Liu and Mikiji Miyata
J. Polym. Sci. PART A: Polym. Chem., **2013**, *51,* 793-800.

International Conferences

[1] Weak Hydrogen Bonds in Cholamide Inclusion Crystals with Aromatic Guests
Wen-Tzu Liu, Kazuaki Aburaya, Yute Kin, Ichiro Hisaki, Norimitsu Tohnai and Mikiji Miyata
XXI Congress and General Assembly of the International Union of Crystallography, Osaka, Japan (Aug. 2008)

[2] Four-Point Chiral Recognition in Inclusion Crystals of Cholic Acid Derivatives
Wen-Tzu Liu, Ichiro Hisaki, Norimitsu Tohnai and Mikiji Miyata
The 11th International KYOTO conference on New Aspests of Organic Chemistry, Kyoto, Japan (Nov. 2009)

[3] Inclusion Behaviors of Inclusion Crystals of 3, 7, 12, 24-Tetrahydroxycholane
Wen-Tzu Liu, Ichiro Hisaki, Norimitsu Tohnai and Mikiji Miyata
5th International Symposium on Macrocyclic and Supramolecular Chemistry, Nara, Japan (Jun. 2010)

[4] Hierarchical Recognition of Inclusion Crystals of 3, 7, 12, 24-Tetrahydroxycholane
Wen-Tzu Liu, Ichiro Hisaki, Norimitsu Tohnai and Mikiji Miyata
22nd International Symposium on Chirality, Sapporo, Japan (Jul. 2010)

[5] Molecular Recognition for Inclusion Crystals of Cholic Acid, 3,7,12,24-Tetrahydroxycholane and 3,12,24-Trihydroxycholane
Wen-Tzu Liu, Ichiro Hisaki, Norimitsu Tohnai and Mikiji Miyata
The 13th Asia Pacific Confederation of Chemical Engineering Congress, Taipei, Taiwan (Oct. 2010)

[6] Inclusion Behaviors and Molecular Recognition of 3, 7, 12, 24-Tetrahydroxycholane
Wen-Tzu Liu, Ichiro Hisaki, Norimitsu Tohnai and Mikiji Miyata
The International Chemical Congress of Pacific Basin Societies, Honolulu, USA (Dec. 2010)

[7] Self-assembly of inclusion complexes threaded with β-cyclodextrins.
Wen Tzu Liu, Norimitsu Tohnai, Ichiro Hisaki, Jui Hsiang Liu and Mikiji Miyata
The 12th Pacific Polymer Conference, Jeju Island, Korea (Nov. 2011)

[8] Inclusion Behaviors and Molecular Recognitions of Cholic Acid Derivatives
Wen-Tzu Liu, Ichiro Hisaki, Norimitsu Tohnai and Mikiji Miyata
The 11th Global COE International Symposium: Bio-Environmental Chemistry, Osaka, Japan (Dec. 2011)

Post Award

[1] Handedness Discrimination of 2_1-Helical Assemblies of Benzene and Its Derivatives in the Crystalline State
Kazuaki Sakaguchi, Toshiyuki Sasaki, Wen-Tzu Liu, Norimitsu Tohnai, Ichiro Hisaki, Mikiji Miyata
Symposium on Molecular Chirality 2011, Tokyo, Japan (May 2011)

Acknowledgements

The author would like to express her sincere gratitude to her supervisor, Professor Mikiji Miyata for his leadership, kind guidance, meticulous comments, intensive discussion, and exceedingly valuable suggestions throughout this work. It has been an honor to work with and learn from him for five and half years.

The author would like to appreciate Professor Shunichi Fukuzimi, Professor Kazuya Kikuchi, Associate Professor Norimitsu Tohnai (Osaka University) and Assistant Professor Ichiro Hisaki (Osaka University).

The author would like to thank Ms. Chiaki Kawamura for her office procedure in the laboratory of Chemistry on Supramolecular Recognition (Professor Miyata's group) at Department of Material and Life Science, Graduate School of Engineering, Osaka University. The author would also like to thank her seniors, Mr. Yute Kim, Mr. Hajime Shigemitsu, Mr. Akihiro Tamugi, Mr. Yohei Morishita, Dr. Tomoaki Hinoue. The author would like to thank Ms. Norie Shizuki, Ms. Hiromi Nakajima, Mr. Taketoshi Murai, Dr. Atsushi Yamamoto, Mr. Chien-Chih Chen, Mr. Kazuaki Sakaguchi, Mr. Toshiyuki Sasaki, Ms. Misa Sugino, Mr. Hirofumi Senga, Mr. Atsuhiko Hasegawa, Mr. Tomofumi Hirukawa, Ms. Eriko Kometani, Mr. Yuta Shigenoi, Mr. Toshiki Matsuoka, Mr. Hirohide Yabuguchi, Mr. Yusuke Araki, Mr. Kenichi Sakai, Ms. Eri Hiraishi, Ms. Noriko Manabe, Mr. Keisuke Hatanaka, Mr. Tomoya Hamada, Mr. Tetsuya Miyano, Mr. Daisuke Yasumiya, Ms. Yoko Ida, Mr. Keisuke Osaka, Mr. Tetsuya Hasegawa, Mr. Syuji Bunno, Mr. Tomonaga Harada, Mr. Shoichi Nakagawa , Mr. Ryunosuke Nishida, Mr. Hirokazu Kawabata and Mr. Yuichiro Yoshinaga.

The author acknowledges financial support from the Global COE (center of excellence) Program "Global Education and Research Center for Bio-Environmental Chemistry" of Osaka University and Japan Student Services Organization (JASSO).

Finally, the author would like to express continuous encouragement and assistant given by her father, mother, brother and friends.

Osaka, Japan
Wen-Tzu Liu

Department of Material and Life Science
Graduate School of Engineering, Osaka University

Appendix

Crystallographic data (excluding structure factors) employed in this thesis have been deposited with the Cambridge Crystallographic Data Centre. Copies of the data can be obtained free of charge on application to CCDC, 12 Union Road, Cambridge, CB2 1EZ, UK (Fax: (+44)1223-336033; e-mail: deposit@ccdc.cam.ac.uk). The deposition numbers are listed below. In the list, CA and CAL denotes cholic acid and 3α,7α,12α,24-tetraoxycholane.

Chapter	**Host**	**Guest**	**Deposition number**	**refcode**
1	CA	*m*-fluoroaniline / indene	747041	-
2	CAL	*o*-chlorotoluene	908618	-
	CAL	2,6-dichlorotoluene	908619	-
3		benzene (space group $P2_1/c$)	-	BENZEN03
		benzene (space group *Pbca*)	-	BENZEN